technische universität dortmund

Max-Planck-Institut für molekulare Physiologie

mpi

A biochemical pacemaker system for robust actin growth

Dissertation

Zur Erlangung des akademischen Grades eines Doktors der Naturwissenschaften

(Dr. rer. nat.)

der Fakultät für Chemie und Chemische Biologie

der Technischen Universität Dortmund

Angefertigt am Max-Planck Institut für molekulare Physiologie in Dortmund

vorgelegt von

Johanna Funk

April 2021

Tag der Abgabe der Dissertation: 10. März 2020
Tag der Disputation: 26. Juni 2020
Von Johanna Funk

Erstgutachter	Prof. Dr. Philippe I. H. Bastiaens
Zweitgutachter	Prof. Dr. Stefan Raunser

The work presented in this thesis was performed in the group of Dr. Peter Bieling in the Department of Systemic Cell Biology lead by Prof. Dr. Philippe I. H. Bastiaens at the Max Planck Institute of Molecular Physiology, Dortmund, Germany.

1 Contents

I. List of Figures

II. List of Tables

III. List of Abbreviations

A	alanine
aa	amino acid
AD	ATPase deficient
ATP	adenosine-5'-triphosphate
bp	basepairs
C	cysteine
D	asparagine
DNA	desoxyribonucleic acid
E	glutamic acid
FH	formin homology
H	histidine
his	histidine
hr(s)	hour(s)
IAEDANS-actin	1,5-IAEDANS at Cys-374
1,5-IAEDANS	5-(2-[(iodoacetyl)-amino]ethyl)aminonaphthalene-1-sulfonic acid
K	lysine
K_D	equilibrium dissociation constant
k_{on}	association rate constant
k_{off}	dissociation rate constant
L	liter
M	methionine
M	molar

min	minutes
mDia	murine protein diaphanous homologue
mM	millimolar
µM	micromolar
nM	nanomolar
ml	milliliter
µl	microliter
nl	nanoliter
µm	micrometer
μm^3	cubic micrometer
ms	milliseconds
ns	nanoseconds
nm	nanometer
PA	profilin-actin
PA-OE	profilin-actin overexpression
Q	glutamine
R	arginine
S	serine
s	seconds
UTRN	Utrophin

2 Abstract & Zusammenfassung

2.1 Abstract

The assembly of actin filaments into different cytoskeletal networks is essential to all eukaryotic cells to maintain their shape and intracellular organization. The actin protein is a major player in very important but complex processes such as contraction, protrusion, endocytosis and motility. Assembly of actin subunits into functional networks requires precise regulation and control over the speed at which actin filaments polymerize. However, eukaryotic cells contain vast but variable amounts of polymerizable actin subunits. It is presently unclear how robust filament assembly can be accomplished at such varying actin monomer concentrations. Actin architectures in vivo are highly dependent on the rate of actin polymerization. In vitro and at sub-physiological monomer concentrations, filament elongation has been reported to scale linearly with the concentrations of available actin monomers. A linear substrate dependency in filament elongation at physiological substrate conditions would translate to corresponding assembly rates and filament lengths as an immediate consequence. In vivo, this would result in changed architectures which might be problematic. It is difficult to conceptualize how cells would set up stereotypic actin networks of invariant architectures to maintain functionality.

To investigate the mechanisms, which might control filament elongation under cell-like conditions, I reconstituted actin assembly in single filament TIRF-M in vitro assays using mammalian cytoplasmic actin at physiologically relevant subunit concentrations. This could be achieved by the use of stoichiometric profilin-actin complexes as a substrate for filament assembly. Profilin prevents the spontaneous nucleation of actin filaments at high concentrations of monomeric actin and profilin-actin is considered the physiological substrate for actin growth. Strikingly, under these conditions we discovered an upper limit to the rate of actin filament assembly. This means that the filament elongation speed becomes insensitive to changes in concentration of polymerizable substrate. By employing profilin mutants with a changed actin binding affinity, we showed that the dissociation of profilin from the filament end constitutes the observed rate-limiting reaction.

In vivo actin filament assembly is regulated through the action of polymerases such as formins. Formins are known to promote filament elongation from profilin-actin. However, since these proteins have previously been studies only at low, non-physiological concentrations, we ask whether they are capable of modulating profilin release as the rate-limiting step in filament elongation. Interestingly, we demonstrate that profilin dissociation from the filament end is directly accelerated by actin polymerases even at saturating substrate concentrations. Under these conditions actin polymerization proceeds with speeds that depend on the type of formin bound to the elongating end.

To probe the physiological relevance of our in vitro results, I expressed fluorescently tagged formin molecules in different mammalian cell types that significantly differ in their profilin-actin levels. The polymerization-driven movement of single formin molecules is used as an indirect readout for actin filament elongation in vivo. Importantly, we demonstrate that actin filament assembly in vivo indeed operates close to the kinetic limits observed in vitro, which are imposed by profilin and formins. Collectively, our results reveal, that profilin and formins synergize to maintain robust actin filament polymerization rates, which are insensitive to changes in the soluble subunit concentration.

2.2 Zusammenfassung

Der Zusammenschluss von Aktinfilamenten zu zytoskeletallen Netzwerken ist ein essenzieller Prozess in allen eukaryotischen Zellen und dient der Aufrechterhaltung von Zellform und intrazellulärer Organisation. Dabei spielt das Aktin Protein eine dominante Rolle in komplexen Prozessen wie Zell-Kontraktion, -Migration, -Endozytose und -Motilität. Der Bau funktionaler Netzwerke aus Aktin-Untereinheiten, sog. Monomeren, erfordert genauste Regulation und Kontrolle der Aktin Polymerisationsgeschwindigkeit. Eukaryotische Zellen enthalten jedoch große und variable Mengen an polymerisierbaren Monomeren. Wie jedoch Zellen eine robuste Aktin Polymerisation unter ständig schwankenden Monomerkonzentrationen aufrechterhalten, ist derzeit nicht geklärt. Aktiarchitekturen in vivo sind stark abhängig von der Geschwindigkeit der Polymerisation. In vitro und unter Bedingungen von sub-physiologischen Monomerkonzentrationen konnte bereits gezeigt werden, dass die Polymerisation von Aktinfilamenten in linearer Abhängigkeit zur Konzentration verfügbarer Monomere steht. Die lineare Substratabhängigkeit in der Polymerisation von Filamenten unter physiologischen Substratkonzentrationen würde jedoch in entsprechenden Polymerisationsraten und Filamentlängen resultieren. In vivo würde ein solcher Effekt Veränderungen in der Architektur ganzer Netzwerke verursachen, die problematisch sein könnten. Es ist schwer zu begreifen, wie es Zellen unter diesen Umständen gelingt Aktin-Netzwerke von invarianter Architektur zu generieren, um Funktionalität aufrechtzuerhalten.

Um die relevanten Mechanismen der Filament-Polymerisation unter physiologischen Bedingungen zu untersuchen, habe ich in dieser Arbeit die Polymerisation von Aktinfilamenten in vitro rekonstruiert. Dabei wurde unter Verwendung von zytoplasmatischen Säuger-Aktin die Polymerisation einzelner Filamente bei physiologisch relevanten Substratkonzentrationen mittels Interner Totalreflexionsfluoreszenzmikroskopie untersucht. Als Substrat habe ich stöchiometrische Komplexe bestehend aus Profilin und Aktin eingesetzt. Profilin verhindert die spontane Nukleation neuer Aktinfilamente in Anwesenheit hoher Monomerkonzentrationen und stellt das physiologische Substrat für Aktin-Polymerisation

dar. Interessanterweise konnten wir unter diesen Bedingungen feststellen, dass die Polymerisation von Aktinfilamenten einen Maximalwert erreicht. Dies bedeutet, dass die Polymerisationsgeschwindigkeit von Aktin stabil gegenüber Änderungen in der Substratkonzentration ist. Weiterhin konnten wir durch die Verwendung von Profilin-Mutanten mit veränderter Bindungsaffinität für Aktin zeigen, dass die Dissoziation von Profilin vom Filament Ende die beobachtete maximale Polymerisationsrate festlegt.

Die Polymerisation von Aktin in vivo wird durch Aktin-Polymerasen wie beispielsweise Formine reguliert. Es ist bekannt das Formine die Polymerisation von Profilin-Aktin begünstigen und beschleunigen. Formine wurden bisher jedoch nur unter niedrigen, nicht physiologisch relevanten Substratkonzentrationen untersucht. Wir stellen daher die Frage, ob Formine ebenso in der Lage sind die Dissoziation von Profilin vom Ende des Aktinfilaments, als Raten-limitierenden Schritt der Aktin-Polymerisation, zu beschleunigen. Interessanterweise können wir zeigen, dass die Profilin-Dissoziation vom Ende des Filaments unter Substratsättigenden Bedingungen durch Aktin-Polymerasen direkt beschleunigt wird. Unter diesen Bedingungen verläuft die Polymerisation von Aktinfilamenten mit Geschwindigkeiten in Abhängigkeit des gebundenen Formin-Typs. Um weiterhin die physiologische Relevanz unserer in vitro Ergebnisse zu untersuchen, exprimierte ich Fluoreszenz-markierte Forminmoleküle in unterschiedlichen Säugerzellen die sich in ihren Profilin-Aktin Mengen signifikant unterscheiden. Die polymerisationsabhängige Bewegung einzelner Forminmoleküle wurde als indirekte Anzeige für die Polymerisation einzelner Aktinfilamente in vivo verwendet. Wir konnten zeigen, dass die Polymerisation von Aktinfilamenten in vivo tatsächlich sehr nahe an den in vitro beobachteten kinetischen Polymerisationsraten liegt die durch Profilin und Formine festgelegt sind. Zusammengenommen zeigen unsere Ergebnisse, dass Profilin und Formine gemeinsam zu einer robusten Polymerisationskinetik von Aktinfilamenten beitragen die stabil gegenüber Änderungen in der Substratkonzentration ist.

3 Introduction

Actin is one of the most abundant proteins in nearly all eukaryotic cells. Actins key cellular function originates from its ability to reversibly and rapidly polymerize into double helical filaments. These filaments constitute the functional units that build a large variety of higher order structures, which are in turn fundamentally important for numerous essential cellular processes such as morphogenesis and motility (Pollard and Cooper, 1984). Vertebrates express three distinct actin isoforms: α-actin found only in muscle cells and β/γ-actin found in both non-muscle and muscle cells alike. These isoforms are very similar and differ mainly in their N-terminus (Herman, 1993). The actin monomer folds into four subdomains (Figure 1): subdomain 1 and 3 are structurally related and have been suggested to emerge from gene duplication, while subdomains 2 and 4 insert into subdomains 1 and 3 respectively. The actin monomer has two central clefts (upper and lower): the base of the upper cleft (between subdomains 2 and 4) binds the nucleotide and a nucleotide-associated divalent cation, while the lower cleft (between subdomains 1 and 3) is predominantly hydrophobic and mediates major longitudinal contacts between actin monomers bound in a filament (Fujii et al., 2010; Oda et al., 2009). The latter cleft also provides the main binding sites for many actin binding proteins such as profilin or WH2(WASP homology 2 domain)-motif containing proteins (Carlier et al., 2011; Dominguez, 2004, 2010).

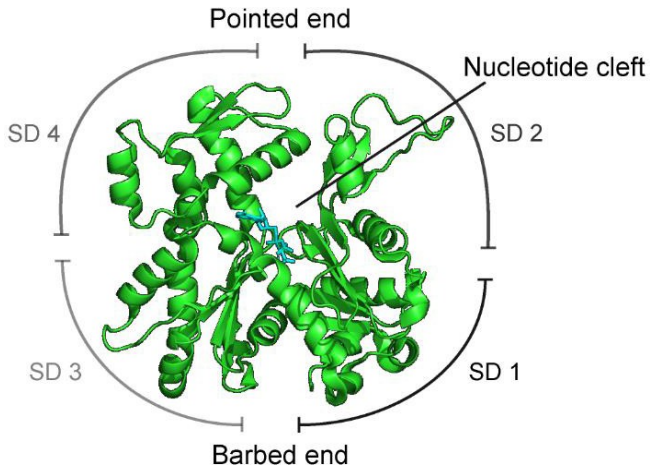

Figure 1: Architecture of the actin monomer. The actin monomer (green) consists of four subdomains 1-4 (SD) with a central nucleotide cleft which binds the nucleotide (cyan) together with an associated divalent cation (modified from PDB:5OOD, (Merino et al., 2018)).

3.1 The nucleation of actin filaments

The basic unit of the double stranded helical actin filament is the actin monomer (Holmes et al., 1990; Kabsch et al., 1990). The assembly of actin monomers into filaments first requires actin filament nucleation. Nucleation of actin describes the generation of a new actin filament built from monomers that orient in a head-to-tail manner. However, the spontaneous nucleation of actin filaments is kinetically unfavorable, because the filament precursors, such as actin dimers, are highly unstable (Figure 2). The kinetic equilibrium constants for the formation of these intermediates have been estimated from in vitro polymerization assays and kinetic simulations (Pollard and Cooper, 1986) to values of 0.1 mM for actin dimers and 0.01 - 0.1 mM for actin trimers (Sept and McCammon, 2001).

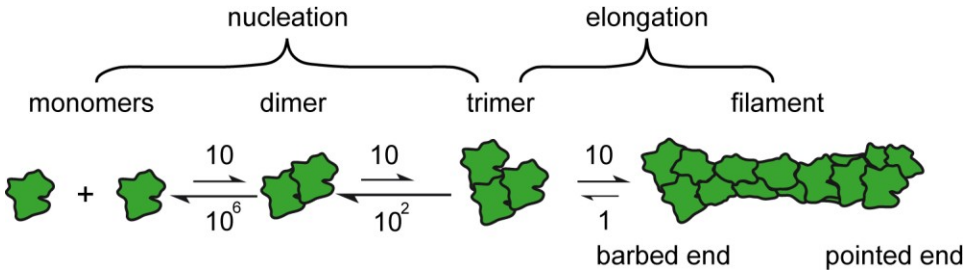

Figure 2: Spontaneous actin filament nucleation and elongation. Actin monomer-to-filament transition: the spontaneous assembly of actin dimers is kinetically unfavorable. Actin dimers are unstable. The association rate constants [$\mu M^{-1}s^{-1}$] and the dissociation rate constants [s^{-1}] are indicated with errors. Once actin trimers are generated, actin polymerization proceeds rapidly from the barbed end. Figure modified from (Pollard and Cooper, 2009).

The nucleation reaction can be promoted by other actin binding proteins such as Arp2/3 or WH2-containing nucleators, which lower the kinetic barrier to nucleation (Kerkhoff, 2006; Renault et al., 2008). These proteins nucleate filaments by distinct molecular mechanisms: While the Arp2/3 complex is generating branched actin networks by binding and nucleating new filament from the site of pre-existing filaments (Amann and Pollard, 2001), linear filaments are generated de novo by either WH2-nucleators from their pointed ends or by formins from their barbed ends (Dominguez, 2016). Importantly, once actin trimers are generated actin filaments rapidly elongate through the addition of actin monomers to the ends of the filaments. However, the two filament ends differ

strongly in their polymerization kinetics (Pollard, 1986b) with the barbed end being much more dynamic than the pointed end (see section 3.3).

3.2 The elongation of actin filaments

Actin filament elongation has been characterized in biochemical reconstitution assays using purified actin over the past decades. The elongation of filaments from ATP-bound monomers is a fast, bimolecular reaction which is thought to be diffusion-limited (Drenckhahn and Pollard, 1986). The thermodynamic balance point of polymerization and depolymerization is described by the critical concentration (C_c). The C_c of actin is calculated from the ratio of the dissociation rate constant to the association rate constant. Under in vitro conditions, the C_c of ATP-bound actin monomers is known to be sub-micromolar.

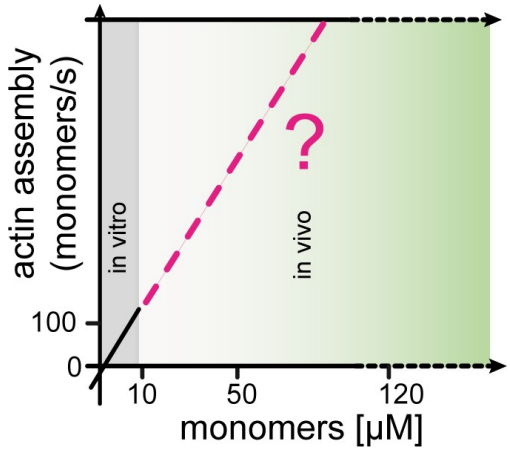

Figure 3: Actin filament assembly and disassembly. Linear dependence of actin assembly from the concentration of actin monomers. Under polymerizing conditions, the monomer concentration has to exceed the critical monomer concentration to start the elongation of filaments. Linear substrate dependence on elongation was only shown for low non-physiological monomer concentrations (≤ 10 µM) (Drenckhahn and Pollard, 1986). Whether the speed of actin assembly is only dependent on the concentration of polymerizable actin subunits at high, in vivo relevant monomer levels, is presently not known.

The diffusional encounter between ends and monomers occurs more frequently when the concentration of monomers rises, which is why the speed of filament assembly has been shown to linearly accelerate with increasing substrate concentrations (Figure 3). Thus the filament elongation rates over a limiting range of substrate concentrations can

be fit with a linear model originally formulated by Oosawa (Oosawa and Asakura, 1975; Pollard, 1986a). The strong, linear dependence of the filament elongation rate on the substrate concentration has become the basis for quantitative models of actin dynamics (Carlier and Shekhar, 2017; Carlsson, 2010). A central drawback, however, is that filament assembly has only been studied for very low, non-physiological substrate concentrations until now.

3.3 Actin filament polarity

The major fraction of the monomer pool in vivo is bound to ATP (Rosenblatt et al., 1995). Given the high physiological Mg^{2+} (millimolar) and the low Ca^{2+} (nanomolar) concentration in the cytoplasm, actin monomers are likely bound to Mg^{2+} rather than to Ca^{2+}, which means that most monomers should be readily polymerizable in the absence of additional regulatory mechanisms (see below). Polymerization of actin filaments from ATP bound monomers is followed by nucleotide hydrolysis. This reaction occurs in two consecutive steps: 1. Fast hydrolysis of ATP to ADP + P_i at a rate of 0.3 s^{-1} followed by 2. Slow dissociation of the inorganic phosphate at a rate of 0.002 s^{-1} (Blanchoin and Pollard, 1999, 2002; Melki et al., 1996) (Figure 4). As a result, most of the aged filament consists of ADP-bound subunits (and ADP + P_i), while ATP-actin is only expected at the filament ends. ATP hydrolysis and the release of phosphate result in actin subunits that are bound to nucleotides in different states along the filament. These different nucleotide states are acting as a molecular timer to coordinate actin network disassembly in space and time. Changes in nucleotide state are essential to many actin binding proteins such proteins involved in disassembly, such as cofilin, to bind to filaments, thereby acting as a readout for the filament age. The actin nucleotide content is used by such proteins to selectively disassemble filaments into monomers or short fragments and thus destabilize whole networks to maintain a constant pool of actin subunits ready for polymerization (Merino et al., 2019).

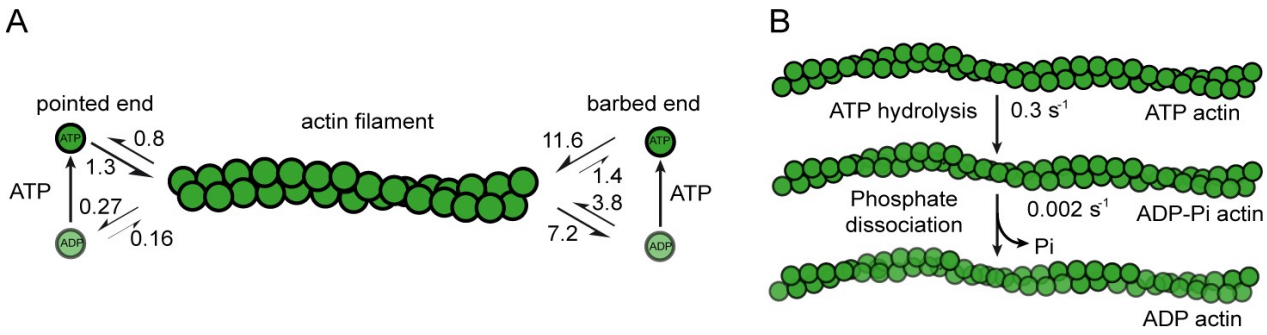

Figure 4: Actin kinetics. A. Rate constants for actin filament elongation from monomers bound to different nucleotides at both ends (Fujiwara et al., 2007; Pollard, 1986b). The unit of the monomer association rate constants is $\mu M^{-1} s^{-1}$. The unit of the monomer dissociation rate constants is s^{-1}. B. Rates for ATP hydrolysis (fast) and γ-phosphate dissociation (slow) after actin polymerization. (Figures modified from (Pollard and Borisy, 2003)).

The polarity of actin filaments manifests kinetically in the difference of monomer addition rates to either filament end. One of the filament ends (barbed end) polymerizes around 10 times faster from ATP-bound monomers than the opposite end (pointed end) (Pollard, 1986a). The difference in actin barbed and pointed end filament elongation rates results in different C_c values at the two ends: 0.1 μM for barbed end and 0.8 μM for pointed end for ATP-bound actin (Kinosian et al., 1993; Pollard, 1986b). Since the critical concentration of the two filament ends are different, filament ends polymerize much faster from their barbed end and depolymerize faster from their pointed end. At steady state, this results in actin dynamics where substrate concentrations are maintained between the C_c of the two ends. Hence filaments of non-changing length are maintained through continuous subunit addition at the barbed end and subunit disassembly at the pointed end, a mechanism which has been reported as “actin treadmilling” (Carlier and Shekhar, 2017).

Currently we do not understand why the addition of monomers onto the pointed end is much slower than the diffusion limit (Pollard, 1986b). It has been suggested that the electrostatic protein interactions are less favorable for monomers to bind to the pointed end (Sept et al., 1999). Furthermore, the conformation of both filament ends might be differently conducive for monomer addition (Courtemanche and Pollard, 2013). Importantly, the differences in the critical concentrations for barbed and pointed filament ends is likely insignificant when considering the actin monomer concentrations found in

living cells (Koestler et al., 2009; Raz-Ben Aroush et al., 2017; Skruber et al., 2018). Because know that cells maintain soluble subunit concentrations orders of magnitude away from the equilibrium critical concentration of either end, the “actin treadmilling” effect (Carlier and Shekhar, 2017) cannot explain actin dynamics in vivo.

Profilin is the dominant monomer binding protein (see section 3.4.1) in vivo, which likely prevents filament elongation from the pointed end, because profilin-actin complexes cannot contact the exposed pointed end face of terminal protomers (Schutt et al., 1993; Vinson et al., 1998). Despite being the only locations of assembly and disassembly, very little is known about the structures of actin filament ends. Up to this point, multiple structures of actin subunits from the internal filament have been solved (Fujii et al., 2010; Galkin et al., 2010; Merino et al., 2018; Oda et al., 2009; Pospich et al., 2017). However, there is only a single structure of the filament pointed end at low (23 Å) resolution available until now (Narita et al., 2011), which indicated the terminal actin in a conformation incompatible with filament assembly. Whether this might account for the slow pointed end assembly kinetics remains to be determined.

3.4 Two major actin monomer binding proteins which control the monomer pool of actin

Cells contain hundreds of distinct proteins that are involved in the regulation of actin dynamics (Paavilainen et al., 2004). These proteins have diverse functions such as regulating or promoting actin filament nucleation and elongation, the termination of filament elongation, filament cross-linking or severing of filaments. The collective biochemical activities of some of these actin interacting proteins are required to maintain the large concentrations of polymerizable actin subunits (Koestler et al., 2009; Pollard et al., 2000; Raz-Ben Aroush et al., 2017; Skruber et al., 2018), which are in turn essential to rapidly assemble actin filaments. In vertebrate cells, there are two major actin monomer binding proteins, profilin and thymosin-β_4, and both contribute to prevent spontaneous actin monomer self-assembly, which would result in the uncontrolled nucleation of new actin filaments. Interestingly, the mechanism by which these two proteins act is profoundly different and will be described in the following sub-sections.

3.4.1 Profilin

Profilin is a small (~ 15 kDa) protein which constitutes the major actin monomer binding protein in all eukaryotic cells. Profilin concentration found in vivo are ranging between 5 – 100 µM depending on the cell type (Pollard et al., 2000). Profilin shows several important actin-related functions which allow for a central role in actin assembly (dos Remedios et al., 2003):

i) Profilin interacts with actin at the barbed end face of the actin monomer (Schutt et al., 1993) (Figure 5). This prevents the actin monomer from partitioning in spontaneous nucleation of new filaments and at the same time it inhibits the elongation of filaments from their pointed ends (Pantaloni and Carlier, 1993; Pollard and Cooper, 1984; Pring et al., 1992). Therefore, profilin-actin complexes can exist at very high concentration in vitro and in vivo in contrast to free actin monomers.

Figure 5: Structure of the actin-profilin complex. Structure of B. Taurus actin (green) and profilin (magenta). The ATP nucleotide and its associated divalent cation are shown in cyan. PDB code: 2BTF (modified from (Schutt et al., 1993)).

ii) Profilin has been shown to catalyze the nucleotide exchange of ADP for ATP in the actin monomer (Korenbaum et al., 1998). However, whether profilin or other abundant actin binding proteins such as CAP (Jansen et al., 2014) are dominant nucleotide exchange factors for actin in vivo is presently not known. Regardless of the activities involved, it is generally believed that the pool of ATP bound actin monomers is replenished very quickly (Rosenblatt et al., 1995).

iii) The binding affinity of profilin for non-muscle ATP-bound actin monomers is very high (K_D = 0.1 µM) (Vinson et al., 1998), whereas profilin binding affinities for muscle ATP-actin and ADP-bound monomers are considerably lower (K_D = 0.5 µM each) (Perelroizen et al., 1996; Vinson et al., 1998). Owing to its high monomer binding affinity for ATP-actin monomers, profilin effectively competes with other monomer binding proteins that overlap with its binding site such as thymosin-β_4. Thus the majority of polymerizable actin in vivo is bound to profilin in a stoichiometric complex (Kaiser et al., 1999; Pantaloni and Carlier, 1993; Rotty et al., 2015; Witke et al., 2001).

iv) Profilin does not only bind to actin. Instead, it can simultaneously bind to proline-rich sequences of other essential actin regulators such as formins in a ternary complex (Ferron et al., 2007). Long, unstructured stretches of proline-rich sequences are often found in actin regulating proteins and are thought to funnel profilin-actin complexes to processes such as elongation and nucleation these proteins promote (Kovar et al., 2006).

Importantly, profilin-actin complexes participate in actin elongation by binding to an exposed filament barbed end with nearly the same rate as free actin monomers (Kinosian et al., 2002; Pollard and Cooper, 1984; Pring et al., 1992). Profilin is therefore considered to act as the major protein (in synergy with thymosin-β_4, see below) which maintains a metastable pool of polymerizable actin subunits ready to elongate free filament barbed ends in vivo (Kaiser et al., 1999; Pantaloni and Carlier, 1993; Pollard et al., 2000). Importantly, the terminal actin filament subunits likely expose binding sites for profilin. How profilin is interacting with the actin filament barbed ends has never been shown by direct structure determination and is therefore still not entirely understood (Yarmola and Bubb, 2006). To continue elongation, profilin has to rapidly dissociate from the filament end. Interestingly, the profilin binding sites at either free actin monomers or terminal filament subunits cannot be equivalent. This can be inferred from the very different profilin-binding affinities for monomers (K_D = 0.1 µM) (Vinson et al., 1998) compared to filament barbed ends (K_D = 20 - 226 µM) (Courtemanche and Pollard, 2013; Pernier et al., 2016). The transition between these two actin configurations is likely co-committed with the filament polymerization.

Studies on profilin revealed that the nature of the nucleotide, which is bound to the terminal actin subunits, dramatically changes the affinities of profilin for the barbed end. Opposite to the effects of nucleotide state changes within actin monomers, the profilin binding affinity for actin filament barbed ends bound to ADP is much higher (K_D = ~ 1 µM) compared to AMP-PNP (non-hydrolysable analogue of ATP) bound filament barbed ends (K_D = 20 - 226 µM) (Courtemanche and Pollard, 2013; Pernier et al., 2016). This suggest that the conformational changes upon ATP hydrolysis and the release of phosphate are different between actin monomers and the subunits of the filament barbed end (Courtemanche and Pollard, 2013; Jegou et al., 2013). However, changes in nucleotide state at the growing filament end are unlikely of physiological relevance. The rate constants for actin ATP hydrolysis and phosphate release determined (Blanchoin and Pollard, 1999, 2002; Melki et al., 1996) are in the regime of seconds to minutes (see section 3.3), much slower than realistic in vivo growth rates. At physiological actin monomer concentrations it is therefore very unlikely that filament barbed ends are found in the ADP-state during the process of polymerization in vivo. There are only a few conceivable cases, such as during filament severing, in which exposed actin barbed ends are likely found in the ADP-state (Bamburg et al., 1980; Nishida et al., 1984). Up to this point, it is unknown whether such barbed ends might be prevented from further elongation because they might be bound tightly by profilin.

The linear dependence of the substrate concentration on the actin filament elongation speed (Drenckhahn and Pollard, 1986) creates several conceptual issues: 1) the subunit addition from profilin-actin onto the filament barbed end requires multiple steps which should not depend on the concentration of free subunits. After profilin-actin has bound to the filament barbed end, profilin has to first dissociate from the terminal subunit to continue elongation since it partially overlaps with the binding site for a new monomer to incorporate into the filament (Courtemanche and Pollard, 2013; Pernier et al., 2016; Pollard and Cooper, 1984). Currently, it is not known how rapidly profilin dissociates from the filament end and whether it changes the dynamics of filament elongation (Blanchoin and Pollard, 2002; Gutsche-Perelroizen et al., 1999; Romero et al., 2004). This question becomes especially important at high profilin-actin concentrations that can be found inside cells and/or in presence of actin polymerases (see section 3.5) when the

addition of new actin subunits becomes very fast. 2) The amount of polymerizable actin subunits varies across eukaryotic cell-types (Koestler et al., 2009; Pollard et al., 2000; Raz-Ben Aroush et al., 2017). Filaments would elongate with significantly different rates among different cell-types if the rate of subunit incorporation would scale linearly with the concentration of available substrate. Importantly, cells contain many different actin networks and their architectures depend on the growth speed by which their filaments elongate. If the actin substrate concentration varies by 2-3 fold among or within cells, the organization of actin architectures can be anticipated to be perturbed due to strongly varying filament lengths which correspond to the level of polymerizable subunits. Adaptations in the actin network organization could then only be anticipated through the action of other actin accessory proteins which are able to tune filament assembly and disassembly rates accordingly.

3.4.2 Thymosin-β4

Thymosin-β4 is a small (5 kDa) peptide (Safer and Nachmias, 1994) which sterically blocks both barbed and pointed end binding sites of actin monomers and thus prevents filament polymerization (Carlier et al., 1993; Yarmola and Bubb, 2004). Part of the thymosin-β4 binding sites overlaps with profilin, which is why these proteins compete for binding of actin monomers (Figure 6) (Safer et al., 1997; Schutt et al., 1993).

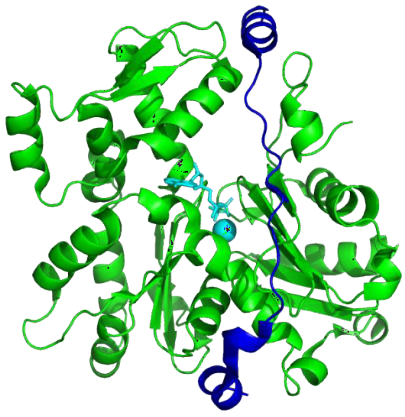

Figure 6: Structure of the actin-thymosin-β4 complex. Structure of K. pastoris actin monomer (green) (Uniprot no. Q9P4D1) bound to human thymosin-β4 (blue) (Uniprot no. P62328). The ATP nucleotide and its associated divalent cation are shown in cyan. PDB code: 4PL7 (modified from (Xue et al., 2014))

Importantly, thymosin-β4 binds much weaker to ATP – actin (K_D = 1.6 µM) compared to profilin (K_D = 0.1 µM) (Pantaloni and Carlier, 1993; Pollard and Cooper, 1984; Vinson et al., 1998). Since thymosin-β4 is a true sequestering protein, actin monomers that are bound to thymosin-β4 are considered as a non-polymerizing monomer reservoir. The concentration of thymosin-β4 in vivo is reported to be between 20 and 550 µM (Barkalow and Hartwig, 1995; Hartwig, 1992; Pollard et al., 2000) and is therefore considered to bind a large fraction of the amount of non-polymerized actin. The reservoir of actin monomers bound to thymosin-β4 can be mobilized for filament growth by rapid exchange with profilin. Upon the polymerization of actin monomers bound to profilin, free profilin competes with thymosin-β4 for ATP-bound actin subunits (Pantaloni and Carlier, 1993; Pollard and Cooper, 1984).

3.5 Actin polymerases

In vivo actin filament elongation is believed to proceed either passively through association of profilin-actin complexes or is actively catalyzed by specific actin polymerases (Chesarone and Goode, 2009; Kovar et al., 2006; Romero et al., 2004). Up to this point, two major protein classes, formin and Ena/VASP proteins, have been described to modulate actin filament elongation. Both protein families catalyze the elongation of filaments from their barbed ends in a processive manner (Alberts, 2001; Kovar and Pollard, 2004; Li and Higgs, 2003; Paul and Pollard, 2008; Pruyne et al., 2002).

3.5.1 Formins

Especially the large formin family, which consists of 15 family members in humans, is essential for many different processes in vivo such as the assembly of different actin structures including filopodia, stress fibers or actin cables in the contractile cytokinetic ring (Faix and Grosse, 2006; Goode and Eck, 2007; Skau and Waterman, 2015). Formins are large multi-domain proteins that share important characteristic features such as the presence of formin homology domains 1 and 2 (Chesarone et al., 2010; Schonichen and Geyer, 2010) which are described in the following sections.

3.5.1.1 The formin homology domain 2 (FH2)

The FH2 domain is the region of highest sequence homology (~25 %) between different formin proteins (Castrillon and Wasserman, 1994) and thus constitutes the defining element of this protein family. The FH2 domain forms a stable, dimeric ring-like structure (Figure 7) (Harris et al., 2004; Moseley et al., 2004). The FH2 ring can nucleate actin filaments in presence of free actin monomers (Pring et al., 2003), or bind processively to the barbed end of existing filaments as it elongates (Kovar and Pollard, 2004; Paul and Pollard, 2008; Pruyne et al., 2002). Previous studies (Kovar et al., 2006; Otomo et al., 2005b; Vavylonis et al., 2006) suggest that the formin FH2 domain bound to the filament end can be in an open or closed configuration (gating, see 3.5.1.2). In combination with the FH1 domain (see 3.5.1.3), formins accelerate the filament barbed end elongation rate (Chesarone and Goode, 2009; Kovar et al., 2006; Romero et al., 2004).

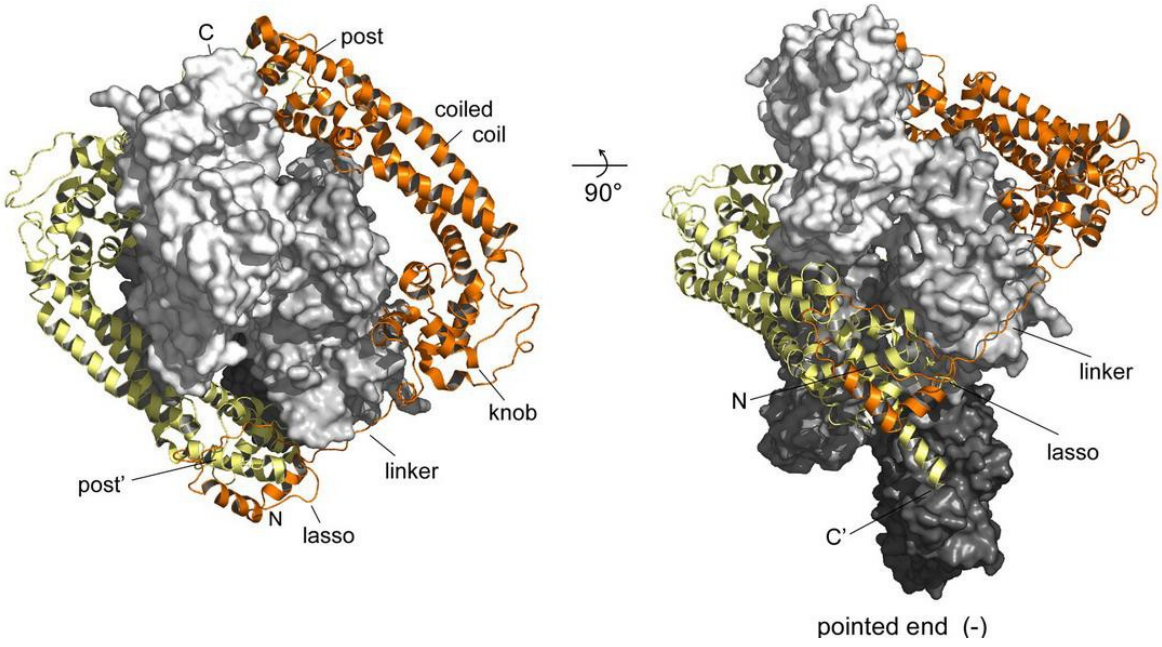

Figure 7: The structure of the FH2 domain. Crystal structure of Bni1 FH2 dimer (yellow and orange) bound to TMR-actin (grey) in a head-to-tail configuration (PDB code: 1Y64) (Otomo et al., 2005b). Image taken from (Schonichen and Geyer, 2010).

Up to this point, only limited structural information of isolated FH2 domain exists (Lu et al., 2007; Otomo et al., 2005b; Shimada et al., 2004; Xu et al., 2004; Yamashita et al., 2007). A FH2 structure, when bound to the filament barbed end, has not been determined yet. Most structural information was gained from FH2 (Bni1, Figure 7)

complexed with actin monomers or from their free states (Otomo et al., 2005b). These structures reveal that two FH2 domains dimerize into an anti-parallel head-to-tail configuration by their N-terminal lasso and C-terminal post regions (Castrillon and Wasserman, 1994). Highly conserved residues in the knob (I1431 in Bni1) and the post (K1601 in Bni1) region mediate the interaction with actin (Lu et al., 2007; Otomo et al., 2005b; Xu et al., 2004).

3.5.1.2 The stepping mechanism of formins

Formins possessively track elongating filament barbed ends. The FH2 domain binds the barbed end with pM affinity and thus stays attached for the assembly of thousands of actin monomers until it dissociates (Breitsprecher et al., 2012; Kovar et al., 2006; Neidt et al., 2008). Molecular dynamics simulations (Baker et al., 2015), biochemical assays (Kovar et al., 2006; Paul and Pollard, 2008; Vavylonis et al., 2006) and structural analysis (Otomo et al., 2005b) discuss potential conformational changes in the terminal barbed end subunits upon FH2 binding. The formin barbed end tracking mechanism is suggested to operate by rapidly alternating contacts of the two FH2 domains with the ultimate and penultimate actin subunits. It is believed that these FH2 alternating movements fluctuate between an open state, allowing for actin monomer addition, and a closed state which prevents monomer addition onto the filament barbed end (Kovar et al., 2006; Moseley et al., 2004; Otomo et al., 2005b; Romero et al., 2004; Zigmond et al., 2003). Actin in absence of formins is constantly in the open state. However, the equilibrium is biased towards the closed state by the binding of FH2 domains. Interestingly, the time formins spend in one or the other state, known as gating factor (Paul and Pollard, 2009), varies dramatically among different formins (from ≤ 5 % for Cdc12 to ≥ 95 % for mDia1) (Kovar et al., 2006; Neidt et al., 2008). However, it is not clear which formin and actin structures or formin gating states are sampled in which order for formins to follow the polymerizing actin barbed end. Up to this point, multiple formin stepping mechanisms on actin filaments have been suggested based on biochemical data. Importantly, none of the described formin states has been directly visualized at filament barbed ends so far.

3.5.1.3 The formin homology domain 1 (FH1)

In contrast to the FH2 domain, the FH1 domain is unstructured and composed of multiple poly-proline stretches. The number and length of poly-proline repeats differs among different formins (Kovar et al., 2006; Kovar et al., 2003; Romero et al., 2004). A requirement to accelerate barbed end elongation is the association of profilin-actin complexes to the poly-proline repeats of the flexible FH1 domains (Chang et al., 1997; Imamura et al., 1997; Watanabe et al., 1997). It is thought that the actin polymerase activity of formins arises from their ability to recruit profilin-actin complexes through their FH1 domains to the immediate vicinity of the barbed end and thereby enhance the frequency of productive encounters (≥ 1000/s) between profilin-actin and the terminal subunits of the filament barbed end (Figure 8) (Chesarone and Goode, 2009; Courtemanche, 2018; Kovar et al., 2006; Paul and Pollard, 2008; Vavylonis et al., 2006).

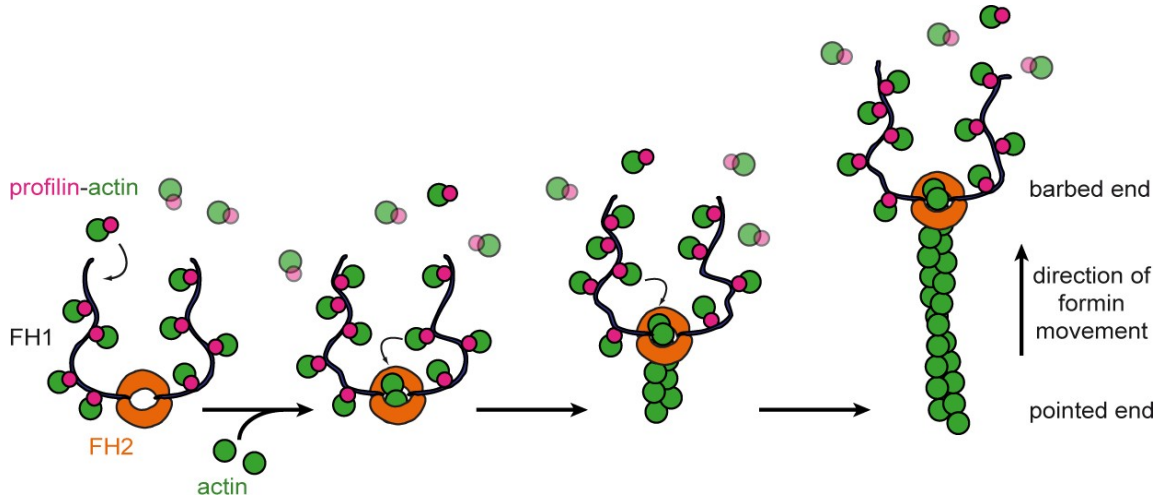

Figure 8: The function of the FH1 domain. Formin mediated elongation of actin filaments from profilin-actin complexes. First actin filaments are nucleated from free actin monomers by an FH2 dimer. Filament nucleation is followed by elongation. During elongation, multiple profilin-actin complexes bind to multiple sites on the unstructured FH1 domains. The FH1 domains rapidly transfer profilin-actin to the filament barbed end. Figure modified from (Pollard, 2007).

Through this mechanism, filament elongation rates can drastically exceed the diffusion - limited association rate of free actin monomers onto the filament barbed end (Kovar et al., 2006; Vavylonis et al., 2006). Thus, it is thought that the rate-limiting step for formin-mediated polymerization is determined by the association rate of the profilin-actin complex onto the poly-proline region in the FH1 domain. Whether, however, formin-

mediated filament assembly in vivo is controlled at the level of profilin-actin binding, is not known.

3.5.1.4 Other formin regulatory domains

The activity of formins is tightly regulated in time and space. Formins are autoinhibited actin polymerases that are only locally activated, most often in response to membrane-associated signals in vivo. These signals are typically small GTPases as well as specific phospholipids such as phosphatidylinositols (PtdIns) that are only found in specific membrane locations inside cells (Ramalingam et al., 2010; van Gisbergen et al., 2012). Previous studies on mDia1 (Ramalingam et al., 2010) show that mDia1 phospholipid-binding sites are positively charged residues in the N-terminus (basic domain) and in the C-terminal region which electrostatically interact with phosphatidylinositol-4, 5-biphosphate (PIP2) which for instance is located at cellular protrusion sites. For mDia1, first the N-terminal basic residues induce clustering of PIP2 followed by the insertion and anchoring of the formin molecule through subsequent lipid interaction at the C-terminus.

In addition of formins anchoring to membranes, diaphanous-type formins (which are the primary focus of this work) are released from auto-inhibition through active Rho-GTPases (Evangelista et al., 1997; Nakano et al., 2002; Watanabe et al., 1997). Domains which regulate formin activity are the diaphanous inhibitory domain (DID) and the diaphanous autoregulatory domain (DAD) (Alberts, 2001; Li and Higgs, 2003; Otomo et al., 2005b; Rose et al., 2005). The DID is recognized and bound by the C-terminal located DAD resulting in the auto-inhibition of formin activity. GTPases can facilitate the displacement of the DAD from its DID recognition site to release intramolecular auto-inhibition when binding to the N-terminal located GTPase binding domain (GBD) (Alberts, 2001; Li and Higgs, 2003). The DAD release induces a conformational change, which is thought to result in higher FH2 dimer flexibility allowing actin binding. Importantly, the sequence of the GBD (Figure 9) (Otomo et al., 2005a; Rose et al., 2005) as well as the phospholipid interaction sites are highly variable among different formin types (Ramalingam et al., 2010; van Gisbergen et al., 2012).

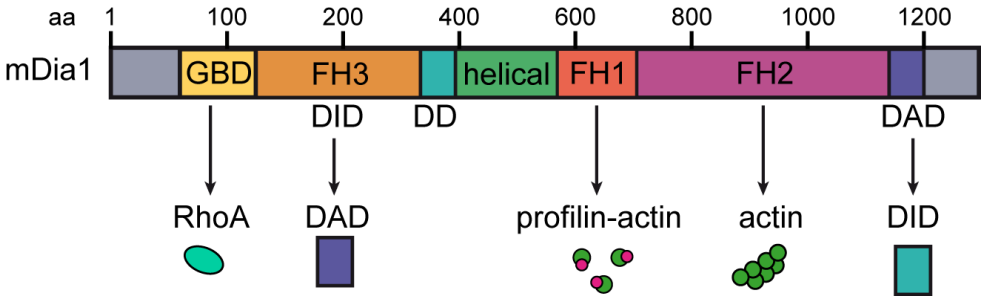

Figure 9: Molecular domains of the mDia1 formin. From N-to-C terminus: GBD – GTPase binding domain which binds RhoA, DID – diaphanous inhibitory domain which binds the C-terminal DAD, DD – dimerization domain, FH1 – formin homology 1 domain which binds profilin-actin complexes, FH2 – formin homology 2 domain which binds to actin and the DAD – diaphanous autoregulatory domain which binds to the DID. aa – amino acids modified from (Schonichen and Geyer, 2010).

In addition to the nucleation and elongation function, other formins show secondary functions including filament bundling, severing or microtubule binding (Harris et al., 2010; Harris et al., 2004; Henty-Ridilla et al., 2016; Moseley and Goode, 2005). Interestingly, the strength by which formins promote actin filament nucleation and elongation varies a lot which may serve different requirements in vivo (Neidt et al., 2008; Vaillant et al., 2008).

4 Objectives

In all eukaryotic cells, actin filament dynamics are crucial for many different processes such as polarity and motility. A common requirement to all actin-driven processes is the growth of actin filaments from soluble monomers. In vivo, the amount of the available monomer substrate for filament assembly is highly variable, not only among different organisms but also between specific cell types and likely even within specific locations inside a cell. It is currently unclear how filament assembly is controlled at these largely varying substrate levels. Because actin polymerization has been considered as being limited by substrate diffusion, one should expect largely varying filament growth rates in vivo.

Importantly, due to technical limitations, actin filament growth has never been studied under physiologically relevant substrate conditions in vitro until now. Therefore, I developed new strategies to follow filament elongation over the full range of physiological subunit levels, which was previously inaccessible. We monitor filament assembly by using total internal reflection fluorescence microscopy (TIRF-M), offering superior optical sectioning compared to other light microscopy methods. To further improve the signal-to-noise ratio, I employed fluorescently labeled filament binding probes, which selectively bind to actin in its filamentous but not in its monomeric form. Previous studies on actin assembly were often limited by spontaneous filament nucleation, which increasingly occurs at increasing amounts of free actin subunits. To prevent spontaneous nucleation we use stoichiometric complexes of profilin and actin as a substrate for filament polymerization. These major improvements enables us for the first time to follow actin elongation at physiologically relevant substrate levels. We investigate whether under these cell-like conditions actin elongation is either limited by the diffusional encounter of profilin-actin complexes to filament end or, alternatively, by another reaction within the elongation cycle.

Following the incorporation of the soluble profilin-actin complex, profilin is bound to the terminal subunit and sterically blocks the filament end for the next monomer to bind. Therefore, profilin first has to dissociate from the end to complete one round of polymerization. We ask whether the release of profilin from the terminal filament subunit constitutes the rate-limiting step in actin assembly. To this end, we design several

affinity perturbed profilin mutants, which we incorporate into our TIRF-M single filament experiments. A change in the maximum filament assembly rate would provide evidence for profilin dissociation being the rate-limiting reaction.

Actin hydrolyzes ATP upon polymerization and profilin dissociation from the filament end has been suggested to require ATP-hydrolysis of the terminal actin subunit (Pernier et al., 2016; Romero et al., 2004). To investigate whether ATP-hydrolysis of the terminal filament subunit controls profilin dissociation, we perform polymerization experiments using a non-hydrolysable actin mutant. If actin ATP-hydrolysis is indeed required for profilin to dissociate from the filament end, we expect that the non-hydrolysable actin to entirely prevent actin assembly from profilin-actin. Similar arguments have previously been made based on experiments employing non- or slowly-hydrolysable ATP analogs.

In vivo, actin polymerization is often facilitated by the action of actin polymerases such as formins. These proteins are thought to increase the binding-rate of profilin-actin to filament barbed ends. However, whether actin polymerases function when the concentration of polymerizable actin is no longer limiting, is presently unclear. To address this question, we introduce different formin proteins into our polymerization assays. To further investigate how our in vitro results on formin-mediated filament polymerization translate to the situation inside living cells, we finally introduce these formin constructs into various mammalian cells, which contain various amounts of profilin-actin. The expression of fluorescently-tagged formin constructs enables us to generate an indirect readout of actin assembly in vivo. The combination of filament polymerization assays in vitro and in vivo allow us to explore how actin binding proteins such as profilin and formins synergize to establish robust actin dynamics at various substrate levels.

5 Materials and Methods

5.1 Materials

5.1.1 Chemicals and Reagents

Substance	Identifier
ATP	Sigma-Aldrich
α-Biotinyl-ω-amino PEG, #133000-25-20	Rapp-polymere
α-Hydroxy-ω-amino PEG, #103000-20	Rapp-polymere
Fibronectin	Sigma-Aldrich
γ–^{32}P–ATP (3000 Ci/mmol)	PerkinElmer
Hellmanex cleaning solution	Hellma, Mühlheim
JASP	Biomol
Latrunculin B	Abcam
Methylcellulose 400PG	Sigma-Aldrich
PDMS	SYLGARD
Phalloidin	Thermo Fisher
Phalloidin-biotin	Thermo Fisher
Phalloidin Alexa647	Thermo Fisher
Pluronic F127	Sigma-Aldrich
Sodium acide	Sigma-Aldrich
TCEP	Sigma-Aldrich
Y27632	Sigma Aldrich

Generally used chemicals have been purchased from Sigma-Aldrich, Merck, AppliChem unless otherwise indicated.

5.1.2 Enzymes and Proteins

Enzyme/Protein	Identifier
AccuPrime *Pfx* DNA polymerase	Invitrogen™ Life Technologies
DNaseI	Sigma Aldrich
Pfu Ultra HF polymerase	Agilent

Precision protease	homemade, Bieling lab
Q5 HF DNA polymerase	New England Biolabs
Restriction enzymes	New England Biolabs
Streptavidin	Sigma-Aldrich
TEV protease	homemade, Bieling lab

5.1.3 Antibodies

Primary antibodies	Identifier
mouse anti – actin	Thermo Fisher
mouse anti – profilin1	Sigma Aldrich
mouse anti – profilin2	Santa Cruz
rabbit anti – GAPDH(14C10)	Cell Signaling

Secondary antibodies	Identifier
IRDye 800CW donkey anti-mouse IgG	LI-COR Biosciences
IRDye 680RD donkey anti-rabbit IgG	LI-COR Biosciences

5.1.4 Commercial Solutions and Kits

100 mM dNTPs	New England Biolabs
2-log ladder	New England Biolabs
Precision Plus Protein Dual color Standards	Bio-RAD
FuGENE HD Transfection Reagent	Promega
Lipofectamine Transfection Reagent	Invitrogen
NucleoBond Xtra Midi Plus EF	Macherey-Nagel
Roti-Prep Plasmid MINI	Carl Roth
Zymoclean Gel DNA Recovery Kit	Zymo Research

5.1.5 Buffers and Solutions

Buffer/Solution	Composition or Identifier
100x BufferA	200 mM Tris 10 mM $CaCl_2$ 20 mM ATP 1 % NaN_3 50 mM TCEP
DMEM	PAN^{TM}Biotech
DNA sample buffer	50 % (v/v) glycerol 0.1 % Orange F 100 mM EDTA
DPBS	PAN^{TM}Biotech
Eagles medium	PAN^{TM}Biotech
Fetal bovine serum (FBS)	PAN^{TM}Biotech
Gibson assembly mix	1x ISO buffer 5.3 µU/ml T5 exonuclease 33 µU/ml Phusion DNA polymerase 5.3 U/ml Taq DNA ligase
200 mM L-Glutamine	PAN^{TM}Biotech
HBSS	PAN^{TM}Biotech

5x ISO buffer	200 mM Tris-HCL pH7.5 20 mM $MgCl_2$ 1.6 mM dNTP mix* *25 mM each: dGTP, dCTP, dATP, dTTP 20 MM DTT 10 % (w/v) PEG-8000 2 mM NAD
10xKMEI	100 mM Imidazole, pH 7.0 500 mM KCl 15 mM $MgCl_2$ 10 mM EGTA
LB medium	10 g/l Bacto-Trypton, pH7.4 5 g/l yeast extract 10 g/l NaCl
10x ME	5 mM $MgCl_2$ 2 mM EGTA
20x MEH	20 mM Hepes, pH 7.0 1.5 mM $MgCl_2$ 1 mM EGTA
1x MES/MOPS SDS-gel buffer	50 mM MES/MOPS 50 mM Tris Base 1 mM EDTA 0.01 % SDS 5 mM $NaHSO_3$

100x non-essential amino-acids (NEAA)	PAN^{TM}Biotech
OptiMEM	Gibco by Life Technologies
1xPBS	137 mM NaCl, pH 7.4 2.7 mM KCl 10 mM Na_2HPO_4 1.8 mM KH_2PO_4
100x Penicillin – Streptomycin	PAN^{TM}Biotech
5x Protein loading buffer	500 mM Tris, pH 6.8 10 % (w/v) SDS 5 mM EDTA 0.5 mM DTT 0.5 % (w/v) Bromphenol Blue 50 % (v/v) glycerol
1x TAE buffer	40 mM Tris-acetate 1 mM EDTA 20 mM NaOAc
TB medium	10 g/l Bacto-Trypton 24 g/l yeast extract 0.4 % (v/v) glucose 0.71 M KH_2PO_4 0.72 M K_2HPO_4
10xTBS	0.2 MTris 1.36 M NaCl

1x Transfer buffer	25 mM Tris 192 mM glycine 20 % (v/v) methanol
Trypsin/EDTA	PAN^{TM}Biotech
SOC medium	20 g/l Bacto-Trypton 5 g/l Bacto yeast extract 0.5 g/l NaCl 2.5 mM KCl 10 mM glucose
100 mM Sodium pyruvate	PAN^{TM}Biotech

5.1.6 Recombinant DNA Constructs

Construct	Source	Identifier
pΔCMV-mNeongreen-mDia1FH1-2	this work	Uniprot: O08808
pΔCMV-mNeongreen-mDia2FH1-2	this work	Uniprot: Q9Z207
pPBCAG-β-actin-P2A-mScarletI-T2A-profilin1	this work	N/A
pETMSUMO-10xHis-SUMO3-h.s. Profilin1_wt	this work	Uniprot: P07737
pETMSUMO-10xHis-SUMO3-h.s. Profilin2_wt	this work	Uniprot: P35080
pETMSUMO-10xHis-SUMO3-h.s. Pro1_S71M	this work	N/A
pETMSUMO-10xHis-SUMO3-h.s. Pro1_E82A	this work	N/A
pETMSUMO-10xHis-SUMO3-h.s. Pro1_R88K	this work	N/A
pETMSUMO-10xHis-SUMO3-h.s. Pro1_K125EE129K	this work	N/A
pCOLDII-10xHis-h.s. Gelsolin_G4-6	this work	Uniprot: P13020
pETM11H10-10xHis-SNAP-h.s. DAAM1 FH1-2	this work	Uniprot: Q9Y4D1
pETMSUMO-10xHis-SUMO-SenP2-ScarW(WH2)	Bieling lab	N/A
pETM11-10xHis-SNAP-FH1(mDia1)FH2(mDia2)	this work	N/A
pETM11-10xHis-SNAP-FH1(mDia2)FH2(mDia1)	this work	N/A

pFL-h.s. β-actin_wt-linker-T4b	this work	Uniprot: P60709
pFL-h.s. β-actin_Q137A_D154A_H161A-linker-T4b	this work	N/A
pETM60-6xHis-NusA-TEV-UTRN261-KCK	Bieling lab	N/A
pETM11H10-10xHis-TEV-h.s. Thymosin β_4	Bieling lab	N/A

5.1.7 Bacterial strains and cells

Bacterial strains	Source/Identifier
XL 10 Gold	Stratagene (regrown in-house)
E. coli BL21 Star pRARE	EMBL Protein Expression Facility
E. coli Rosetta	Novagen, #70954

Cells (cell type)	Origin	Source/Identifier
Sf9	insect	Andrea Musacchio, MPI Dortmund
TnaO38	insect	Andrea Musacchio, MPI Dortmund
HT080	human	ATCC® CCL-121
B16F10	human	ATCC® CRL-6475
BMDC	mouse	Matthieu Piel, Institut Curie, Paris
El4	mouse	Marcus Taylor, Berlin
Primary neutrophils	mouse	Matthieu Piel, Institute Curie, Paris

5.1.8 Material and Equipment

AKTA pure system	GE Healthcare
DEAE resin	BIO-RAD
HA resin	BIO-RAD
HiPrep 26/10 column	GE Healthcare, Cat# 17508701
HiTrap chelating column	GE Healthcare, Cat# 17040901
HPLC Ultimax 3000 dionex	Thermo Fisher
Microfluidizer	Hyland Scientific
MonoS / Q	GE Healthcare
Nickel NTA superflow	Qiagen, Cat# 30430

Ni sepharaose excel column	GE Healthcare, Cat# 17371205
Plasma cleaner	Diener electronic
Tekan Spark plate reader	Tecan
SepharoseQ	GE Healthcare
Superdex 200 XK 16/60	GE Healthcare, Cat# 28989335
Superdex 200 XK 26/60	GE Healthcare, Cat# 28989336
Superdex 200 10/300 GL increase	GE Healthcare, Cat# 28990944
Superose 6 10/300 GL	GE Healthcare, Cat# 17517201
Superdex 75 XK 16/60	GE Healthcare,
Stopped flow	Photophysics
Syringe pumps	Scientific instrument services
Szinticounter, Triathler multilabel tester	Hidex
Zeba Spin column	Thermo Fisher

Equipment that is not separately listed here corresponds to the general laboratory equipment.

5.1.9 Software, Tools and Databases

ImageJ	Wayne Rasband, NIH-USA
OriginPro 9.0G	OriginLab Corporation
ApE	M. Wayne Davis
Expasy-ProtParam	SIB, Swiss
KAlign	EMBL-EBI
UniProt	EMBL-EBI
MATLAB 2017b	MathWorks
Adobe Illustrator CS4	ADOBE

5.2 Methods

5.2.1 Molecular Biology

5.2.1.1 Polymerase chain reaction (PCR)

The amplification of DNA fragments from plasmids of DNA gene fragments by PCR was performed using specific primers and a DNA polymerase (either AccuPrime for short DNA fragments (<1.5 kbp) or Q5 High-Fidelity DNA Polymerase to amplify long fragments and vector backbones (≥1.5 kbp)). A typical standard PCR reaction was prepared as follows (Table 1):

Table 1: Composition of a typical standard PCR reaction for the amplification of DNA by AccuPrime DNA Polymerase.

Component	Volume [µl]
10x AccuPrime™ PCR Buffer (containing dNTP mix)	5
FW Primer (10 µM)	2
RV Primer (10 µM)	2
AccuPrime™ *Taq* DNA Polymerase, High Fidelity (5 U/µl)	0.3
Template DNA (1-50 ng)	X
Water	to 50

FW - forward/sense Primer, RV - reverse/anti-sense Primer, dNTPs - deoxynucleotide-triphosphates, X - volume of template DNA depending on its concentration.

For multiple reactions and colony PCR reactions, a master mix was prepared containing all common components. All components were mixed in a 250 µl PCR tube on ice and transferred to a thermo-cycler. Specific cycling conditions (elongation time and primer annealing-temperatures) are highly dependent on the primer-design and the DNA-length. A standard PCR-protocol as for DNA amplification by the AccuPrime DNA polymerase is shown in the following Table 2:

Table 2: Standard PCR-protocol for the amplification of DNA by AccuPrime DNA Polymerase.

Cycle-step	Temperature [°C]	Time [s]	Number of cycles
Initial denaturation	97	120	1
Denaturation	97	30	30
Annealing	X	30	
Elongation	68	1 kb per min	
Final elongation	68	120	1
Storage after cycling	4	forever	

X – annealing temperature depends on the primer sequence, calculated using the online tool OligoCalc (Kibbe, 2007).

5.2.1.2 Site directed mutagenesis

Site directed mutagenesis was performed to generate specific point mutations in a DNA sequence. For this work several profilin1 and β-actin mutants have been created through site-directed mutagenesis. Primers were designed based on the template DNA sequence with changes in the nucleotide sequence of the specific codon that should be redesigned. The primers consist of at ≥ 43 nucleotides with at least 20 nucleotides left and right of the redesigned triplet. After vector PCR amplification within 20 cycles, the PCR product was treated with 10 U DpnI for 1 hr at 37 °C to cleave residual methylated template vector DNA. Following DpnI digest the enzyme was inactivated by incubation at 80 °C for 10 min and transformed into chemically competent E. coli XL10 Gold cells.

5.2.1.3 Gibson assembly

To join multiple DNA fragments Gibson assembly (Gibson, 2011; Gibson et al., 2009) was performed as follows:

First, Gibson primers were designed containing a 20-30 bp overlapping sequence for each of the adjacent DNA fragments that will be combined. Furthermore, a appropriate

restriction site was selected and cleaved in the plasmid backbone for DNA insertion during Gibson assembly. After DNA fragment amplification using the Gibson primers, all fragments (100 ng each, 5 µl) were mixed with 15 µl homemade Gibson assembly mix and incubated at 50 °C for 1 hr following transformation of 10 µl Gibson assembly mix into E. coli XL 10-Gold cells.

5.2.1.4 Restriction enzyme digestion

Restriction enzymes were used in order to isolate a specific DNA sequence out of a plasmid or to generate compatible ends for DNA ligation. The restriction digestion was performed by incubating 1 µg of DNA with 10 U of restriction enzyme in the recommended buffer in a total volume of 30 µl for 1 hr at 37 °C.

5.2.1.5 Agarose gel electrophoresis

Agarose gel electrophoresis was performed to separate DNA strands upon their size on a agarose gel matrix. The agarose gel was prepared in a concentration of 1 % (w/v) with TAE-buffer and supplemented with RedSafe (50 µl/l) as a nucleic acid staining solution. All DNA samples loaded were prepared in DNA loading buffer and the gel electrophoresis was performed at 120 V. To determine the DNA fragment sizes, the DNA bands were compared to a 2-log DNA ladder profile on a GelDoc XR System. To further process the size separated DNA fragments of interest, DNA bands showing the desired size were cut out of the agarose gel following electrophoresis. The DNA was extracted using the Zymoclean™ Gel DNA Recovery Kit from Zymo Research following the manual instructions.

5.2.1.6 Transformation of chemically competent E. coli cells

Transformation of plasmid DNA was performed using either XL 10-Gold E. coli cells (for sub-cloning or preparation of plasmid DNA) or E. coli cells suitable for protein expression (Rosetta or BL21 star pRARE). First, the chemically competent E. coli cells were thawed on ice and supplemented with 75 mM DTT. After the addition of DNA to the

cells, the mix was incubated on ice for 20 min following a heat-shock for 45 sec at 42 °C. Next, cells were immediately chilled on ice for 30 sec after heat-shock. 400 µl of SOC medium was added to the cells followed by incubation for 1 hr at 37 °C while shaking. Following incubation, cells were centrifuged at 4.000xg for 2 min and the cells pallet was plated onto a pre-warmed agar plate containing the appropriate antibiotics. Agar plates were incubated over night at 37 °C.

5.2.1.7 Preparation of Plasmids and determination of DNA concentration

To isolate DNA plasmids out of single E. coli cells after DNA transformation, single E. coli clones were inoculated into 10 ml LB liquid medium supplemented with the appropriate antibiotics. After 16 hr incubation at 37 °C, E. coli cells were centrifuged at 4.000xg for 10 min. The cell pellet was processed and plasmid DNA was isolated from the cells using the NucleoSpin Plasmid kit from Machery-Nagel following the manual instructions. The concentration of DNA was determined with a Nanodrop ND-1000 spectrophotometer from Peqlab at the absorption wavelength of 260 nm.

5.2.1.8 DNA Sequencing

DNA sequencing was performed by Eurofins GATC sequencing service. For sequencing, 2.5 µl of DNA (100-200 ng/µl) was diluted in 5 µl water and mixed with 2.5 µl of the specific sequencing Primer (10 µM).

5.2.2 Protein design

5.2.2.1 Design of structural barbed end complexes

To build models of three dimensional structures of the binding of profilin, formin mDia1 FH2 or profilin-formin mDia1 FH2 to the barbed end of actin filaments, the MODELLER program (Webb and Sali, 2016) was used. As a actin filament template the structure of α-actin in complex with beryllium fluoride (PDBID 5OOF) (Merino et al., 2018) was taken. The profilin models were generated by superimposing the actin monomer in the

profilin/β-actin crystal structure (PDBID 2BTF) (Schutt et al., 1993) to the ultimate or the penultimate protomer of the actin filament barbed end.

The generation of the FH2 domain of mDia1 (aa 750-1163) bound to a barbed end occupied with profilin was performed by superimposing subdomains 1 (aa 1-33; 70-137; 348-375) and 3 (aa 138-180; 274-347) of an Bni1p-actin subunit from the Bni1p-actin crystal structure (PDBID 1Y64) (Otomo et al., 2005b) with the terminal protomers in F-actin-BeFx resulting in the right positioning of the formin mDia1 FH2 domain in the actin filament. However, the structure of Bni1p has a non-physiological helical arrangement of the formin and thus the loop between the Knob and Lasso regions (aa 804-831 in mDia1) were erased and further built de novo to recover the known dimeric conformation of the mDia1 FH2 domains. In addition to increase the quality of the formin FH2-actin filament end models two crystal structures of mDia1 FH2 domains (PDBID 1V9D and 3O4X) (Nezami et al., 2010; Shimada et al., 2004) were included.

5.2.2.2 Design of profilin mutations

RoesttaScripts framework (Fleishman et al., 2011) within Rosetta (Leaver-Fay et al., 2011) was applied to detect possible mutations that increase the binding affinity of profilin for actin. The strategy to design the profilin mutations was modified from the protocol of the Baker lab (Berger et al., 2016). The design of the profilin mutations is based on the crystal structure of profilin-β-actin (Schutt et al., 1993) and the F-actin-profilin models (see previous section 5.2.2.1). Thereby, mutations into the amino acids Cys, Trp, Pro and Gly were not allowed at the interface with actin. While 1920 possible profilin sequences had been generated for each actin conformation, the top 50, meaning the ones with the lowest energies, were examined in further analysis. Then, single point mutations that were likely to increase the binding affinity of profilin for actin were selected and incorporated into binding- and TIRF single filament polymerization assays.

5.2.3 Protein Biochemistry - Protein expression, purification and labeling

5.2.3.1 Protein expression in insect Sf9 and TnO38 cells

For protein expression from insect cells, 2-4 µg of the vector DNA were gently mixed with 250 µl of SF900 media and incubated with 4 µl FUGENE transfection reagent for 20 min at room temperature. Meanwhile, 3 ml of $3 * 10^5$ SF9 cells were transfered into a 8.8 cm^2 sized sterile culture dish. After the cells had time adhere for 30 min at 27 °C, the transfection mix was carefully added to the cells and incubated for 5 days at 27 °C. Next, the transfected cells were resuspended with 10 ml of $1 * 10^6$ SF9 cells. Following 4 days of incubation, the transfected cells were centrifuged for 10 min at 150 xg and the virus containing supernatant was filtered through a 0.2 µm syringe filter. To further amplify the virus, 50 ml of $1 * 10^6$ SF9 cells were transfected with 500 µl of virus and were again incubated for 4 days shaking at 200 rpm at 27 °C. Following the virus amplification, the virus was again separated through centrifugation and filtering. To start the protein expression, 2 L of $1 * 10^6$ TnaO38 cells were infected by the addition of the virus (1 : 50) and the proteins were expressed over 3 days. After protein expression, the cells were harvested at 2000 xg for 20 min at 18 °C and the cell pellets were either snap frozen in liquid nitrogen and stored in -80 °C or the protein was directly purified.

5.2.3.2 10xhis-Gelsolin G4-6

Murine Gelsolin G4-6 was cloned together with a N-terminal 10xhis tag into a pCOLD vector. The protein was expressed in E. coli BL21 Rosetta cells for 16 hrs in TB medium at 16 °C starting at a OD_{600} of 1.2. For the Gelsolin purification, cells were lysed by resuspending them in lysis buffer (20 mM Tris-Cl pH 8.0, 300 mM KCl, 5 mM $CaCl_2$, 10 mM imidazole 0.2 mM ATP, 0.5 mM β-mercaptoethanol, 1 mM PMSF, DNAseI) and passing them 3 times through a microfluidizer. Following a hard spin, the supernatant was passed over a 40 ml Ni^{2+} superflow column for 3 rounds. Following the circulation, the column was washed (with 20 mM Tris-Cl pH 8.0, 300 mM KCl, 5 mM $CaCl_2$, 10 mM imidazole 0.2 mM ATP, 0.5 mM β-mercaptoethanol) until the UV signal reached its baseline. The his-tagged Gelsolin G4-6 was gradient (0-100 %) eluted (20 mM Tris-Cl pH 8.0, 300 mM KCl, 5 mM $CaCl_2$, 0.2 mM ATP, 500 mM Imidazole) over 10 column volumes followed by size exclusion chromatography over a Superdex 200 26/600 into

storage buffer (5 mM Tris-Cl pH 8.0, 50 mM KCl, 5 mM $CaCl_2$, 0.1 mM ATP, 0.5 mM TCEP). The protein was concentrated up to 14 mg/ml by spinning the protein solution in vivaspin concentrators at 3000xg and 4 °C. After the addition of 20 % glycerol, the protein was snap frozen in liquid nitrogen and placed in -80 °C for long-term storage.

5.2.3.3 Native β, γ actin

To purify native β, γ cytoplasmic actin isoforms 400 g of fresh bovine thymus was weight out, cleaned from connective tissue and blood vessels and severed into small fragments. The thymus pieces were then mixed with Holo-Extraction buffer (10 mM Tris-Cl pH 8.0, 7.5 mM CaCl2, 1 mM ATP, 5 mM β-mercaptoethanol, 0.03 mg/ml benzamidine, 1 mM PMSF, 0.04 mg/ml trypsin inhibitor, 0.02 mg/ml leupeptin, 0.01 mg/ml pepstatin, 0.01 mg/ml apoprotein) at 4 °C in a precooled blender until the tissue was homogenized to a mash. After homogenizing the thymus tissue, additional 2.5 mM β-mercaptoethanol was added to the lysate. Following the initial 30 min centrifugation at 13.000xg the lysate was filtered through a 100 µm nylon membrane followed by another hard spun for 1 hr at 140.000xg. After the aspiration of the remaining upper lipid layer, the volume of the cleared supernatant was measured out and the salt and imidazole concentrations were adjusted to 50 mM KCl and 20 mM imidazole. The supernatant was mixed with 10xhis-gelsolin G4-6 (see previous section) to promote the formation of gelsolinG4-6-actin complexes. To form the complex, 4 mg of 10xhis-gelsolin G4-6 were added for each g of thymus to the lysate. The lysate was then dialyzed into IMAC wash buffer (10 mM Tris-Cl pH 8.0, 50 mM KCl, 20 mM imidazole, 5 mM CaCl2, 0.15 mM ATP, 5 mM β-mercaptoethanol) at 4 °C over night. On the next day, the lysate was circulated over a 80 ml Ni^{2+} superflow column for 2 rounds. After circulation, the column was washed into IMAC wash buffer. As soon as the UV signal reached baseline, actin monomers were eluted into a collection tray containing 2 mM $MgCl_2$ (final concentration) using Elution buffer (10 mM Tris-Cl pH 8.0, 50 mM KCl, 20 mM imidazole, 5 mM EGTA, 0.15 mM ATP, 5 mM β-mercaptoethanol). Following monomer elution, the actin containing fractions could be identified and pooled by gelation. After adjusting to 1xKMEI and 0.5 mM ATP the fractions were further polymerized for 3-4 hrs at RT and afterwards spunned at 140.000xg for 1 hr. The pellet

was resuspended in F buffer (1xKMEI, 1xBufferA) after centrifugation and stored in dialysis at 4 °C exchanging the dialysis buffer every 4 weeks. To depolymerize actin filaments into monomers, actin was dialyzed in G buffer for 6 days exchanging the dialysis buffer every 2 days.

1.5-IAEDANS labeling: For fluorescence measurements actin monomers were labeled with 1.5-IAEDANS at position Cys374 similar as described in (Hudson and Weber, 1973; Miki et al., 1987). Briefly, filamentous actin was mixed with 10x molar excess of 1.5-IAEDANS at RT and incubated for 1 hr and shielded from light. To stop the reaction, 1 mM DTT was added to the mix and incubated for 10 min. Then the filaments were separated from free dye by ultracentrifugation at 500.000xg for 30 min and the actin pellet was resuspended and dialyzed in BufferA at 4 °C for 2 days. After dialysis actin monomers were separated from residual filaments and aggregated dye by ultracentrifugation at 300.000xg for 30 min. The monomer concentration and the degree of labeling were determined by measuring the absorption at 280 nm/336 nm.

5.2.3.4 Recombinant human β actin

Human β actin (wt and Q137A+D154A+H161A) was designed with a C-terminal linker sequence (ASRGGSGGSSGGSA) followed by human β thymosin sequence and a 10xhis tag (Noguchi et al., 2007) and cloned into a pFL vector for insect cell expression. The ATPase deficient (AD) β actin triple mutant (Q137+D154A+H161A) was generated by site directed mutagenesis. Both β actin versions were expressed in insect TnaO38 cells for 3 days at 27 °C. For the β actin purification, the insect cells were resuspended in a 5x pellet volume of lysis buffer (10 mM Tris-Cl pH 8.0, 50 mM KCl, 7.5 mM $CaCl_2$, 1 mM ATP, 5 mM imidazole, 5 mM β-mercaptoethanol, 0.03 mg/ml benzamidine, 1 mM PMSF, 1x complete protease inhibitor cocktail). Following resuspension, the cells were lysed by passing them through a microfluidizer for 2-3 times. The lysate was centrifuged at 80.000 xg for 40 min and afterwards filtered through a 0.45 µm syringe filter and passed 3 times through a Ni^{2+}-sepharose excel column. After the column was washed with 10 mM Tris-Cl pH 8.0, 50 mM KCl, 5 mM $CaCl_2$, 0.15 mM ATP, 5 mM imidazole, 5 mM β-mercaptoethanol, the protein was eluted (10 mM Tris-Cl pH 8.0, 50 mM KCl,

0.15 mM ATP, 300 mM imidazole, 5 mM β-mercaptoethanol) with a linear 0-100 % gradient over 6 column volumes followed by dialysis overnight into BufferA. On the next day, the protein was cleaved with TLCK treated chymotrypsin in a molar ratio of 250 : 1 (actin over chymotrypsin) at 25 °C for 10 min. The reaction was quenched by the addition of 0.2 mM PMSF at 4 °C and the protein was circulated over a Ni^{2+}-sepharose excel column which was equilibrated with BufferA. Next, the flow through fraction was polymerized for 3-4 hrs at 25 °C upon the addition of 1xKMEI, 2 mM $MgCl_2$ and 0.5 mM ATP final concentration. The polymerized actin fraction was separated from non-polymerizable monomers as well as residual cleavage contaminants through ultracentrifugation at 250.000 xg for 1 hr. The actin filament pellet was resuspended into BufferF (1xKMEI, 1xBufferA) and stored in dialysis at 4 °C while exchanging the dialysis buffer every 3-4 weeks.

5.2.3.5 Native α actin

The purification of native mammalian skeletal α actin was performed starting from 10 g of rabbit acetone powder purchased from Sigma (#-M6890). First, the acetone powder was dissolved in 200 ml BufferA at 4 °C stirring for 30 min following centrifugation at 18.000 xg for 1 hr. Next, 1xKMEI and 0.1 mM ATP final concentration was mixed into the supernatant to initiate polymerization. After polymerization for 1 hr at 23 °C while slightly stirring the polymerization reaction was transferred to 4 °C for an additional hour. Following polymerization, solid KCl was slowly added to the solution (800 mM KCl final concentration) over a time course of 30 min. Next, the actin fraction that polymerized into filaments was separated from polymerization incompetent actin and other contaminants by ultracentrifugation at 185.000xg for 2 hrs and the actin filament pellet was resuspended in BufferF and stored in dialysis at 4 °C while exchanging the dialysis buffer every 3-4 weeks.

5.2.3.6 Recombinant tagged and non-tagged profilin 1 and 2

Human profilin 1 and 2 were designed either as non-tagged or N-terminal SUMO3-10xhis tagged proteins. The proteins were expressed in E. coli BL21 Rosetta cells at

30 °C for 4.5 hrs. Profilin1 mutants were generated via site-directed mutagenesis (E82A, R88K, S71M and K125E+E129K) and expressed with an N-terminal SUMO3-10xhis tag that was removed through protease cleavage during the purification. To purify the tagged profilin versions, the cells were resuspended in buffer (20 mM Tris-Cl pH 8.0, 300 mM NaCl, 10 mM imidazole, 0.5 mM β-mercaptoethanol, 15 µg/ml benzamidine, 1 mM PMSF and DNaseI) and lysed by passing them through a microfluidizer for 2-3 times. After centrifugation at 80.000 xg for 40 min the supernatant was circulated over a 5 ml HiTrap Chelating column. After column wash, the N-terminal SUMO3-10xhis tag was cleaved off from the protein by SenP2 cleavage on the column over night. Profilin containing the natural N-terminus was located in the flow through after cleavage and was gelfiltered over a Superdex 200 16/600 column into storage buffer (20 mM Tris-Cl pH 7.5, 50 mM NaCl, 0.5 mM TCEP). The non-tagged profilin isoforms were purified by ammonium sulfate precipitation described by (Bieling et al., 2018). Briefly, after resuspending the cells in lysis buffer (10 mM Tris-Cl pH 8.0, 50 mM NaCl, 1 mM EDTA, 2 mM DTT, 1 mM PMSF and DNaseI) and cell lysis by passing the cells 2 times through a microfluidizer, the lysate was centrifuged at 80.000 xg for 40 min. Next, 35 % ammonium sulfate was gently added to the supernatant while stirring for 30 min. After centrifugation at 80.000 xg for 45 min, additional ammonium sulfate was added to a final concentration of 61 %. Following a 30 min incubation and another round of centrifugation the pellet was resuspended in 40 ml lysis buffer and dialyzed into the same buffer overnight. After dialysis, the protein suspension was load onto a 100 ml DEAE ion exchange column followed by column wash (10 mM Tris-Cl pH 8.0, 50 mM NaCl, 0.2 mM EDTA, 2 mM DTT, 1 mM PMSF). The flow through and the wash were collected and dialyzed into HA buffer (5 mM KPi pH 7.5, 1 mM DTT) over night. Next, the protein solution was load onto a 100 ml hydroxylapatite (HA) column and the flow through and was fractions were collected and gelfiltered over a Superdex 200 16/600 into storage buffer (20 mM Tris-Cl pH 7.5, 50 mM NaCl, 0.5 mM TCEP). After the purification, the proteins were snap frozen in liquid nitrogen with the addition of 20% glycerol in the storage buffer and were stored at -80 °C.

5.2.3.7 Profilin-Actin complex

Due to high affinity of profilin binding to actin monomers, profilin - actin complexes could be generated in batch and gelfiltered to separate the complex from free species. Briefly, filamentous mammalian cytoplasmic actin was depolymerized into BufferA (2 mM Tris, 0.2 mM ATP, 0.1 mM $CaCl_2$, 0.1 µg/ml NaN_3, 0.5 mM TCEP) and gelfiltered over a Superdex 200 16/600. After gelfiltration a 1.5x molar excess of profilin was added to the actin monomers and incubated at 4 °C for minimum 3 hrs up to over night to form profilin-actin complexes. Next, the complex was separated from excess free species by gelfiltration over a Superdex 200 10/300 GL into BufferA. The complex was concentrated to a working concentration between 200–400 µM and stored at 4 °C up to 3 weeks without inducing nucleation of filaments.

5.2.3.8 β4-thymosin

H. sapiens β4-thymosin was cloned with an N-terminal 10xhis-tag and expressed in E. coli Rosetta cells for 16 hrs at 18 °C by the addition of 0.25 mM IPTG. For the purification, the cells were resuspended in lysis buffer (20 mM Tri-Cl pH 7.5, 200 mM NaCl, 15 mM imidazole, 0.5 mM β-mercaptoethanol, 15 µg/ml benzamidine, 1 mM PMSF, DNaseI) and lysed by passing the cell suspension through a microfluidizer for 2-3 rounds. Next, the lysate was centrifuged at 80.000 xg for 40 min followed by IMAC purification using 5 ml HiTrap Chelating column. After circulating the protein for 2-3 times over the HiTrap column, the column was washed until UV baseline was reached and the protein was eluted (20 mM Tri-Cl pH 7.5, 200 mM NaCl, 200 mM imidazole, 0.5 mM β-mercaptoethanol, 1 mM PMSF) in a gradient over 10 column volumes. Based on the elution profile the peak fraction was pooled and the 10xhis-tag was cleaved overnight using TEV protease (1:30, Protein over TEV) while dialyzing back into wash buffer (20 mM Tri-Cl pH 7.5, 200 mM NaCl, 15 mM imidazole, 0.5 mM β-mercaptoethanol, 1 mM PMSF). After TEV cleavage, the protein was recirculated over the 5 ml HiTrap Chelating column following gelfiltration over a Superdex 75 16/600 into storage buffer (5 mM Hepes pH 7.5, 25 mM KCl, 0.5 mM TCEP). Next, the protein was snap frozen in liquid nitrogen with the addition of 20% glycerol in the storage buffer and stored at -80 °C.

5.2.3.9 Formins

M. musculus mDia1 FH1-2 (aa 548-1154), mDia2 FH1-2 (aa 515-1013), mDia1 FH2 (aa 752-1163), chimera mDia $FH1_{mdia1}FH2_{mdia2}$ (aa 548-751/453-1013), chimera mDia $FH1_{mdia2}FH2_{mdia1}$ (aa 515-612/645-1154), *h. sapiens* DAAM1 FH1-2 (aa 490-1029), were expressed with an N-terminal 10xhis-SNAP-tag. All constructs were expressed in E. coli BL21 Star pRARE cells for 16 hrs at 18 °C. For the purification, the cells were resuspended in lysis buffer (50 mM $NaPO_4$ pH 8.0 (pH 7.5 for mDia chimera constructs), 400 mM NaCl, 0.75 mM β-mercaptoethanol, 15 µg/ml benzamidine, 1x complete protease inhibitors, 1 mM PMSF, DNaseI) and lysed by passing the cell suspension through a microfluidizer for 2-3 rounds. Next, the lysate was hard spunned at 80.000 xg for 40 min followed by IMAC purification using 5 ml HiTrap Chelating column. After circulating the protein for 2-3 times over the HiTrap column, the column was washed until UV baseline was reached and the protein was eluted (50 mM $NaPO_4$ pH 7.5, 400 mM NaCl, 400 mM imidazole, 0.5 mM β-mercaptoethanol) in a gradient over 12 column volumes. Based on the elution profile the peak fraction was pooled and the 10xhis-tag was cleaved over night using TEV protease (1:30, Protein over TEV). After TEV cleavage, the protein was desalted into low salt Mono S buffer (10 mM Hepes pH 7.0 (pH 7.5 for chimera constructs), 90 mM NaCl, 0.5 mM TCEP) over a HiPrep 26/10 desalting column. Next, the protein was loaded onto a Mono S column followed by elution in a linear 25 column volume gradient to high salt Mono S buffer (10 mM Hepes pH 7.5, 1 M NaCl, 0.5 mM TCEP) followed by gelfiltration over a Superdex 200 16/600 into storage buffer (20 mM Hepes pH 7.5, 200 mM NaCl, 0.5 mM TCEP, 20 % glycerol).

Following the purification the proteins were either snap frozen and stored in –80 °C or directly used for SNAP-labeling. For the reaction a 3x molar excess of SNAP Cell TMR Star was mixed with the protein and incubated for 6 hrs at 16 °C following an overnight incubation at 4 °C. Post labeling the protein was gelfiltered over a Superose 6 10/300 GL column into storage buffer. The degree of labeling (50–70 %) was determined by absorbance at 280 nm and 554 nm.

5.2.3.10 Myosin and biotinylated heavy - mero – myosin (HMM)

Skeletal muscle myosin was prepared from chicken according to (Pollard, 1982). Briefly, 300 g muscle tissue were mixed with 4x volumes of extraction buffer (0.15 mM KH_2PO_4 pH 6.5, 0.3 M KCl, 5 mM $MgCl_2$, 0.1 mM ATP, 20 mM EDTA) while blending. The pH was adjusted to 6.6 afterwards. After centrifugation at 25.000xg for 40 min, the supernatant was taken and diluted with 10 x volumes of cold water and the precipitate was separated from solution by centrifugation at 9.000xg for 30 min. Next, the pellet was resuspended in buffer 8 (3 ml buffer per g of pellet, 60 mM KH_2PO_4 pH 6.5, 1 M KCl, 25 mM EDTA) and dialyzed against buffer 9 (25 mM KH_2PO_4 pH 6.5, 0.6 M KCl, 10 mM EDTA, 1 mM DTT) over night. Following dialysis, an equal volume of cold water was added to the myosin solution and stirred for 30 min. After centrifugation for 30 min at 15.000xg, the supernatant was diluted with 7 volumes of cold water and again spun for 30 min at 9.000xg. The pellet fraction was then resuspended into buffer 10 (20 mM Tris-Cl pH 7.0, 0.6 M KCl, 10 mM DTT) and treated with α-chymotrypsin (25 µg/ml final) at 25 °C for 15 min. The reaction was stopped by the addition of 0.3 mM PMSF. After protease treatment, the myosin was dialyzed into buffer 11 (10 mM NaPi pH 7.2, 35 mM NaCl, 10 mM DTT). On the next day, the HMM was separated by ultracentrifugation for 1 hr at 300.000xg. The supernatant was desalted into buffer 11 without DTT and incubated with 15x molar excess of EZ-Link maleimide-PEG11-biotin for 2 hrs at 4 °C. The reaction was stopped by the addition of 1 mM DTT. The protein was desalted into buffer 11 containing 20 % glycerol, snap-frozen and stored at –80 °C.

5.2.4 Biochemical protein characterization

5.2.4.1 Fluorescence anisotropy experiments

The measurements were performed in 96 well CORNING black bottom plates with a TECAN SPARK plate reader. A constant concentration of 150 nM actin monomers were stabilized with 25 µM latrunculin B and mixed with 4 nM Atto488-WAVE1(WCA) (Bieling et al., 2018) as a fluorescent competition binding partner. Profilin was titrated to the Atto488-WAVE1(WCA):actin complex to final concentrations of 0–20 µM and equilibrated for 5 min at RT before the measurement. The assay was performed in 1xTIRF buffer (20 mM Hepes pH 7.0, 100 mM KCl, 1.5 mM $MgCl_2$, 1 mM EDTA, 20 mM

β-mercaptoethanol, 0.1 mg/ml β-casein, 1 mM ATP). For the determination of anisotropy values, Atto488-WAVE1(WCA) was excited at 485/20 nm and the emission was detected at 535/25 nm.

5.2.4.2 Fluorescence quenching measurements

Fluorescence measurements were performed in 96 well CORNING plates with a TECAN SPARK plate reader. A constant concentration of 150 nM 1.5-IAEDANS labeled actin monomers were pre-mixed with 25 µM latrunculin B in 1xTIRF assay buffer (see Fluorescence anisotropy experiments) and thymosin-β_4 was titrated over a range of 0–200 µM. After 5 min of equilibration, the 1.5-IAEDANS actin was excited at 336 nm and the emission and thus the fluorescence change of the 1.5-IAEDANS actin bound to thymosin-β_4 was detected at 490 nm.

5.2.4.3 Endpoint hydrolysis measurements via HPLC

To determine the nucleotide species of different actin wt and mutant proteins before and after polymerization endpoint hydrolysis measurements by HPLC were performed. All HPLC measurements were initiated by loading actin monomers and profilin-actin with Mg-ATP. First, 40 µM monomers or profilin-actin were incubated in presence of 1 mM $MgCl_2$ and 1 mM ATP for 1 hr at 23 °C. Next, the proteins were desalted into 2 mM Tris-Cl pH 8.0 using a Zeba Spin Desalting column. Actin seeds were polymerized from the desalted actin monomers by adjusting to 1xKMI (50 mM KCl pH 7.0, 1.5 mM $MgCl_2$, 10 mM imidazole) for 1 hr at 23 °C. To start the reaction, 5 µM pre-polymerized actin seeds were mixed with 40 µM profilin-actin in presence of 1xKMI and incubated for 1.5 hrs incubation at 23 °C. To separate the nucleotides from the protein after polymerization, the samples were boiled at 99 °C for 5 min followed by ultracentrifugation at 280.000xg for 1 hr. The supernatant was carefully aspired and injected onto a C18-column equilibrated with 16 % acetonitrile, 50 mM KP_i pH 6.6, 10 mM TBABr. As a negative control, profilin-actin were stabilized with 5 mM latrunculin B and the seeds were supplied with 5 mM phalloidin before mixing, otherwise the samples were treated as described above. All nucleotide retention times were measured

using an UltiMate 3000 HPLC Dionex – System. The nucleotide signal intensity was recorded at 254 nm.

5.2.4.4 Radioactive ATPase assay

To monitor ATP-hydrolysis over time, the generation of inorganic radioactive phosphate upon polymerization from β-actin (wt and Q137A+D154A+H161A) was measured. Starting from 100 µM Mg-ATP-actin that was dialyzed into BufferA for 7 days and gelfiltered over a Superdex200 16/60 column afterwards. Next, the monomer fraction was split into two fractions. One monomer fraction was incubated with 1.5x-molar excess of profilin1 for 4 hrs to form profilin-actin complexes that were isolated by gelfiltration over a Superdex200 10/300 GL. Following desalting of both actin monomers and profilin-actin complex fractions into ATP free BufferA (2 mM Tris-Cl pH 8.0) over a Zeba Desalting column, 1 ml of 10 µM actin monomers was incubated with 2xKMEI to polymerize actin for 1 hr at 23 °C. In the meantime, 1 ml of 10 µM profilin-actin was incubated with 0.2 mM EGTA, 0.132 mM $MgCl_2$ and 0.06 mM γ–^{32}P–ATP (3000 Ci/mmol, PerkinElmer #NEG002A) for 30 min at 4 °C and afterwards desalted over a Zeba Desalting column into 2 mM Tris–Cl pH 8.0, 0.2 mM EGTA, 0.132 mM $MgCl_2$. Immediately before starting the polymerization reaction, the pre-polymerized actin seeds were sheared through a 27 G needle. The reaction was initiated by mixing 6 µM of actin seeds with 6 µM of γ–^{32}P–ATP labeled profilin-actin. 100 µl samples were taken at different time points over a time course of 48 min and rapidly quenched with an equal volume of silicotungstic–sulfuric acid (4.3 % aqueous silicotungstic acid in 2.8 N sulfuric acid). Next, the samples were recovered in 1 ml of a 1:1 isobutanol/xylene solution and immediately rigorously mixed with additional 100 µl of 10 % ammonium molybdate for 20 s. Following a 4 min centrifugation at 200xg, the upper phase containing the phosphate molybdate complex was aspired and diluted in LSC cocktail (Hidex). The number of counts was detected using a liquid scintillation counter (Triathler multilabel tester, Hidex).

5.2.4.5 Tryptophan fluorescence quenching by stopped flow

The measurement of the association rate constant for profilin binding to actin monomers was performed by selectively detecting changes in the intrinsic actin (tryptophan) fluorescence due to conformational transitions upon profilin binding. To determine the association rate constant for profilin binding to actin monomers, increasing profilin concentrations were mixed in a 1:1 volume with a fixed concentration of 0.5 µM actin monomers at 25 °C. The assay was performed in 20 mM Hepes pH 7.0, 100 mM KCl, 1.5 mM $MgCl_2$, 1 mM EDTA, 20 mM β-mercaptoethanol, 1 mM ATP and 1.5 µM latrunculin B. The tryptophan fluorescence intensity of actin was recorded by a SX20 double mixing stopped flow device (Photophysics) using excitation and emission wavelengths of 280 and 320 nm, respectively. The time courses of actins tryptophan fluorescence was recorded and fitted with a single exponential function to yield the observed pseudo-first order reaction rate (k_{obs}) as a function of profilin concentration.

5.2.4.6 Quantitative western blot analysis

Quantitative western blots from cell lysates were performed using 12 % SDS gels. To determine actin and profilin amounts per cell, purified actin and profilin references of known concentration were titrated into 1xPBS on the same gel as the cell lysate samples. The number of cells was counted by a Vi-CELL Viability Analyzer from Beckmann Coulter. Cells were lysed in 5 mM Tris–Cl pH 7.5, 150 mM NaCl, 1 mM EDTA, 1 % Triton X-100 and 10 min of sonication. All protein samples were prepared in 1x Laemmli sample loading buffer (Cold Spring Harbor Protocols, 2007). Precision Plus Protein Standard All Blue (Biorad) was used as a molecular weight marker. SDS Gel electrophoresis was performed in a Mini-PROTEAN Tetra Cell System (BioRad) using Tris-Glycine buffer and proteins were transferred onto a PVDF membrane (Merck Chemicals) at 100 V for 90 min by wet-blotting. After protein transfer, membranes were blocked with Odyssey TBS blocking solution (LI-COR Biosciences) for 1 hr at RT and probed with one of the following antibodies: monoclonal mouse anti – actin (1:1000, **#**MA5-11869 ThermoFisher) / profilin1 (1:20000, #061M4892 Sigma) / profilin2 (1:20000, **#**sc-100955 Santa Cruz) and monoclonal rabbit anti – GAPDH(14C10) (1:5000, #2118) as primary antibodies. As secondary antibody infrared labeled - donkey

anti-mouse and donkey anti-rabbit were used (1:10000, #925-32212, #926-68073 LI-iCOR). All antibodies were incubated for 1 hr at RT and the membrane was washed with TBS-T (TBS + 0.05 % Tween20) in between. The antibody signal was visualized by fluorescence detection on a LI-COR Odyssey CLx imaging system.

5.2.4.7 Cell volume measurements by fluorescence eXclusion

Cell volumes were determined for different cell lines and primary cells outlined in this study. Measurements were performed as described in (Cadart et al., 2017) for all cell types in suspension and attached to a glass surface using fibronectin. Briefly, cells were transferred into a PDMS chamber with a specific known height and reference-pillars in order to calibrate the fluorescence signal intensity together with the appropriate cell culture media. Before microscopic imaging, the media was supplemented with a Alexa488 dye coupled to dextran. Thus, dextran is too large to diffuse through cellular membranes, no fluorescent signal is detected in the intracellular volume. It has been shown, that the displacement of fluorescence is proportional to the cell volume (Bottier et al., 2011). When imaging the cells it was necessary to have at least one reference-pillar in each field of view. After image normalization, cells were manually tracked. The data analysis was performed using custom written codes for MATLAB 2017b software created by QuantaCell (Cadart et al., 2017). For each cell type ≥ 300 single cells were analyzed and the distribution of the single cell volumes were plotted as a histogram and a lognormal distribution curve was fitted to the histogram. Last, the mean volume [μm^3] and the error (SD) for each cell type were calculated.

5.2.5 Cell Biology

5.2.5.1 Cell culture

HT1080 cells were cultured in DMEM and supplemented with 2 mM glutamine, 1 % NEAA and 10 % FBS. B16F10 cells were cultured in DMEM and supplemented with 4 mM glutamine, 1 % NEAA and 10 % FBS. Mouse EL4 cells were cultured in RPMI-1640 with 10 % FBS. The cells were cultivated at 37 °C with 5 % CO_2 in a humidified incubator. BMDCs were cultured according to (Vargas et al., 2016a, b). Mouse

neutrophil cells were extracted from mouse blood and kindly provided by M. Piel, Institute Curie-Paris.

5.2.6 Microscopy

5.2.6.1 Single filament experiments on functionalized glass coverslips using TIRF-Microscopy

For TIRF-M single filament experiments flow chambers were prepared from microscopy counter slides passivated with PLL-PEG and coverslips (22x22 mm, 1.5H, Marienfeld-Superior) that were functionalized according to (Bieling et al., 2010). Briefly, coverslips were cleaned with 3 M NaOH for 30 min followed by another cleaning with Piranha solution for 45 min. Following silanization with 3-(Glycidoxypropyl)trimethoxysilane (GOPTS) for 30 min at 60 °C the coverslips are separated in acetone and functionalized with PEG-biotin / hydroxy (5:95 %) for 4 hrs at 60 °C. For the single filament assays the flow cell surfaces were blocked for 5 min with a Pluronic block solution (0.1 mg/ml κ-Casein, 1 % Pluronic F-127, 1 mM TCEP, 1xKMEI), followed by 2 washes with 40 µl of wash buffer (0.5 mM ATP, 1 mM TCEP, 1xKMEI, 0.1 mg/ml β-Casein). Next, the channel was incubated with 75 nM streptavidin for 3 min, followed by washing and incubation of 90 nM biotin-phalloidin for 3 min. For experiments in low profilin-actin concentration regimes (in absence of formins) were spontaneous nucleation of filaments was not rapid enough pre-polymerized phalloidin stabilized actin seeds were prepared and immobilized in the flow channel for 2 min prior to the addition of the reaction mixture.

Visualization of single filament polymerization by TIRF-M was performed following a modified protocol as outlined in (Hansen and Mullins, 2010; Kuhn and Pollard, 2005). Briefly, 9 µl of a 4.44x µM profilin-actin solution was mixed with 1 µl of 10x ME (0.5 mM $MgCl_2$, 2 mM EGTA) and 4 µl oxygen scavenging system (1.25 mg/ml glucose-oxidase, 0.2 mg/ml catalase, 400 mM glucose) (Aitken et al., 2008; Bieling et al., 2010; Rasnik et al., 2006). The Mg-ATP –profilin-actin was then combined with 26 µl reaction buffer mix containing additives including 10 nM Cy5-$UTRN_{261}$, (plus additives as described in the specific results section and in the corresponding figure legends) and TIRF buffer with the

final composition of: 20 mM Hepes pH 7.0, 100 mM KCl, 1.5 mM $MgCl_2$, 1 mM EDTA, 20 mM β-mercaptoethanol, 0.1 mg/ml β-casein, 0.2 % methylcellulose (cP400, M0262, Sigma-Aldrich), 1 mM ATP and 2 mM Trolox.

Filaments that appeared to either stop growing due to surface defects or that showed very large movements out of the TIRF field due to lower surface tethering were not analyzed. All single filament polymerization experiments were performed using profilin-actin as a substrate unless otherwise indicated in the specific results section and the figure legends.

5.2.6.2 Microfluidic single filament experiments by TIRF-Microscopy

Single filament TIRF-M experiments under constant flow were performed as the TIRF-M experiments described in the previous section. Furthermore, the polymerization reaction of single filaments were conducted in microfluidic PDMS chambers that were mounted on a PEG-biotinylated glass coverslip (see previous section) via plasma treatment as described in (Duellberg et al., 2016). The microfluidic chambers were designed with 2 or 3 inlets and 1 observation channel. After pluronic block (0.1 mg/ml κ-Casein, 1 % Pluronic F-127, 1 mM TCEP, 1xKMEI) for 5 min, 75 nM streptavidin was flowed through the channel for 3 min. Next, prep-polymerized and biotinylated Alexa647-phalloidin stabilized actin seeds were bound to the surface via streptavidin. To start actin filament polymerization, profilin-actin was diluted in TIRF buffer and directly transferred via a syringe pump into the reaction chamber to visualize filament elongation immediately under the TIRF-microscope. The flow speed was set to 14-16 µl/min.

5.2.6.3 Single formin visualization in vivo

To visualize single formin molecules in cells, constitutively active constructs of mDia1 FH1-2 (aa 548-1154) and mDia2 FH1-2 (aa 515-1013) were cloned individually with an N-terminal mNeonGreen sequence into a pΔCMV vector. For transient transfection, 20.000 cells were seeded into a well of an 8 well Lab-Tek 1.5H that was coated with fibronectin (40 µg/ml). After 24 hrs, 1.5 µl FUGENE (Promega) were incubated in 150 µl OptiMEM (Gibco) for 5 min at 23 °C followed by a 15 min incubation with 0.5 µg DNA.

The entire transfection mix was directly transferred to the cells. $2x10^6$ EL4 cells were resuspended in 100 µl Nucleofector solution with 2 µg DNA and electroporated by Lonza Amaxa NUcleofector II with the program C009 for EL4 cells. After electroporation, the cells were transferred into 1.5 ml medium. To minimize the transfer of cell debris, cells were once passaged on the following day. Finally, the cells were seeded onto a mouse ICAM-1 coated Lab-Tek 1.5H. For either cell type after 18 hrs after transfection (HT1080) or initial passage (EL4), the cell culture medium was replaced by HBSS (PAN Biotech #P04-32505) before imaging at 23 °C. Only cells with very low formin expression (<35 single molecules per cell per image) were chosen for image acquisition. Moreover, only single molecules that were translocating freely in the interior of the cell and did not move close towards the periphery were chosen for analysis to prevent an influence of mechanical resistance through the plasma membrane on formin movement.

Control experiments were performed incubating the cells at least 10 min with either 500 nM latrunculin B, 10 µM Y-27632 or 8 µM JASP (Peng et al., 2011). The single molecule imaging was performed before and after drug treatment.

5.2.6.4 TIRF-Microscopy data acquisition

All in vitro experiments were performed at RT using an custom built TIRF microscope (OLYMPUS IX81). Image acquisition was done by a EM CCD Andor iXon 888 camera controlled by Micromanager 1.4 software (Edelstein et al., 2014). Fiji ImageJ was used for image and data analysis. Dual color imaging was performed through a 60x OLYMPUS APO N TIRF objective using TOPTICA IBeam smart 640s and 488s/or OBIS 561nm LS lasers and a Quad-Notch filter (400-410/488/561/631-640). Shutters, optical filters, dichroic mirrors and the Andor camera were controlled by Micromanager 1.4 software. Images were acquired within intervals of 0.14 – 10 s using exposure times of 30 – 200 ms to avoid bleaching.

All in vivo single molecule experiments were performed at 23 °C unless otherwise specified using a customized Nikon TIRF Ti2 microscope and a Nikon perfect focus system. Image acquisition was achieved by a dual camera EM CCD Andor iXon system controlled by NIS – Elements software. Dual color imaging was performed through an

Apo TIRF 60x oil DIC N2 objective using a custom multilaser launch system (AcalBFi LC) at 488 nm and 560 nm. Images were acquired at intervals of 0.075 – 0.15 s.

5.2.7 Overexpression of profilin1 and β - actin in HT1080 cells

Polyclonal stable HT1080 cells were generated using the PiggyBac system according to System Bioscience protocols. Briefly, for profilin-actin overexpression, the following sequences were cloned in a PiggyBac vector containing a CAG promotor through Gibson assembly: human β-actin – P2A (ggcagcggcgccacaaacttctctctgctaaagcaagcaggtgatgttgaagaaaaccccgggcct) – mScaletI – T2A (ggctccggcgagggcaggggaagtcttctaacatgcggggacgtggaggaaaatcccggccca) – human profilin1. After transfection, the transgenetic cells were selected using puromycin (1 µg/ml) followed by cell sorting through a flow cytometer (BD FACSAria). The cells were sorted according to their mScarletI fluorescence intensity into distinct sub-populations which were grown separately. Quantitative western blot analysis were performed to measure the amounts of profilin1 and β-actin in these distinct cell populations.

5.2.8 Quantification and statistical data analysis

All analyzed data was plotted and fitted in Origin9.0G. All microscopy experiments were analyzed in ImageJ either manually via kymograph analysis or automated by using the TrackMate plugin (Tinevez et al., 2017) unless otherwise described. Microscopic cell volume measurements were analyzed with MATLAB 2017b using a script created by QuantaCell.

5.2.8.1 Profilin binding affinity for actin monomers by fluorescence anisotropy competition

The binding of profilin to actin monomers can be monitored by change in anisotropy of a small fluorescent profilin competition partner. In this work the equilibrium dissociation constant (K_D) for profilin (wt and mutants) binding actin monomers (wt and AD-actin)

was determined from competition with a small Atto488-fluorescently labeled peptide (WCA domain of WAVE1). This peptide binds actin monomers with a known affinity of 28 nM. To determine the equilibrium dissociation constant, all mean anisotropy values that were calculated from at least three independent measurements (with errors representing the SD), were plotted against the increasing total profilin concentration [nM]. The anisotropy data was fitted by an competitive binding model as described in (Wang, 1995) that analytically solves for the concentrations of the bound and free species from the known total concentrations of all proteins and the equilibrium dissociation constants for each of the two competing ligands as follows:

Equation1 (anisotropy as a function of the concentration of the profilin-actin complex):

$$r = r_f + (r_b - r_f)[PA]$$

With r being the measured anisotropy, r_f and r_b the anisotropy of the free and the bound species, respectively and [PA] the profilin-actin complex concentration.

The concentration of the profilin-actin complex can be determined from:

Equation 2 (concentration of the profilin-actin complex):

$$[PA] = \frac{[P]_0(2\sqrt{a^2-3b}\,\cos\left(\frac{\theta}{3}\right)-a)}{3K_P+(2\sqrt{a^2-3b}\,\cos\left(\frac{\theta}{3}\right)-a)}$$

With $[P]_0$ = total concentration of profilin, K_P = equilibrium dissociation constant for the interaction between profilin and actin.

And concentration of the WAVE1-WCA complex can be determined from:

Equation 3 (concentration of the WAVE1-WCA:actin complex):

$$[WA] = \frac{[W]_0(2\sqrt{a^2-3b}\,\cos\left(\frac{\theta}{3}\right)-a)}{3K_W+(2\sqrt{a^2-3b}\,\cos\left(\frac{\theta}{3}\right)-a)}$$

with

Equation 4:

$$\theta = \cos^{-1}\frac{-2a^3+9a-27c}{2\sqrt{(a^2-3b)^3}}$$

and

Equation 5: $$a = K_P + K_W + [P]_0 + [W]_0 - [A]_0$$

and

Equation 6: $$b = K_P([W]_0 - [A]_0) + K_W([P]_0 - [A]_0) + K_P K_W$$

and

Equation 7: $$c = -K_P K_W [A]_0$$

with $[A]_0$ being the total actin concentration, $[P]_0$ the total concentration of profilin, $[W]_0$ the total concentration of Atto488-WAVE1(WCA,) K_P the equilibrium dissociation constant for the interaction between profilin and actin and K_W the equilibrium dissociation constant for the interaction between Atto488-WAVE1(WCA,) and actin.

5.2.8.2 Thymosin-β4 binding affinity for actin monomers by fluorescence measurements

The binding of thymosin-β4 to actin monomers can be monitored by change in fluorescence intensity of IEDANS-labeled actin. Here the equilibrium dissociation constant (K_D) for thymosin-β4 binding actin monomers was determined by plotting the mean decrease in fluorescence intensity [au] against the increasing total thymosin-β4 concentration. The mean intensity values were calculated from at least three independent experiments per condition, error bars represent the SD. The data was fitted to a quadratic binding model as described in (Zalevsky et al., 2001):

Equation 8: $$I = I_f + (I_b - I_f)\frac{([K_D]+[A]+[T]) - \sqrt{([K_D]+[A]+[T])^2 - 4[A][T]}}{2[T]}$$

With [A] being the total concentration of IEDANS-labeled actin, [T] the total concentration of thymosin-β4, I_f and I_b the fluorescent intensities in the free and bound state, respectively and K_D being the equilibrium dissociation constant.

5.2.8.3 Calculations of free actin, profilin and thymosin-β4 species

Free actin, profilin, thymosin-β4 (if added) and profilin-actin complex concentrations were calculated from the total concentration of actin, profilin and thymosin-β4 (if added) in the

single filament TIRF-M assays (see Figure 18B). For the calculations of free species, an exact two species competition model as described in (Wang, 1995) and previous (see section 5.2.8.1) was used.

5.2.8.4 Cell volume measurements by fluorescence eXclusion measurements

Data analysis was performed using codes for MATLAB 2017b software designed by QuantaCell. First, the raw images were normalized following a manual cell tracking as it has been described earlier from (Cadart et al., 2017). For each cell type ≥ 300 single cells were analyzed. The cell volume distribution was plotted as a histogram and a lognormal distribution curve was fitted over the histogram. The mean volume [μm^3] and the error (SD) for each cell type and each condition was calculated.

5.2.8.5 Association rate constant for profilin binding to actin monomers by stopped flow

To determine the association rate constant for profilin binding to actin monomers, changes in tryptophan fluorescence were monitored over time upon profilin titration into a constant amount of actin. The measured decrease in tryptophan fluorescence [au] (tryptophan quenching) over time was plotted on a logarithmic scale for all profilin concentrations. Next, the data was fitted with the following mono-exponential decay function to determine the observed reaction rate k_{obs}:

Equation 9: $$I(t) = (I_f - I_b) * e^{(-k_{obs}x)} + I_b$$

With I(t) being the measured fluorescent intensity over time, I_f and I_b the tryptophan fluorescence in the free and the bound state respectively and k_{obs} being the observed reaction rate.

Following the determination of the association rate constant (k_{on}) from linear regression fits of the k_{obs} values as function of the total profilin concentration, the dissociation rate constant (k_{off}) could be calculated from the known equilibrium dissociation constants (K_D) and association rate constants (k_{on}) as follows:

Equation 10: $k_{off} = K_D * k_{on}$

Errors for the dissociation rate constants were calculated using error propagation:

Equation 11: $\Delta k_{off} = \sqrt{(\Delta K_D * k_{on})^2 + (\Delta k_{on} * K_D)^2}$

5.2.8.6 Quantification of in vivo profilin and actin by western blot analysis

The quantification of profilin and actin amounts per cell was performed by quantitative western blot analysis. The signal of fluorescently labeled secondary antibodies was detected by an Odyssey Imaging System (LI-COR Biotechnology). The detected fluorescence signal intensity of the distinct protein bands on membranes scans were analyzed in ImageJ first by selecting each of the detected intensity areas (cellular protein and reference protein) with the *rectangular tool*. After equal sized areas were selected, all lanes were plotted in an intensity plot profile reflecting the pixels across the selected area using the command *plot lanes*. Next, by drawing a straight line through the intensity curve at a basal height created by the background intensity, the signal intensity of the background was excluded from the protein intensity profile. Then, the protein signal intensity, which is represented as the area under the intensity profile, was measured by selecting the *tracing tool* and clicking anywhere under the curve to integrate the intensity signal of the area of the plot profile. To determine in vivo profilin and actin amounts, intensities of the corresponding reference protein samples were plotted over the loaded protein mass [ng]. After fitting the calculated values to a linear function, the mass of the in vivo proteins could be calculated from the slope of the reference protein.

To calculate protein concentration per cell, it was necessary to determine the average single cell volume next to the protein mass. While actin and profilin are excluded from the endomembrane system (ER, Golgi, Mitochondria etc.) that occupies roughly 50 % of the cell measured by tomography methods, only half of the total cellular volume was considered to calculate profilin and actin concentrations per cell. The protein concentration of actin and profilin was calculated as follows:

Equation 12: $protein\ concentration = \frac{protein\ mass}{molecular\ weight * 0.5 * cell\ volume}$

This assumption results in an overestimation of the protein concentration by maximally 2x-fold in the most extreme cases where it would be possible that both, profilin and actin, can explore the complete cellular volume.

5.2.8.7 Barbed end elongation velocity from single filaments by TIRF-microscopy

Image sequences were opened with ImageJ followed by the adjustment of brightness and contrast, image sequences were converted into a time-projection. All filaments were manually tracked using the *segmented line tool* from ImageJ. Next, two-dimensional space-time plots were created using the *kymograph plugin*. To calculate polymerization rates of individual filament barbed ends, the slopes of the corresponding kymographs were measured. The pixel size/length was converted into monomers/s or microns/s. One actin monomer contributes to 2.7 nm of the actin filament length. The filament barbed end polymerization velocity was measured from ≥40 filaments in 3 independent experiments for each experimental condition. The calculated polymerization rates were reported as mean values with bars representing the standard deviation (SD). The filament polymerization speed (growth velocity) as a function of the total profilin-actin concentration was fitted by a hyperbolic model:

Equation 13: $$v([PA]) = \frac{v_{max}[PA]}{K_{0.5}+[PA]}$$

With [PA] representing the total profilin-actin concentration, v_{max} the maximal filament polymerization velocity at saturated profilin-actin concentrations and $K_{0.5}$ the profilin-actin concentration at half-maximal polymerization speed.

5.2.8.8 Formin single molecule velocity in vivo

Movements of single formin molecules in vivo were either manually tracked with the *segmented line tool* from ImageJ after generating a time-projection of the image sequence or analyzed by automated tracking via the ImageJ *TrackMate plugin*. For the manual tracking, kymographs were generated (as described earlier for the single filament analysis) and the slopes were measured to determine the single formin velocity. The pixel size/length was converted into microns/s. One actin monomer contributes to

2.7 nm of the actin filament length. For each experimental condition ≥10 cells and ≥35 single molecules per cell were analyzed. The calculated mean speed values were plotted as a histogram and fitted with a Gaussian function. The error is representing the SD.

6 Results

6.1 Profilin and actin levels in mammalian cells

The actin cytoskeleton has numerous important roles in all eukaryotic cells including the determination of the cellular shape and the organization and maintenance of the interior of cells. The cytoskeleton is built from actin monomers which assemble into actin filaments. Actin filaments undergo polymerization and depolymerization via the assembly and disassembly of monomers at the filament ends. In vivo, actin monomers are bound to monomer binding proteins. The major actin monomer binding protein is profilin. Profilin binds actin in a 1:1 stoichiometry and prevents spontaneous filament polymerization by shielding the barbed end face actin. However, since the pointed end face of the actin monomer is not bound to profilin, these complexes are still able to polymerize. Profilin-actin complexes are considered to act as the physiological substrate for filament polymerization in cells. A crucial aspect in the regulation of filament assembly speed is the concentration of available substrate. The amount of polymerizable monomers was identified as a key factor which directly controls filament growth in a linear fashion (Figure 10). The conclusion of a linear relationship between filament growth speed and available profilin-actin has been drawn from results of in vitro reconstitution experiments. Importantly however, these experiments were carried out at non-physiological monomer concentrations only. How filament assembly is controlled at much higher and variable amounts of soluble monomers, found in vivo, is still a key unresolved question (Figure 10).

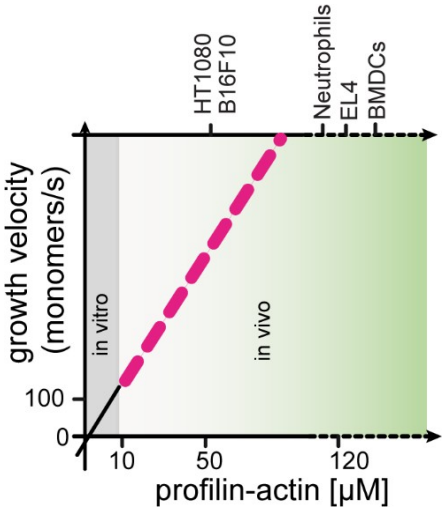

Figure 10: Scheme of actin filament barbed end growth rate linearly depending on the profilin-actin substrate concentration. Top axis shows determined profilin-actin concentrations for different cell types as indicated (see Figure 11). Black line: filament growth rate from in vitro reconstitution studies, magenta dashed line: assumed filament growth dynamics at in vivo profilin-actin levels.

To study actin filament polymerization in vitro under physiologically relevant profilin-actin concentrations, we determined the total concentration of actin and profilin (isoforms 1 and 2) (Mouneimne et al., 2012) across a selection of several mammalian cells (Figure 11). Cell types that were analyzed in terms of their profilin and actin concentration were HT1080 (mesenchymal), B16F10 (epithelial) or immune cells (EL4-T-cells, BMDC-dendritic cells and neutrophils). The class of immune cells was especially interesting because of their ability to move rapidly (Vargas et al., 2016a) possibly caused by fast turnover of the actin cytoskeleton. For the determination of in vivo profilin and actin concentrations we performed quantitative western blot analysis combined with fluorescence eXclusion single cell volume measurements (see methods) (Cadart et al., 2017). The quantifications showed, that both actin and profilin were expressed to high levels (with total actin >150 µM and total profilin >50 µM) in all tested cell types (Figure 11). These results are consistent with earlier studies (Pollard et al., 2000; Witke et al., 2001). The amounts of the profilin isoforms 1 and 2 were determined with profilin1 being the dominant isoform in contrast to profilin2, which was not expressed at substantial levels except in the primary dendritic cells (Figure 11). In all tested cell types, the total actin concentration was always equal to or exceeding the total profilin concentration. This result was expected because actin polymerizes into filaments and

binds to monomer binding proteins such as profilin as well as others (e. g. thymosin-β4). Importantly, profilin binds much more tightly to mammalian cytoplasmic actin monomers (K_D~18 nM, see Figure 13A) than other monomer binding proteins (e. g. thymosin-β4 K_D~1.2 µM, see Figure 13B). The amount of actin monomers is therefore likely large enough to completely bind all profilin molecules in vivo. We thus estimate the profilin-actin concentration to a range of 52 to 144 µM in the examined mammalian cell types (Figure 11).

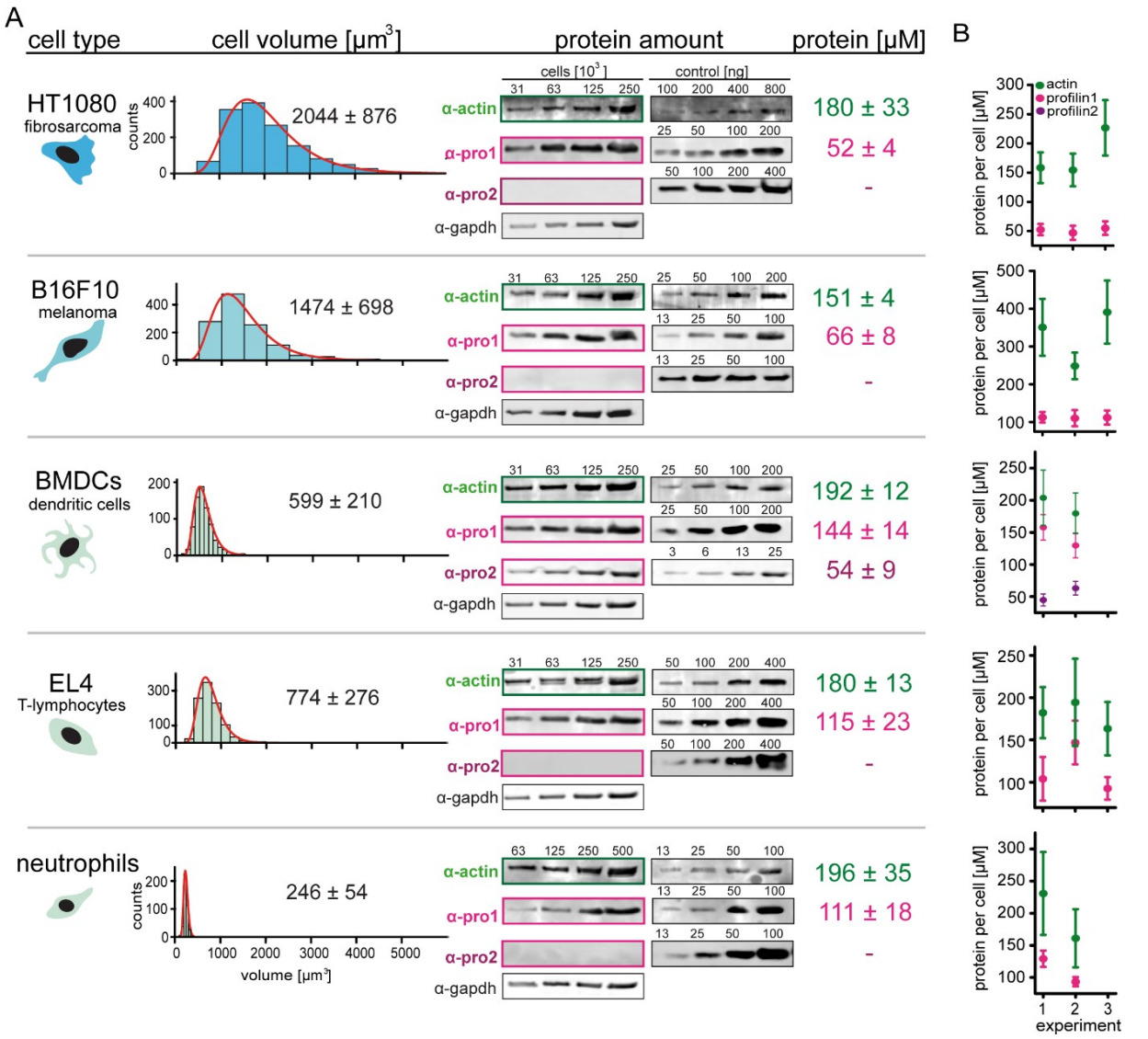

Figure 11: Profilin-actin levels in vivo. A. Measurements of profilin-actin in various cell types as indicated. Left to right: cell type, single cell volume histogram, quantitative western blots of actin, profilin1/2 (with left-cell titrations, right-reference curve of recombinant proteins), mean protein values (N=3) and SD. As a loading control GAPDH was detected by a specific monoclonal antibody. B. Plotted profilin and actin protein concentrations from individual experiments.

Importantly, the profilin:actin ratio was shifted to profilin being higher expressed in the smaller sized immune cells. This result is in line with their fast motility. To rapidly move and adhere to low-adhesive surfaces, these cells have to rapidly generate actin-rich lamellipodia. To this end immune and other fast migrating cells have to maintain a larger pool of polymerizable actin substrate than other non-motile cells.

6.2 Characterization of actin and its major monomer binding proteins

Up to this point actin filament elongation dynamics have only been shown for a very limited concentration regime far below the profilin-actin levels found in cells. This reveals a large gap in understanding the actin dynamics at actin levels that are of physiological relevance. So far we do not know how cells control filament growth under these conditions.

To assess, whether filament polymerization is limited at high physiologically relevant profilin-actin levels, we studied polymerization dynamics over a wide concentration regime which was previously inaccessible using TIRF-M imaging. Up to this point, most previous studies performed filament polymerization assays using labeled actin monomers (Kuhn and Pollard, 2005). This strategy however is limited since it leads to increasing fluorescent background signal upon increasing monomer concentrations. Another issue in previous experiments was an increase in spontaneous polymerization of filaments by the use of free actin monomers as a substrate. Above a certain threshold, the increasing density of filaments becomes incompatible with the data analysis. Furthermore, we improved the filament tethering on the surface of our assay chamber since tethering efficiency becomes important when following filament ends at high polymerization rates. In case of low filament tethering, growing filaments undergo high random movements which will interfere with a precise data analysis.

Up to this point, most studies (Breitsprecher et al., 2009; Kuhn and Pollard, 2005; Winterhoff et al., 2016) have specifically used the muscle α-actin isoform which is very easy to purify in high yields from muscle tissue. The α-actin isoform is however, the most divergent among all three actin isoforms. α-actin was often combined with a chemical label located close to the profilin binding site. The position of the actin label

lead to different biochemical properties of the profilin-actin interaction resulting in conflicting findings in the field and thus created controversy (Blanchoin and Pollard, 2002; Courtemanche and Pollard, 2013; Kinosian et al., 2000, 2002; Pernier et al., 2016; Romero et al., 2007; Vavylonis et al., 2006). However, all of these biochemical limitations were improved in this work and will be discussed individually in the following sections.

To study actin filament elongation dynamics under physiologically relevant substrate conditions, we first developed new methods to purify high amounts of mammalian cytoplasmic actin isoforms β and γ (Hatano et al., 2018; Ohki et al., 2009). We developed strategies to purify cytoplasmic actin from two different sources as follows (Figure 12A):

1. Native bovine actin (β, γ – isoforms) purified from thymus tissue which is identical in sequence to the human cytoplasmic actin isoforms (Figure 12A left). Briefly, I lysed and mixed fresh thymus tissue with the appropriate amount of 10xhis-tagged gelsolin G4-6. After gelsolin-actin complex formation, the complex was bound onto an IMAC column and the actin monomers were eluted by Ca^{2+} sequestration. Next, I separated functional actin monomers from non-polymerizable actin and other contaminants by one cycle of polymerization and depolymerization.

2. Recombinant human β actin purified from insect cell expression (Figure 12A right). Following the expression of actin fused to his-tagged thymosin-β_4, I purified the protein over an IMAC column. Next, I cleaved thymosin-β_4 off the actin monomers by α-chymotrypsin. After complex elution I separated the actin monomers from non-polymerizable monomers/non-cleaved complex by one cycle of polymerization and depolymerization.

Both purification strategies succeeded in high yields and protein purity. Furthermore, the cytoplasmic mammalian actin from either native or recombinant origin was polymerizing into actin filaments with overall similar rates (Figure 12B) to muscle or cytoplasmic isoforms from other organisms (Hansen and Mullins, 2010; Kuhn and Pollard, 2005).

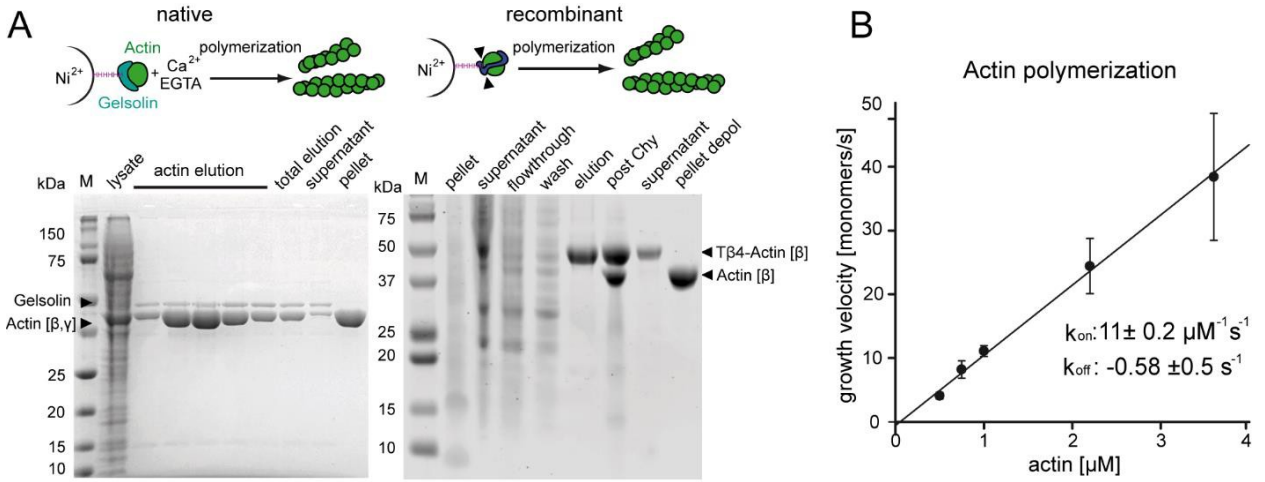

Figure 12: Purification scheme of isoform mixed β, γ and isoform pure β cytoplasmic actin and characterization of actin polymerization dynamics. A. Purification of mammalian cytoplasmic actin from two sources. Top: schematic workflow of the cytoplasmic actin purification. Left: Native purification of β, γ – actin by gelsolin affinity chromatography. Complexes composed of gelsolin and actin were formed in a presence of calcium. After IMAC purification calcium was sequestered through EDTA and actin monomers were eluted. Functional actin monomers were separated from non-polymerizable actin and other contaminants through polymerization. Right: Purification of recombinant isoform pure h. s. β – actin. β – actin was expressed with a C-terminal linker-thymosin β_4 -10xhis and purified by IMAC followed by chymotrypsin cleavage (▼) to separate monomers from the linker-thymosin β_4. Finally monomers were separated from contaminants through polymerization. Both purification protocols result in very pure and high yields of protein which is ascertained from the last pellet fraction. B. Actin filament barbed end polymerization rate of mammalian cytoplasmic β, γ - actin as a function of the actin monomer concentration. The mean values were fitted with a linear function and the following rate constants were calculated from the fit: k_{on} = 11 ± 0.2 μM^{-1} s^{-1} and k_{off} = -0.58 s^{-1}.

In order to examine the binding of the physiological most abundant monomer-binding proteins profilin1/2 and thymosin-β_4 to actin monomers prepared for this work, I performed competition - and actin monomer-binding assays at near-physiological ionic strength. Similar to previous studies working with cytoplasmic actin (Bieling et al., 2018; Didry et al., 2012; Kinosian et al., 2002), the binding affinity measured for both human profilin isoforms (1 and 2) to actin monomers in the ATP bound state was remarkably strong (K_D ~ 18 nM) (Figure 13A). In contrast, I could show that the binding affinity of thymosin-β_4 to ATP bound actin monomers was very low (K_D ~ 1.2 μM) (Figure 13B). Indeed it is known that thymosin-β_4 does not directly participate in filament polymerization but rather sequesters soluble actin monomers.

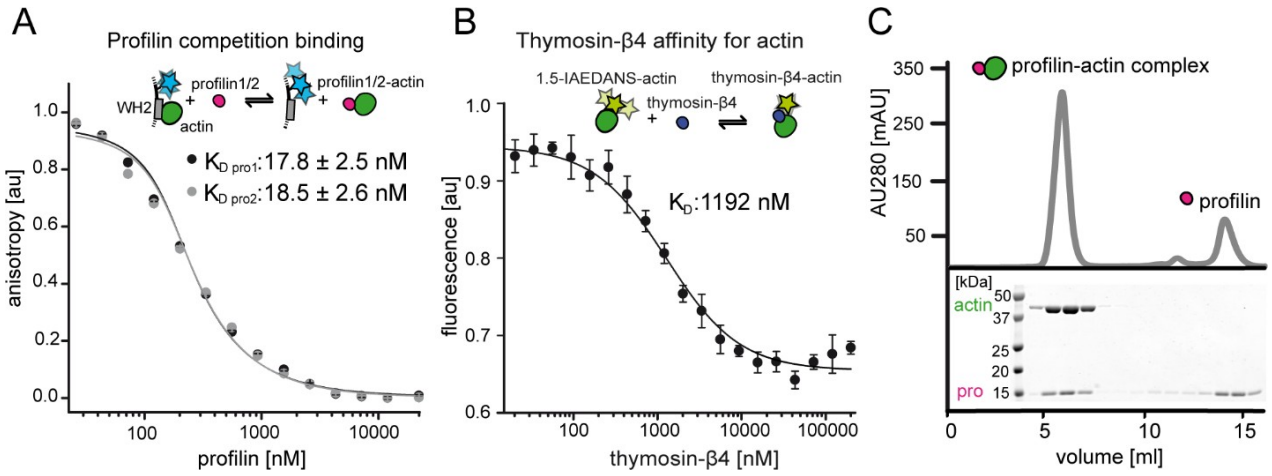

Figure 13: Characterization of the actin monomer binding proteins profilin1/2 and thymosin β₄ and the purification of profilin-actin complexes. A. Determination of binding affinities for profilin1 and 2 to ATP bound cytoplasmic actin monomers by fluorescence anisotropy competition experiments. Fluorescence anisotropy of Atto488WAVE1$_{WCA}$ [4 nM] was monitored at indicated increasing profilin1 and 2 concentrations in presence of fixed amount of 150 nM ATP-bound actin monomers. Mean values [N = 3] were fitted by an exact analytical competition model (Wang, 1995). Errors are SD. B. Determination of thymosin β$_4$ binding to ATP-bound cytoplasmic actin monomers by fluorescence change experiments. Fluorescence measurements of 150 nM 1.5-IAEDANS labeled ATP-bound cytoplasmic actin monomers as a function of increasing thymosin β$_4$ concentration (as indicated). Mean values [N = 3] were fitted to a quadratic binding model (see Methods). Errors are SD. C. Purification of stoichiometric profilin-actin complexes from free profilin by size exclusion chromatography. Both, gel and chromatogram, reveal high purity of the complex fraction.

Due to the strong binding of profilin to cytoplasmic actin monomers, I could isolate heterodimeric profilin-actin complexes and separate them from free species by size-exclusion chromatography (Figure 13C). In the absence of monovalent salts and magnesium ions, I could concentrate the complex higher than 500 µM without initiating spontaneous nucleation of actin filaments. In contrast to the tight binding of profilin to cytoplasmic actin isoforms, profilin binding to α-actin monomers is rather weak (K_D ~ 500 nM) as previous studies could show (Vinson et al., 1998). Thus, complexes of profilin and α-actin could not be produced to similar high levels due to low affinity resulting in the accumulation of free monomers which cause spontaneous nucleation of filaments upon complex concentration.

6.3 Visualization of actin filament assembly at near-physiological monomer levels

To study the dependency of filament growth speed on available monomers at physiologically relevant monomer levels, I visualized the elongation of actin filaments close to a glass surface by using total internal reflection fluorescence microscopy (TIRF-M) (Figure 14 left and Figure 16A). I used a streptavidin – biotin-phalloidin linker (Bieling et al., 2010) to tether actin filament onto a PEG-biotinylated glass surface upon polymerization (Figure 16A&B, see methods). Similar experiments in the past were carried out using labeled actin monomers to follow filament elongation (Kuhn and Pollard, 2005). However, labeled monomers can only be used in a very low monomer concentration regime (Figure 14 upper), because of two reasons: i) the label (commonly located at position C374 at the monomer) interferes with profilin binding and thus promotes spontaneous nucleation, ii) labeled monomers create a high fluorescent background with increasing monomer concentrations preventing filament visualization at monomer concentrations greater than 10 µM.

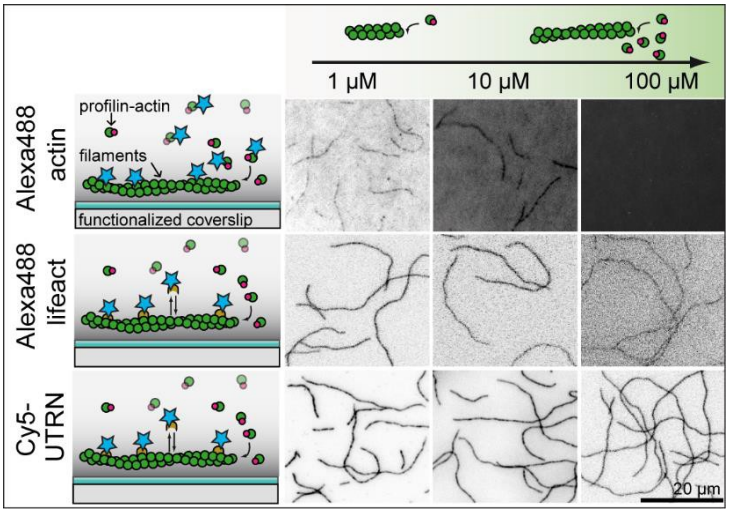

Figure 14: Labeled actin monomers versus actin filament binding probes. Left: Scheme of different filament polymerization TIRF-M assays using either labeled actin monomers (upper) or filament binding probes (middle, lower) as indicated. Right: TIRF-M images of polymerized filaments at indicated profilin-actin concentration visualized by either using Alexa488-labeled monomers (20 % labeled, top) or actin filament binding probes: middle – 10 nM Alexa488-LifeAct, lower – 10 nM Cy5-UTRN$_{261}$. While the filament detection at high profilin-actin concentrations (100 µM) is impossible using labeled monomers, both of the filament binding probes show good signal to noise ratios under all conditions with Cy5-UTRN$_{261}$ being the most efficient labeling probe.

To overcome these limitations, we established a different approach based on the use of fluorescently tagged, filament binding proteins. Therefore, I applied low amounts (10 nM) of fluorescently tagged filament binding probe to the polymerization assay, to monitor filament elongation in real time at physiologically relevant monomer levels (Figure 14 middle and lower).

Both utrophin ABD - $UTRN_{261}$ (Figure 14 lower) (Burkel et al., 2007), or LifeAct (Figure 14 middle) (Riedl et al., 2008), filament binding probes used in this study, provided sufficient contrast to visualize filament elongation and furthermore did not filament assembly kinetics (Bieling et al., 2018).

Although spontaneous nucleation of actin filaments is minimized by the polymerization of filaments from profilin-actin complexes rather than from free monomers, spontaneous nucleation will increase upon increasing complex concentration. This is resulting from actin being in a dynamic equilibrium with profilin. To further reduce spontaneous filament nucleation, we supplemented the reaction mix with low amounts of either free profilin (<2 µM profilin at 10-100 µM profilin-actin) or thymosin-β_4 (<15 µM thymosin-β_4 at profilin-actin >100 µM) (Figure 15A&B). Free profilin or thymosin β_4 were shown to inhibit actin polymerization by blocking the barbed end (Courtemanche and Pollard, 2013). Importantly, we ruled out that filament elongation rates did not saturate because of the accumulation of free profilin. Based on mass-action calculations, we could reveal that not more than 5 µM free profilin and or 11 µM of free thymosin β_4 is accumulating in our experiments. These low amounts of free profilin or thymosin-β_4 did not alter the overall filament elongation kinetics since polymerization rates were constant under all conditions (Figure 18B). Together the combination of all technical improvements described allowed the monitoring of actin filament polymerization at physiologically relevant concentrations up to 200 µM of mammalian cytoplasmic actin in real time for the first time.

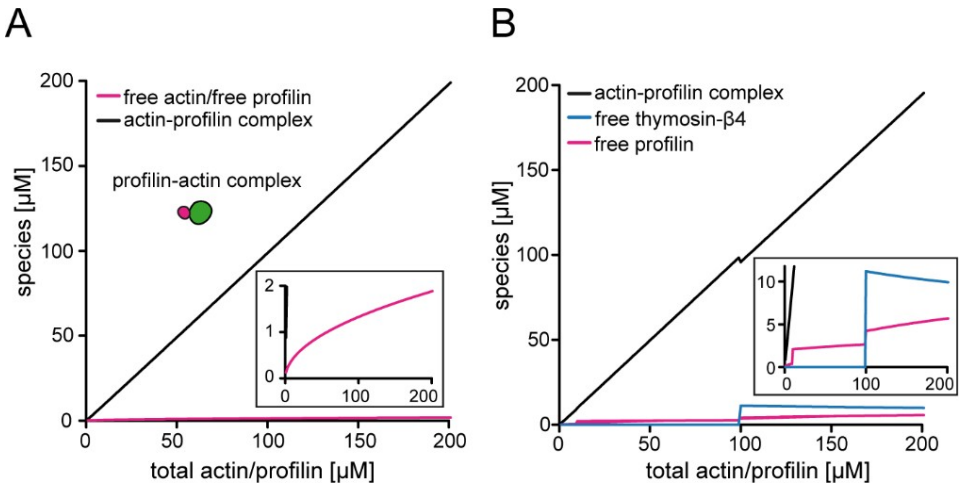

Figure 15: Calculations of free and complexed species upon increasing total actin and profilin. A. Calculations of free actin, free profilin (see also inset) and profilin-actin complex [µM] as a function of the total profilin-actin concentration (see methods). B. Calculations of free profilin, free thymosin β_4 (see also inset) and profilin-actin complex [µM] as a function of the total profilin-actin concentration (see methods) in presence of additional 2 µM profilin (between 10-100 µM total profilin-actin) or 15 µM thymosin β_4 (≥100 µM total profilin-actin) to minimize residual spontaneous filament nucleation (see methods).

6.4 The actin filament elongation cycle is kinetically limited at physiologically relevant profilin-actin concentrations

As it was described by previous studies (Blanchoin and Pollard, 2002; Jegou et al., 2013), we detected a linear increase in actin filament growth speed upon increasing monomer levels up to 10 µM profilin-actin (Figure 16C inset). Strikingly we could show that a further increase in profilin-actin >20 µM surprisingly lead to a deviation of the filament elongation speed from linear growth rates detected at lower substrate levels. Notably, at high profilin-actin levels (≥100 µM) filament growth speed started to saturate and leveled off at elongation rates of around 500 monomers * s^{-1} (Figure 16C).

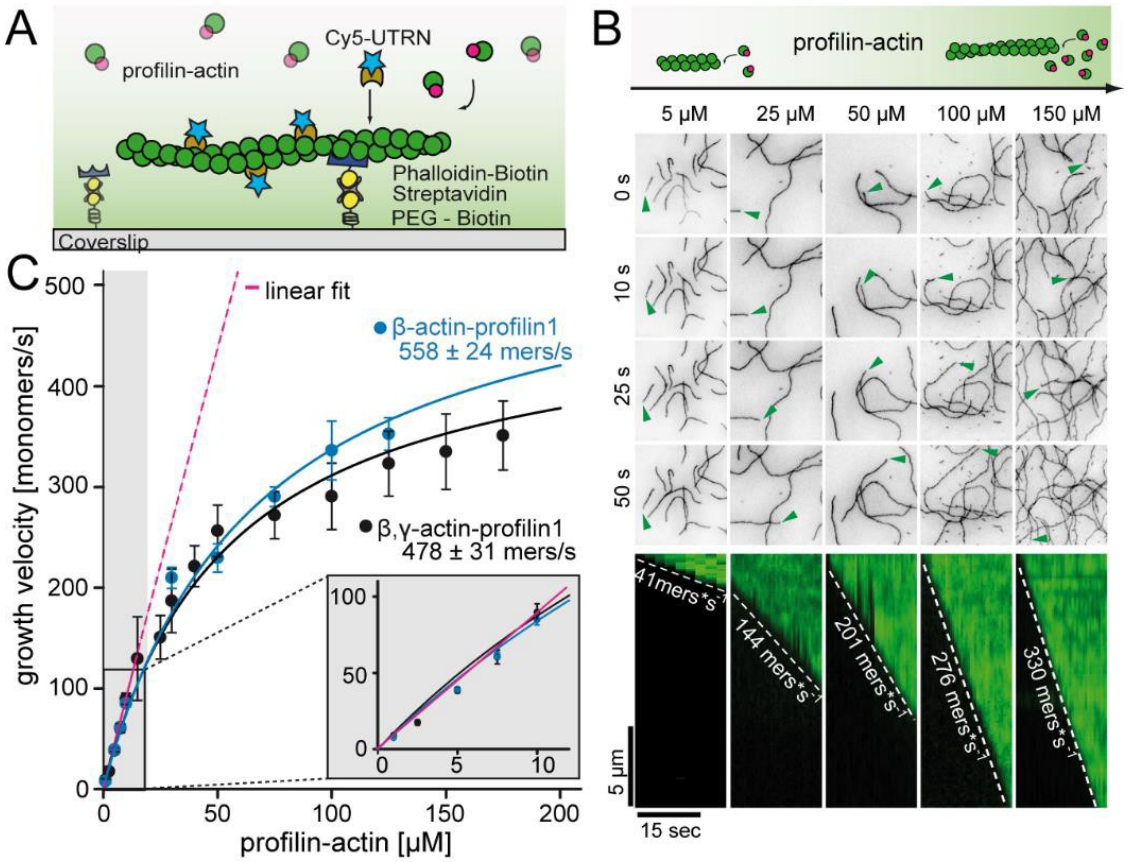

Figure 16: Actin filament elongation from physiologically relevant profilin-actin levels is kinetically limited. A. Scheme of TIRF-M single filament assays. Filaments are tethered to the PEG-biotin functionalized glass coverslip surface by a streptavidin-biotin-phalloidin linker and visualized by Cy5-UTRN filament binding probe. B. Time-lapse images from TIRF-M assays (top) and representative kymographs (bottom) of actin filament elongation at different time points and increasing profilin-actin concentrations as indicated (green error follows a single filament barbed end). C. Barbed end growth velocities from single filament TIRF-M assays at different profilin-actin concentrations as indicated. Mean velocities [N ≥ 40 for each condition, error = SD] were fit by a hyperbola function (see methods), in addition the low substrate concentration regime was fit by a linear function.

Importantly, filament polymerization rates were very similar when performing polymerization assays with recombinant β isoform actin only or native purified β, γ actin (Figure 16C).

To further assess whether the rate limiting reaction in filament elongation is sensitive to the profilin isoform bound to actin monomers, I performed polymerization assays from either profilin1- or profilin2-actin complexes. Importantly, the maximal filament elongation rates were nearly identical when using either profilin1 or profilin2 isoforms in complex with actin monomers as substrate for polymerization (Figure 17). Together the data

indicates, that the rate-limiting reaction in filament elongation is neither sensitive to changes in the actin isoform nor sensitive to the profilin isoform.

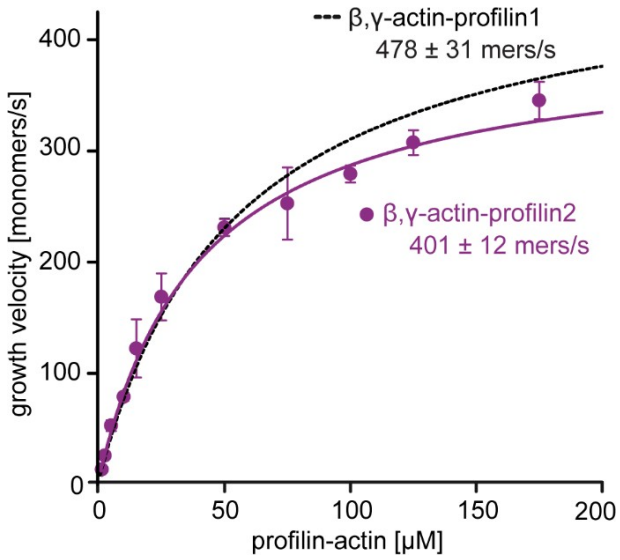

Figure 17: Filament barbed end polymerization velocities measured for profilin1 and 2 isoforms complexed with β, γ - actin. Calculated mean values [N≥ 40 for each condition, error = SD] of the filament polymerization rate at distinct profilin – actin concentrations as indicated were fit to a hyperbola function. Maximum filament growth velocities from the fits are indicated.

Why do the observed filament growth rates saturate with increasing substrate concentration? In order to exclude, that this is not an artificial result potentially created by the nature of the filament labeling probe or the filament tether, control experiments were performed (Figure 18A): Single filament polymerization assays (Figure 18A) using different actin filament labeling probes (utrophin or LifeAct) did not show any changes in filament elongation speed. This verifies that the maximal elongation rate does not depend on the nature of the filament binding probe. To assess whether the type or the degree of surface tethering interferes with actin filament elongation at the barbed end, we applied different filament tethering molecules (biotinylated heavy-mero-myosin or biotin-phalloidin linker) to the surface of the cover slip and we were testing different low or high concentrations of biotin-phalloidin linker (20 and 200 nM). The filament elongation speed at 100 μM was very similar for all tested conditions, which shows that neither the type nor the degree of filament surface tethering limits filament elongation (Figure 18A).

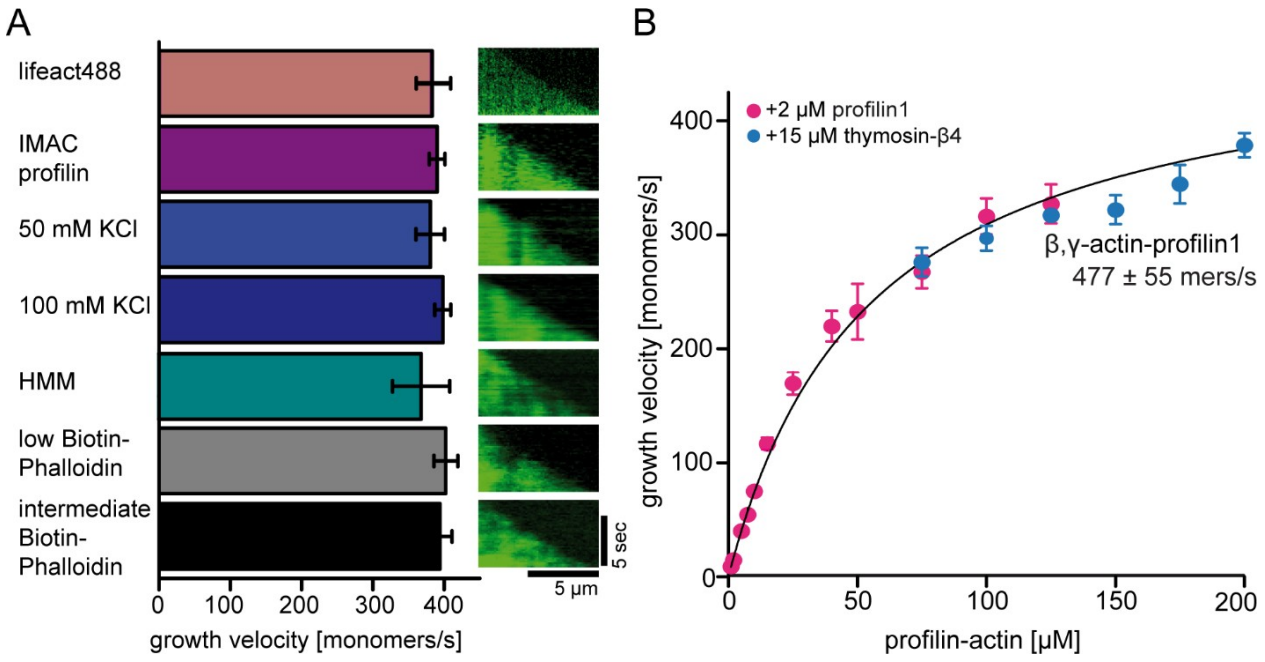

Figure 18: Single filament TIRF-M control experiments. A. Control experiments showing that the maximum filament barbed end polymerization rate is not impaired by the filament binding probe, the profilin purification strategy, the ionic strength of the reaction buffer or the surface tethering. Left: Bar diagram of the filament barbed end growth velocity at 100 µM profilin – actin. The results of the following conditions are represented: filament binding probes (upper 1_{st} –lifeact488, all others – Cy5UTRN$_{261}$), profilin purification strategy (upper 2_{nd} – IMAC purified, all others – native purification), ionic strength (50 and 100 mM KCl), surface tethering (HMM, biotin-phalloidin either at low – 20 nM or at intermediate – 200 nM concentration). Right: Kymographs representing individual filaments under the specific reaction condition (see left). B. Filament barbed end polymerization velocities measured in TIRF-M single filament experiments using profilin1 - β, γ actin as a substrate. In addition, 2 µM free profilin1 (magenta) or 15 µM thymosin $β_4$ (blue) were included into the reaction mix at individual and overlapping profilin-actin concentrations as indicated. Calculated mean values [N≥ 30 for each condition, error = SD] of the filament polymerization rate at distinct profilin – actin concentrations were fit to a hyperbola function yielding the maximum filament growth rate at saturation as indicated.

Does the interaction of free profilin with the filament barbed end lead to a slow-down in actin elongation? Previous studies (Courtemanche and Pollard, 2013; Pernier et al., 2016; Pollard and Cooper, 1984) showed that an increase in free profilin concentration has an inhibitory effect on filament barbed end polymerization through barbed end interaction with free profilin. We thus tested whether: i) the accumulation of free profilin is responsible for a slow-down of filament polymerization and ii) free amounts of additionally added profilin and thymosin-$β_4$ to prevent spontaneous polymerization, were decreasing elongation rates (Figure 18B). Importantly, we show that additional amounts of free profilin or thymosin-$β_4$ did not change polymerization dynamics. Moreover,

polymerization experiments were monitored over a short time course. During this time, the filament growth speed was constant which is represented in the non-changing angle from the two-dimensional space-time plots (Figure 16B & 18A).

To further make sure, that the profilin-actin substrate concentration is always kept constant and the accumulation of free profilin can be excluded, we performed polymerization experiments under constant substrate flow in a microfluidic chamber (Figure 19A-C).

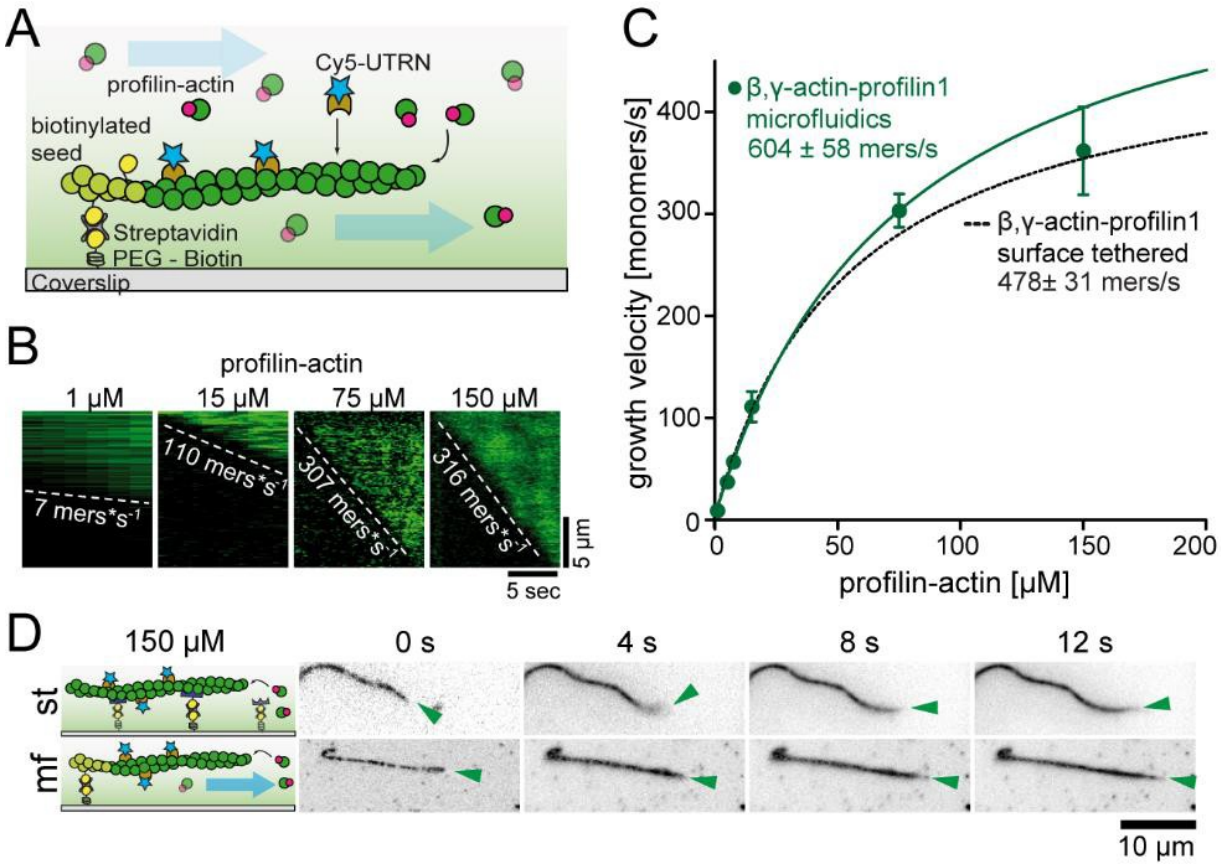

Figure 19: TIRF-M single filament experiments using a microfluidic setup. A. Scheme of experimental microfluidic setup. Actin filaments were grown under flow from biotinylated surface tethered seeds and visualized by Cy5-labeled filament binding probe UTRN. B. Kymographs of representative filaments elongating under flow at distinct indicated profilin-actin substrate concentrations. C. Filament barbed end polymerization velocities measured in TIRF-M single filament experiments using profilin1 - β, γ actin as a substrate. Elongating filaments were either surface tethered along their length (black dashed, as quantified in Figure 16C) or grown from seeds in microfluidic channels (green). Calculated mean values [N≥ 40 for each condition, error = SD] of the filament polymerization rate at distinct profilin – actin concentrations were fit to a hyperbola function. D. Time lapse images from TIRF-M single filament experiments showing representative filaments over time that were either surface tethered (st) along their length or grown in a microfluidic setup (mf) from a stabilized surface tethered seed only. Experiments were carried out at 150 µM profilin-actin. The growing filament barbed end is indicated by a green error.

To examine filament elongation under constant influx of fresh profilin-actin, all filaments were grown from the barbed end of short phalloidin stabilized filaments while the pointed end was anchored to the surface of the flow chamber (Figure 19D, see methods). Importantly, elongation rates of surface tethered filaments and filaments grown under flow were very similar (Figure 19C).

Because filament elongation rates were constant over time under all conditions, we ruled out accumulation of free profilin as a reason for the saturation of filament elongation rates. Collectively our findings demonstrate, that actin filament elongation at physiologically relevant substrate concentrations is not controlled by the diffusion-limited association of profilin-actin onto the filament barbed end. Instead, we find a kinetic limiting reaction within the elongation cycle that proceeds with a rate constant of around 500 s^{-1}.

Which step of the actin elongation cycle might constitute the kinetic rate-limiting reaction we observe? Previous studies suggested that the incorporation of profilin-actin transiently caps the barbed end (Courtemanche and Pollard, 2013). It is proposed (Courtemanche and Pollard, 2013) that the profilin bound to the actin monomer which incorporates into the barbed end will sterically block the binding site on the filament barbed end for the next actin monomer (Figure 20A&B). Therefore, the release of profilin from the terminal subunit of the barbed end is essential to vacate the penultimate filament site for the next monomer to bind and to continue elongation (Figure 20B). In contrast to the very tight (K_D~ 18 nM) profilin-actin monomer interaction shown in Figure 13A, the binding affinity of profilin to the filament barbed end is significantly lower (K_D~ 20 µM) (Courtemanche and Pollard, 2013; Pernier et al., 2016). This large difference in profilin-binding affinity suggests that the conformation of actin subunits in the monomer state must be significantly different from the terminal bound subunit. In fact, the structures of actin monomers that are part of the internal filament and the monomer that is bound in a complex with profilin have been shown to be different (Carlier et al., 2015). Interestingly these observations argue for structural changes in the terminal actin subunit of the barbed end which would be required to promote profilin release. Interestingly, either of these two subsequent reactions: i) structural change of terminal actin subunit structure or ii) dissociation of profilin from the terminal actin

subunit; could constitute the rate-limiting reaction. Thus, changes in the profilin-actin binding interface should only affect the dissociation of profilin but not the conformation of the terminal filament subunit. To test whether the ii) hypothesis constitutes the kinetic bottleneck in actin assembly, we introduced point mutations into the actin binding interface of profilin1 (Figure 21) to either increase or decrease profilin affinity for actin monomers.

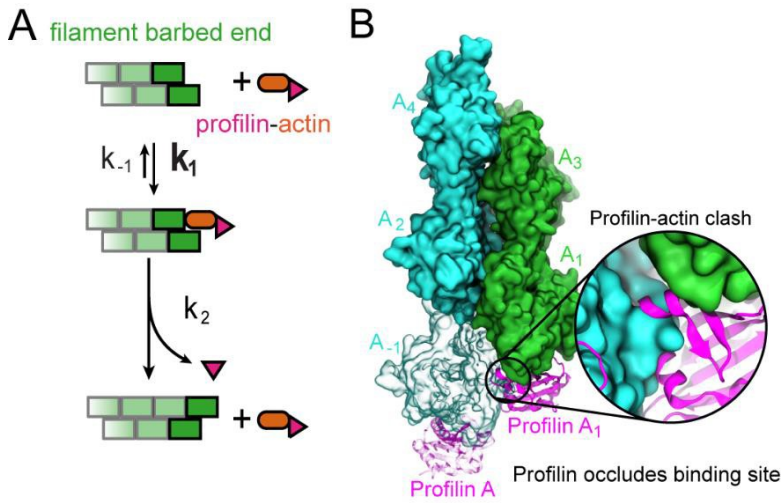

Figure 20: Limiting reactions at the actin filament barbed end. A. Scheme o filament barbed end elongation from profilin-actin with reaction rate constants (k_1, k_{-1}, k_2). B. Structural model of the actin filament barbed end decorated with profilin1 (see methods). Actin is drawn as a green surface, profilin1 as magenta ribbon structure and the new incoming profilin-actin complex is transparent. The model (inset) shows a structural clash between the profilin1 molecule located on the ultimate barbed end face and the new actin monomer that is being incorporated onto the barbed end.

6.5 Profilin dissociation kinetically limits actin filament polymerization at physiologically relevant monomer concentrations

Our structural model (see section 6.4) suggest that binding of profilin-actin onto the filament barbed end transiently caps the terminal protomer. Because profilin sterically clashes with the binding of the next actin monomer, profilin release from the barbed end first is required for elongation to continue. The release of profilin from actin monomers as well as filament ends should be directly affected by structural interactions of the profilin-actin binding interface. To alter the rate of release of profilin from the barbed end, we introduced specific point-mutations into profilin1 at positions located in the profilin-

actin binding interface. We selected specific mutated amino acids (K125/E129 and S71) based on a model built on the crystal structure of profilin-β-actin (Schutt et al., 1993) (see methods) which increase profilin binding affinity for actin (Figure 12A). Furthermore, we generated profilin mutants (E82A, R88K) which are known (Boopathy et al., 2015) to be involved in profilin-actin binding and thus decrease actin binding affinity upon mutation (Figure 12A).

I first performed competition anisotropy experiments to characterize the binding affinities of the profilin1 mutants to mammalian cytoplasmic actin monomers (Figure 21B). The combination of K125E+E129K mutations resulted in a ~ 5x-fold increase in monomer binding affinity, whereas both E82A and R88K single point mutations decreased (~ 1.5x and ~ 4x – fold, respectively) actin monomer affinity (Figure 21B&E). However, larger changes in the affinity were not compatible with single filament polymerization assays. Here, severely weakening mutants would cause accumulation of free actin resulting in massive filament nucleation. In contrast, very tight binding profilin mutants would result in the complete inhibition of filament growth (see Figure 23). We then performed stopped flow experiments to determine the dissociation rate constant of profilin1 mutants from actin monomers (Figure 21C&D). Combined, our results show that the observed changes in actin binding affinity were caused by an altered actin monomer dissociation rate constant, but not by an altered association rate constant (Figure 21E). Importantly, the release of wt and mutant profilin from the actin monomer is way too slow ((k_{off} = 0.77 s^{-1} for wt profilin (Figure 21C-E)) to account for the kinetic limiting step (~ 500 s^{-1}). However, since the k_{off}- measurements were performed on actin monomers, we suggest that actin monomers undergo large structural changes at least in the profilin-actin binding interface upon filament incorporation which promotes profilin to dissociate from the filament end.

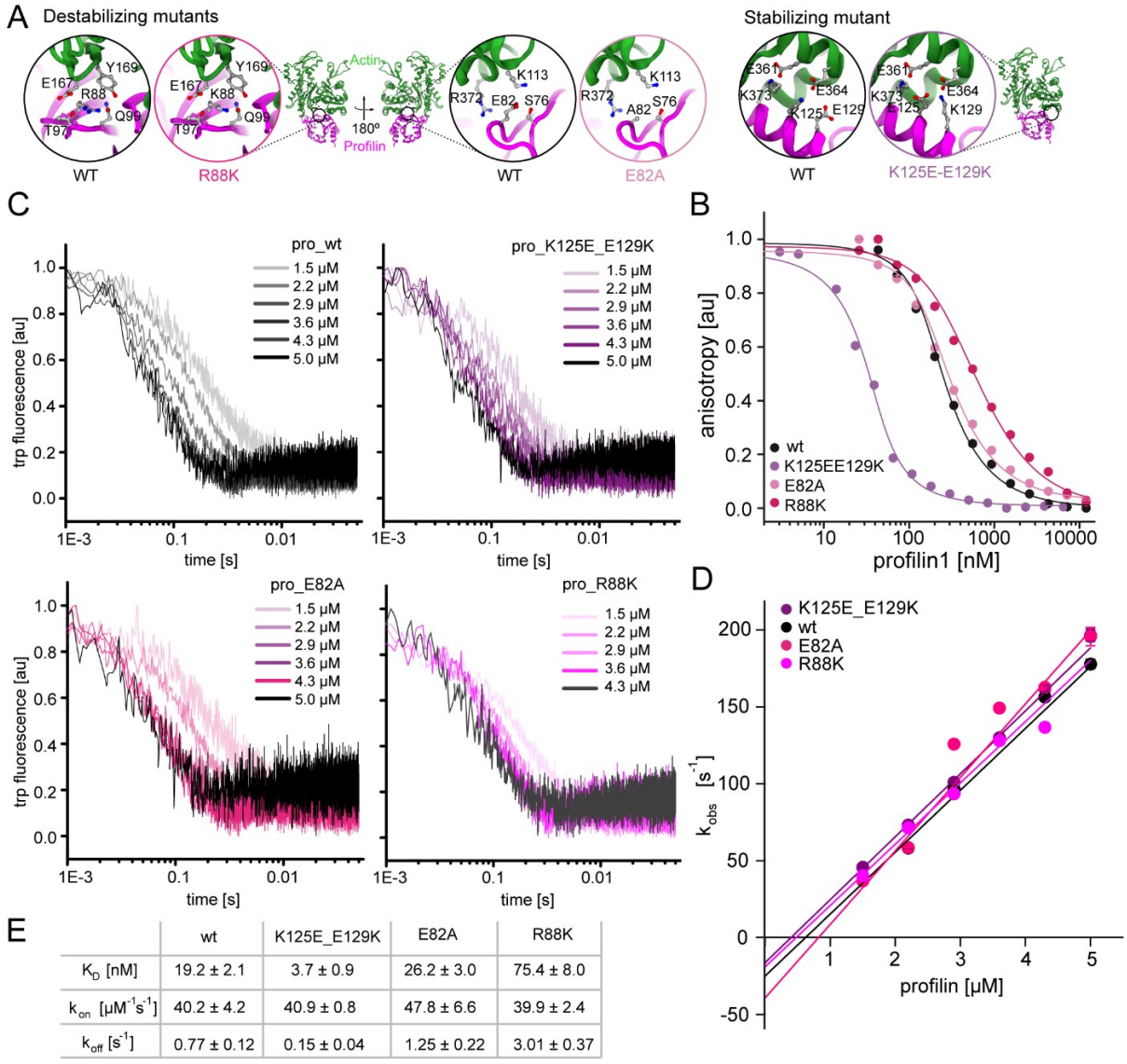

E

	wt	K125E_E129K	E82A	R88K
K_D [nM]	19.2 ± 2.1	3.7 ± 0.9	26.2 ± 3.0	75.4 ± 8.0
k_{on} [$\mu M^{-1}s^{-1}$]	40.2 ± 4.2	40.9 ± 0.8	47.8 ± 6.6	39.9 ± 2.4
k_{off} [s^{-1}]	0.77 ± 0.12	0.15 ± 0.04	1.25 ± 0.22	3.01 ± 0.37

Figure 21: Characterization of stabilizing and destabilizing profilin-mutants. A. Structural models of stabilizing (K125E + E129K) and destabilizing (R88K and E82A) profilin1 mutants (magenta) complexed with an actin monomer (green). Inset: highlighting the position of the point-mutation introduced into the profilin-actin binding interface region and changes in the amino-acid environment. B. Determination of binding affinities for profilin1 (wt and mutants) to ATP bound cytoplasmic actin monomers by fluorescence anisotropy competition experiments. Fluorescence anisotropy of Atto488WAVE1$_{WCA}$ [4 nM] was monitored at indicated increasing profilin1 concentrations in presence of fixed amount of ATP-bound actin monomers (150 nM for wt and weakly binding profilin or 40 nM for tightly binding profilin). Mean values [N ≥ 3] were fitted by an exact analytical competition model (Wang, 1995). Errors are SD. C. Tryptophan fluorescence quenching upon the complex formation of profilin (wt or mutant as indicated) - actin over time. To perform the experiments, a fixed actin concentration of 0.5 µM together with different profilin concentrations (as indicated) was used. The mean values [N ≥ 3 for each condition] were fit to a mono-exponential decay function (see methods) to derive the observed reaction rates (k_{obs}) plotted in D. D. The calculated K_{obs} values (derived from data shown in C) for distinct profilin concentrations (as indicated) were fit to a linear function and the association rate constants (k_{on}) could be calculated from the slope of the linear fits. E. Summarizing table of the equilibrium dissociation constant (K_D), the association rate constant (k_{on}) and dissociation rate constant (k_{off}) for the interaction of profilin1 (wt and mutants as indicated) and actin monomers. The dissociation rate constants were calculated from the measured equilibrium dissociation constant and association rate constants (see methods).

Next, we tested the impact of these profilin mutations in filament polymerization assays. Remarkably, the maximal velocity of filament polymerization scaled with the monomer dissociation rate constant and was inversely proportional to the monomer binding affinity. In line with the monomer binding affinity and the dissociation rate constants, weak binding profilin (E82A and R88K) increased whereas the tight binding profilin (K125E+E129K) decreased the maximum polymerization velocity (Figure 22A-C).

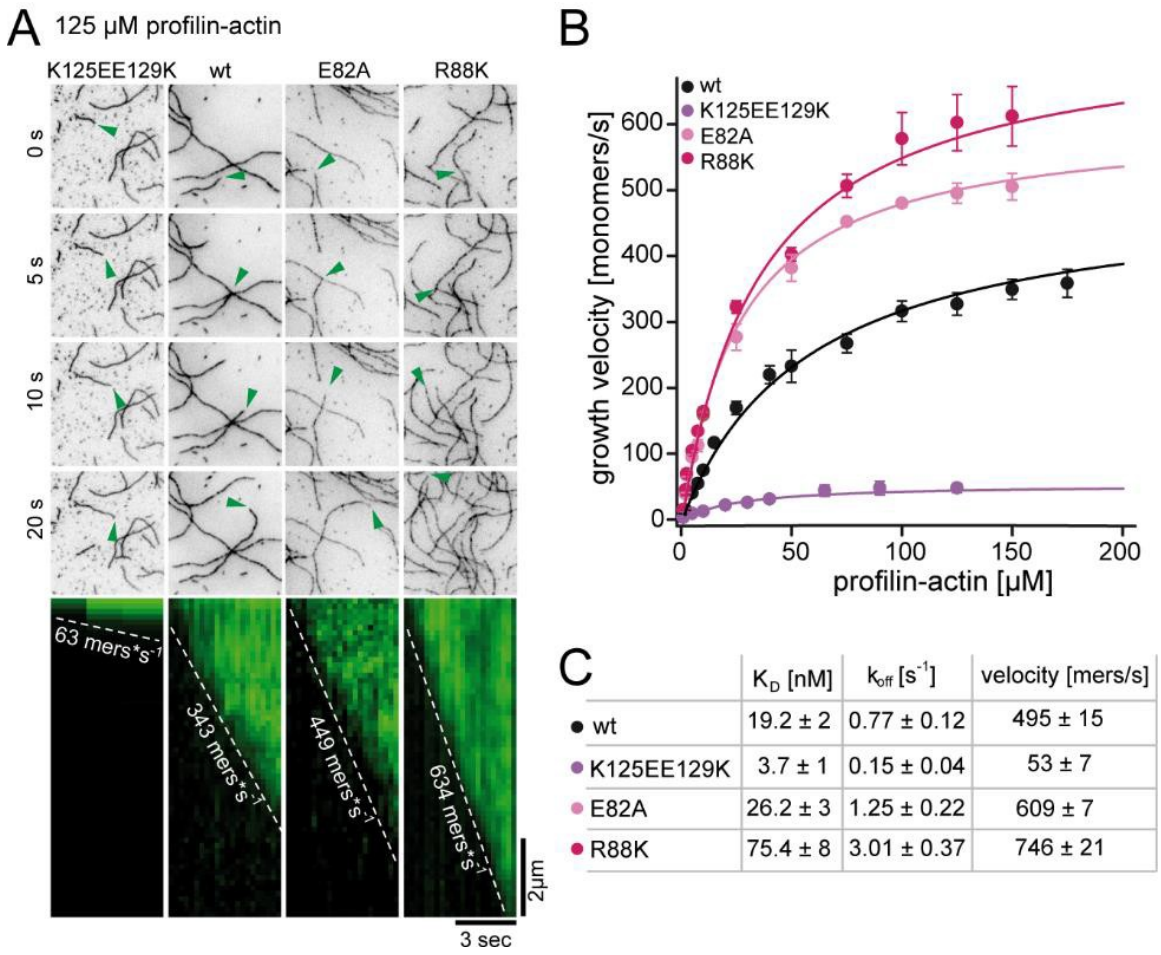

Figure 22: Actin filament elongation from actin complexed with weakly and tightly binding profilin1 mutants. A. Time-lapse images from TIRF-M assays (top) and representative kymographs (bottom) of actin filament elongation at different time points from profilin (wt and mutants as indicated) – actin complexes at 125 µM. The green error follows a single filament barbed end. B. Barbed end growth velocities from single filament TIRF-M assays at different profilin-actin concentrations as indicated for wt and mutant profilin1-actin complexes. Mean velocities [N ≥ 40 for each condition, error = SD] were fit by a hyperbola function (see methods). C. Summarizing table of the maximal filament elongation velocities for profilin1 (wt and mutants) – actin measured by TIRF-M single filament polymerization assays.

Aside from profilin mutants showing a moderate increase or decrease in monomer affinity, we generated a ultra-tight binding profilin mutant (S71M) with a binding affinity in the sub-nanomolar regime (K_D = 1.7 nM) (Figure 23A). This drastic increase in monomer binding affinity lead to the complete inhibition of filament elongation (Figure 23B).

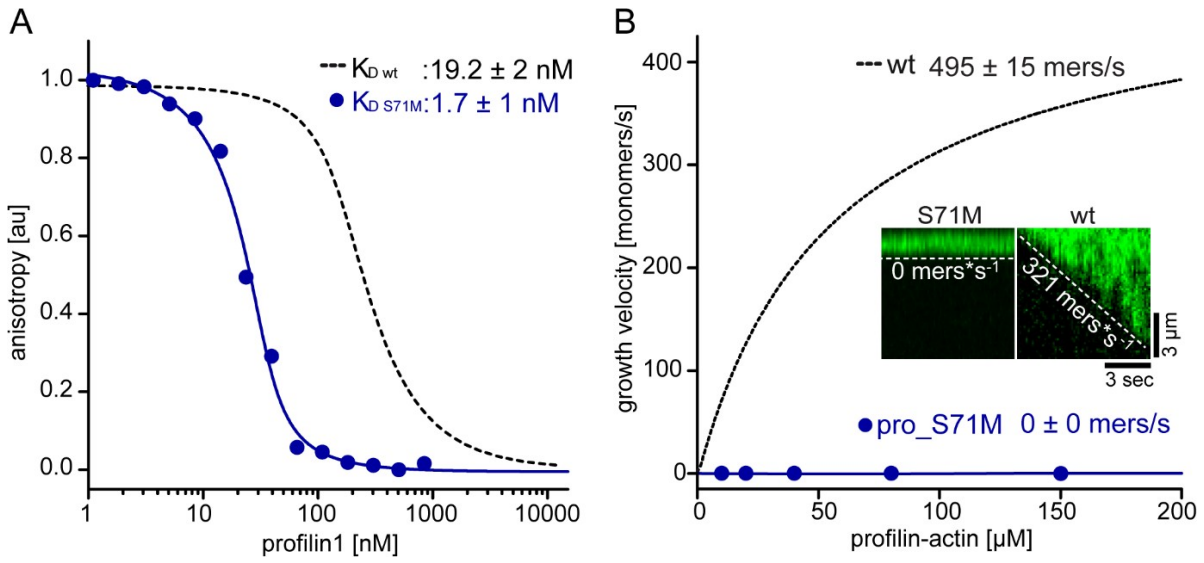

Figure 23: Design and characterization of a super-tight binding profilin1 mutant. A. Determination of binding affinities for profilin1 (wt and S71M) to ATP bound cytoplasmic actin monomers by fluorescence anisotropy competition experiments. Fluorescence anisotropy of Atto488WAVE1$_{WCA}$ [4 nM] was monitored at indicated increasing profilin1 concentrations in presence of fixed amount of ATP-bound actin monomers (150 nM for wt or 40 nM for tightly binding profilin). Mean values [N = 3, error = SD] were fitted by an exact analytical competition model (Wang, 1995). C. Filament barbed end polymerization velocities measured in TIRF-M single filament experiments using profilin1 (wt or S71M) – actin as a substrate. Calculated mean values [N≥ 40 for each condition, error = SD] of the filament polymerization rate at distinct profilin – actin concentrations were fit to a hyperbola function. Inset: Kymographs of individual filaments growing at 150 µM profilin-actin.

Collectively we can draw three main conclusions from these results: i) Profilin mutations at the profilin-actin binding interface lead to changes in the dissociation rate constant of profilin from soluble actin monomers but more importantly from the terminal actin subunits at the filament barbed end similarly. ii) Profilin release from the barbed end constitutes the kinetic limit to the actin elongation cycle which is modulated by iii) the profilin-actin interaction strength.

6.6 Profilin release from the filament barbed end is not linked to ATP hydrolysis

Actin is a ATPase that rapidly hydrolyses ATP during polymerization. In the actin filament, the hydrolysis of the ATP nucleotide occurs in two subsequent steps: i). cleavage of ATP to ADP + P_i, followed by ii). the release of the phosphate resulting in the ADP state (Laki, 1951; Straub and Feuer, 1950; Wegner, 1976).

Some previous studies (Pernier et al., 2016; Romero et al., 2004) claim that profilin only releases from the actin barbed end upon ATP hydrolysis of the terminal actin monomer. In this way, filament barbed end assembly would be coupled to ATP hydrolysis and thus restricts the actin polymerization rate to the rate of hydrolysis of the bound nucleotide.

The rate of ATP hydrolysis in filamentous actin is fast with previously measured rates of 1.4 - 0.3 s^{-1} (Blanchoin and Pollard, 2002; Pollard, 1986b; Rould et al., 2006). Hence, ATP hydrolysis would be too slow to account for the maximum rate of filament polymerization I observe (500 s^{-1}). To conclusively address whether profilin dissociation from the terminal protomer of the barbed end directly requires ATP hydrolysis, we designed an ATPase-deficient actin mutant. The generation of ATPase deficient (AD) actin was performed by the alanine substitution of three distinct amino-acids that are located proximal to the three γ-phosphate residues of the nucleotide in the catalytic core of actin (Q137A+D154A+H161A) (Figure 24A). To verify ATPase deficiency, we performed two different experiments: i) observation of the ATP hydrolysis (phosphate release) after initiation of polymerization over time by radioactive ATPase assays (Figure 24B) and ii) determination of the nucleotide state after actin polymerization by HPLC (Figure 24C).

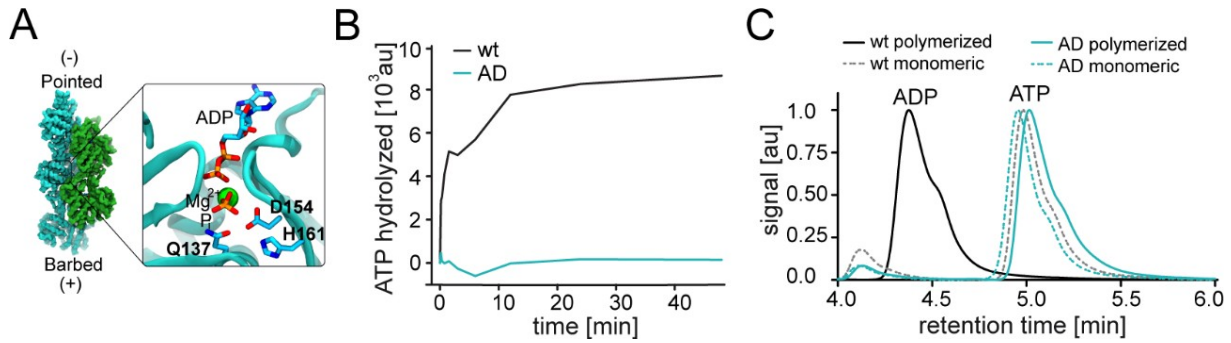

Figure 24: Characterization of the hydrolysis efficiency of an actin mutant. A. Structural model of the actin filament nucleotide binding site. Inset: highlights three amino acids (Q137, D154, H161) in the active site (PDBID 6FHL) relevant for ATP-nucleotide hydrolysis. To generated hydrolysis deficient actin, the three amino acids were mutated into alanine. B. HPLC endpoint assays to measure the nucleotide content (ADP and ATP) after 1.5 hrs of seeded filament polymerization from profilin-actin (either wt or ATPase-deficient (AD)). Latrunculin B stabilized profilin-actin was used as a non-polymerizing control sample (see methods). C. Radioactive ATPase assay to monitor cleaved γ-^{32}P over time from wt and AD – actin after polymerization. To start the reaction, radioactive-ATP containing profilin1-actin complexes were mixed with pre-polymerized filaments in a 1:1 molar ratio (see methods).

Both HPLC and ATPase assays showed that the amino-acid substitutions in the triple mutant prevent ATP hydrolysis upon polymerization from profilin-actin but did not prevent nucleotide binding.

Importantly, AD actin did not alter the profilin binding affinity (Figure 25A) and heterodimeric profilin-actin complexes could be generated as for wt-actin. To test whether the ATPase deficiency of actin affects the dissociation of profilin at the terminal actin subunit, I performed TIRF-single filament polymerization assays as described previously (Figure 25B).

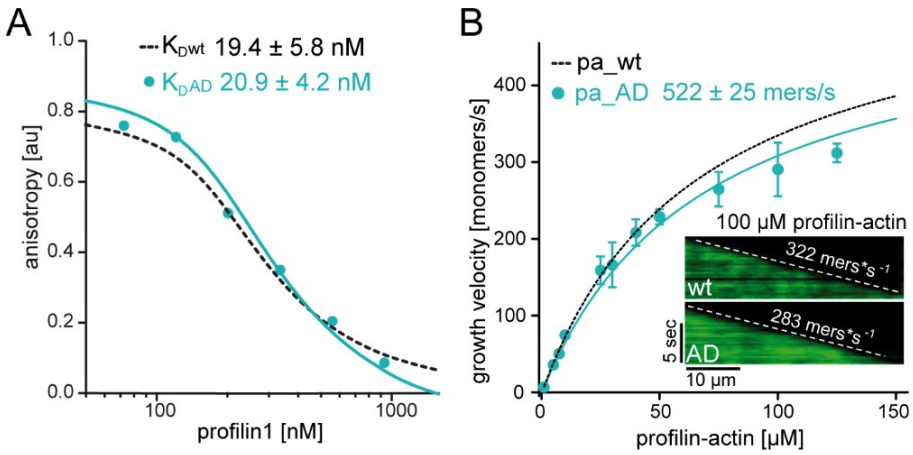

Figure 25: Actin binding and filament polymerization with ATPase deficient actin. A. Determination of binding affinities for profilin1 to ATP bound cytoplasmic actin monomers (wt - black dashed and AD - cyan) by fluorescence anisotropy competition experiments. Fluorescence anisotropy of Atto488WAVE1$_{WCA}$ [4 nM] was monitored at indicated increasing profilin1 concentrations in presence of fixed amount of 150 nM ATP-bound actin monomers. Mean values [N ≥ 3] were fitted by an exact analytical competition model (Wang, 1995). Errors are SD. B Filament barbed end polymerization velocities measured in TIRF-M single filament experiments using profilin1 - actin (wt or AD actin) as a substrate. Calculated mean values [N≥ 40 for each condition, error = SD] of the filament polymerization rate at distinct profilin – actin concentrations were fit to a hyperbola function. Inset: Kymographs of filaments growing at 100 µM profilin-actin.

Interestingly, at saturating profilin-actin amounts, actin filaments polymerize with very similar rates from ATPase deficient actin compared to wt. Together our results show, that neither actin filament polymerization is limited by ATP hydrolysis, nor that the release of profilin from the terminal protomer is coupled to nucleotide hydrolysis.

6.7 The function of formin actin polymerases

In vivo, actin filaments elongate from profilin-actin complexes. More importantly, the elongation reaction from the filament barbed end can be facilitated by actin polymerases. Actin polymerases such as formins are known to accelerate barbed end elongation in vitro (Jegou et al., 2013; Kovar et al., 2006; Romero et al., 2004) as well as in vivo (Higashida et al., 2004). Up to this point formins function has been described as increasing the association rate of profilin-actin complexes to the filament barbed end they processively associated with (Paul and Pollard, 2009). However, such a mechanism can only be expected to work under conditions when the binding of profilin-actin complexes onto the barbed end is limiting. We were therefore wondering how actin

polymerases affect filament polymerization at saturating, physiologically relevant, profilin- actin concentrations (Figure 26).

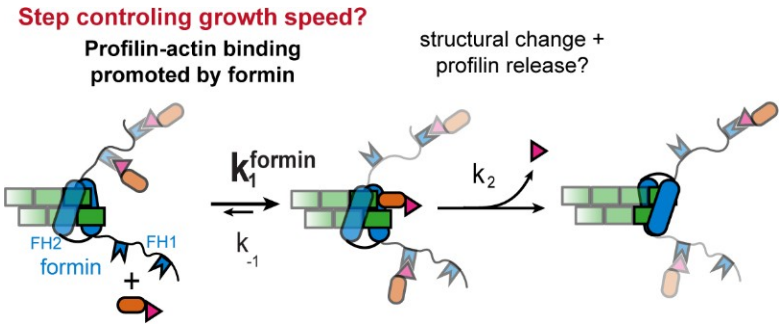

Figure 26: The function of actin polymerases at physiologically relevant profilin-actin concentrations is unclear. Scheme of the actin filament barbed end elongation from profilin-actin complexes mediated by actin polymerases. Can actin polymerases accelerate the rate limiting step (profilin release) through structural changes in the terminal actin subunit?

6.8 Formin actin polymerases directly accelerate the rate-limiting reaction in filament elongation

Initially we focused on the most established growth promoting diaphanous-type formins because of their established polymerase function. Formin proteins consist of a series of different functional domains, with the formin homology 1 and 2 (FH1 and 2) being the most important domains for the polymerase function. All actin polymerases included in the experiments of this work are constitutively active constructs, only containing the profilin-actin interacting FH1 domain and the barbed end binding FH2 domain (see methods), but did not include auto-inhibitory sequence elements. We fixed the concentration of actin polymerases (15 nM) to an amount that was sufficient to saturate all free filament barbed ends (Figure 27A). Since formin decorated filament barbed ends were growing much faster compared to filaments which were not bound to formins, we also could determine the degree of formin decoration on filament barbed ends based on the filament barbed end elongation velocity (Figure 27B).

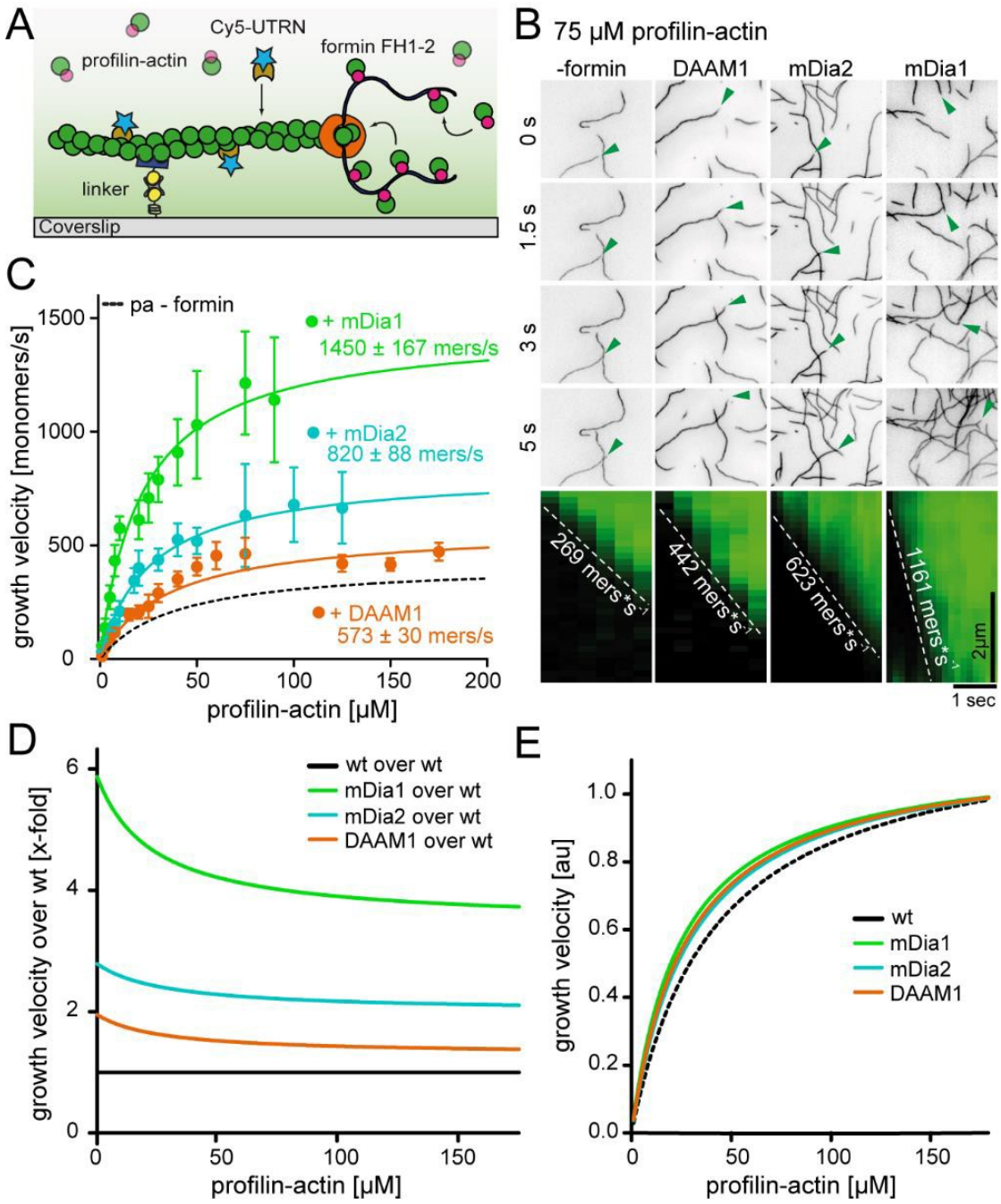

Figure 27: Actin filament elongation from physiologically relevant profilin-actin levels is accelerated by formins. A. Scheme of TIRF-M filament polymerization catalyzed by formins FH1-2 domains on a functionalize glass coverslip (see methods). B. Time-lapse images from TIRF-M assays (top) and representative kymographs (bottom) of actin filament elongation at different time points in absence or presence of 15 nM formins (mDia1, mDia2 or DAAM1 as indicated) at 75 µM (green error follows a single filament barbed end). C. Barbed end growth velocities from single filament TIRF-M assays at different profilin-actin concentrations as indicated in absence or presence of formins as indicated. Mean velocities [N ≥ 40 for each condition, error = SD] were fit by a hyperbola function. D. Fits of the relative x-fold growth rate enhancement of formin mediated filament elongation over wt (without formin) derived from the fitted data in C. E. Normalization of filament elongation rates derived from the fits in C either in presence or absence of formins (as indicated).

In line with previous studies (Jegou et al., 2013; Kovar et al., 2006), both mDia1 and mDia2 very potently accelerated filament barbed end elongation at limiting profilin-actin substrate levels (≤20 µM). mDia1-mediated filament elongation appears to be more than twice as potent as mDia2 in promoting filament elongation. Interestingly, both mDia 1 and 2 formin mediated filament polymerization still saturated at high profilin-actin concentrations (≥50 µM) (Figure 27B&C). However, the maximal rates were different for both tested formins: 1450 mers/s for mDia1 and for 820 mers/s mDia2.

The relative rate enhancement in elongation velocity calculated from the individual hyperbola fits show that the increase in polymerization speed only decreased slightly for all tested formin constructs when increasing the concentration of profilin-actin (Figure 27D). This indicates, that all formins were maximally efficient at low profilin-actin levels, however, the polymerase function is still maintained at high saturating substrate concentrations. Thereby the maximal elongation rates that were achieved at substrate saturation were strikingly higher (by 4x and by 1.6x for mDia1 and mDia2, respectively) than in the absence of either formin-type (Figure 27D). Collectively our findings indicate that formin-type actin polymerases can accelerate the rate-limiting reaction in filament elongation at saturating profilin-actin levels with mDia1 being more potent than mDia2.

In order to address whether the property of formins accelerating the rate-limiting step in the actin filament elongation cycle is not only a feature of diaphanous but also among all formins, we tested the non-diaphanous formin DAAM1 in similar TIRF-M assays. Consistent with diaphanous formin-types mDia1 and mDia2, DAAM1 could also enhance filament barbed end growth under substrate limiting as well as under saturating profilin-actin conditions, however less substantial than either mDia formin, by a factor of 1.2x (Figure 27B-D).

Importantly, our results show that all tested diaphanous and non-diaphanous formins are capable of accelerating the rate-limiting step in filament growth to various degrees. (Figure 27E). In this way formins broaden the regime of available profilin-actin concentrations over which filament elongation speed is invariant.

6.9 Profilin release from the actin filament barbed end is accelerated through formins FH2 domain

All actin polymerases tested in this work were capable to enhance maximum filament elongation at saturating substrate concentrations to specific rates. Previous studies (Higgs and Peterson, 2005) have already discussed the FH2 domain as a characteristic feature of formins which possess a clear consensus sequence among all formins. In contrast to the FH2 domain, the FH1 domain is highly variable in its sequence depending on species and isoform. To assess whether either both, or an individual FH domain determines the difference in the maximal filament elongation velocity, we designed mDia chimeric constructs (mDia1FH1-mDia2FH2 and mDia2FH1-mDia1FH2) by interchanging their FH1 and FH2 domains (Figure 28A).

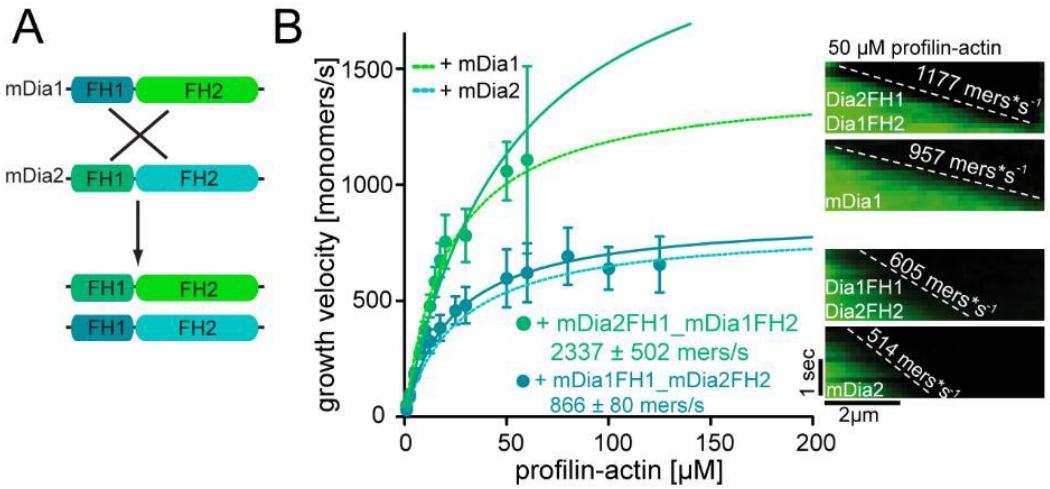

Figure 28: Formins FH2 domain accelerated profilin release from the filament barbed end and determines new individual actin elongation speed limits. A. Scheme of the design of formin mDia chimera constructs. Individual FH1 and FH2 domains are interchanged between the mDia1 and mDia2 molecules. B. Left: Barbed end growth velocities from single filament TIRF-M assays at different profilin-actin concentrations as indicated in presence of formins (wt formins- dashed lines or chimeras – continuous lines, as indicated). Mean velocities [N ≥ 40 for each condition, error = SD] were fit by a hyperbola function. Right: Kymographs of individual representative filaments (as indicated) at 50 µM profilin1-actin.

Both chimeric constructs potently accelerated filament elongation to distinct maximal growth rates at non-limiting profilin-actin concentrations which were notably higher than in their absence (Figure 28B). Strikingly, however, mDia2FH1-mDia1FH2 displayed very

similar maximal polymerization rates as mDia1, whereas the maximal elongation rate mediated by mDia1FH1-mDia2FH2 was comparable to the rate of mDia2. Collectively these results suggest that the barbed-end associated formin FH2 domain is determining the maximal filament elongation velocity.

6.10 Actin polymerase mediated filament elongation is limited by profilin release and does not depend on nucleotide hydrolysis

To test which biochemical reaction limits formin-mediated actin growth, we polymerized filaments (in presence of mDia1) from profilin-actin complexes which either contained a very tight binding profilin or a ATPase deficient actin. Importantly, the ATPase deficient actin was elongating with kinetics indistinguishable from wt actin (Figure 29). The tight binding profilin mutant (K125E + E129K, see section 6.5) however, dramatically slowed down mDia1-mediated elongation speed. Together these results demonstrate, that formin-mediated filament elongation at saturation is not limited by ATP nucleotide hydrolysis. Instead, maximum polymerization velocities can be drastically modulated by changing the profilin dissociation rate constant. This shows that filament polymerization speed (in presence and absence of formins) is limited by the release of profilin from the barbed end. Together these results reveal two distinct functions of formin polymerases: i) formins promote the binding of profilin-actin complexes onto the filament barbed end and ii) formins directly accelerate the release of profilin from the filament barbed end specifically by their FH2 domains. Strikingly, both formin functions together provide a constant enhancement of the filament elongation speed over a wide regime of profilin-actin concentrations. Additionally we reveal that formins elongate actin filaments with distinct rates allowing these molecules to act as pacemakers. Formin-mediated filament elongation rates are buffered and therefore are insensitive to changes in the profilin-actin concentration under physiologically relevant conditions.

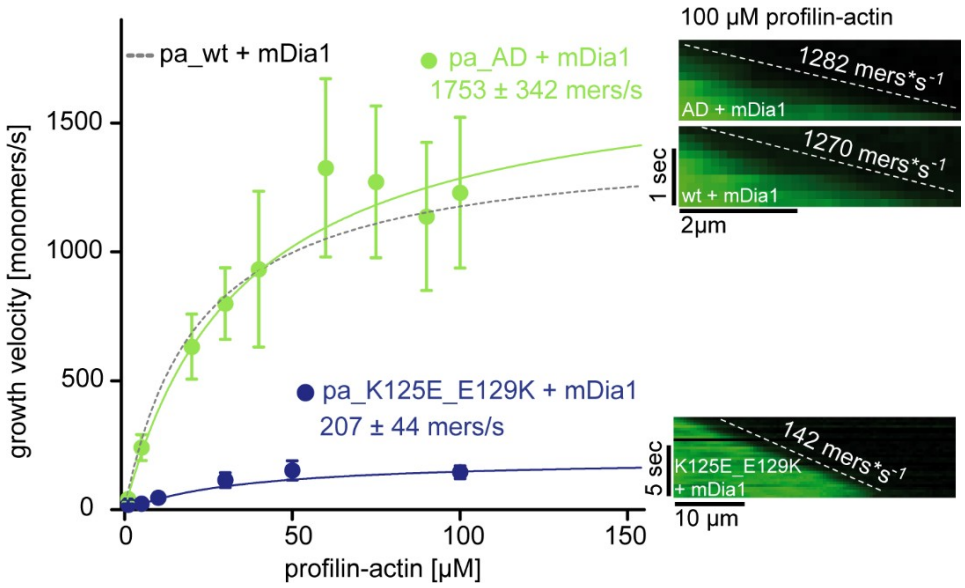

Figure 29: Formin-mediated actin filament polymerization is independent of ATP hydrolysis but depends on profilin1 release. Left: Barbed end growth velocities from single filament TIRF-M assays at different profilin-actin concentrations as indicated in presence of 15 nM mDia1 with either wt profilin - actin (dashed black), profilin - ATPase deficient actin (green) or tight binding profilin K125E_E129K – actin (violet). Mean velocities [N ≥ 40 for each condition, error = SD] were fit by a hyperbola function. Right: Kymographs of individual representative filaments (as indicated) at 100 µM profilin1-actin.

6.11 Actin filament polymerization mediated by formin actin polymerases is robust to variations in profilin-actin levels

To examine the physiological relevance of the data that we collected from in vitro single filament reconstitution assays, single molecule TIRF-M experiments were established to measure single filament barbed end elongation rates in vivo. Since actin is one of the most abundant proteins in eukaryotic cells that builds many different structures within a cell, the length and meshsize of actin filaments is extremely dense. As a consequence, actin elongation cannot be directly imaged using TIRF microscopy or other live-cell microscopy techniques, since the resolution of individual filament barbed ends is not possible in these dense cellular networks. However, formin molecules have previously been used to visualize single growing filament ends in vivo (Higashida et al., 2004). I therefore established constitutively active mNeonGreen tagged formin FH1-2 domains (mDia1 and mDia2) as an indirect readout for single actin filament elongation in vivo (Figure 31A). I was designing formin constructs containing a low expressing ΔCMV-promotor for recombinant protein expression. The decreased promotor strength ensured

low expression of the single formin molecules to avoid protein aggregation, filopodia formation and the consumption of high monomer amounts through increased numbers of formin molecules. Cell types to measure formin mediated actin polymerization were either mammalian mesenchymal HT1080 cells or EL4 T-lymphocytes because of their ≥ 2x-fold difference in profilin-actin concentration (Figure 11). We performed all in vivo formin single molecule experiments at 23 °C (for better comparison to the results from the in vitro single filament assays) using TIRF-microscopy.

Remarkably, single formin molecules that were moving with constant speed close to the surface within the cellular actin cortex could be monitored over multiple µm distances in real time (Figure 31B&C). Furthermore we performed control experiments with either actin – or myosin inhibitors to verify that the directed formin molecule movements were only driven by actin filament polymerization and were independent of myosin-II activity (Figure 30). To confirm that the observed single molecule movements were actin driven, we performed three different strategies (Peng et al., 2011): i). All available actin monomers were polymerized into filaments by jasplakinolide (JASP) (Figure 30B). ii). To selectively prevent actin filament polymerization, all actin monomers were bound to latrunculin B (Figure 30C). and iii). By treating the cells with the ROCK kinase inhibitor y27632 all myosin-II driven processes were suppressed (Figure 30D). Together, the results from our control experiments show that the formin movement is only driven by actin filament polymerization.

For all experiments, only cells expressing very low numbers of formin molecules were selected for data analysis given that strong formin overexpression could potentially perturb the pool of polymerizable substrate (Dimchev et al., 2017). Further, for data analysis we only selected formin molecules that were freely moving in the area of the cell body. Thus we exclude obstacles as for instance mechanical resistance in areas like the cell periphery. In these areas formin movement can be negatively influenced by the plasma membrane.

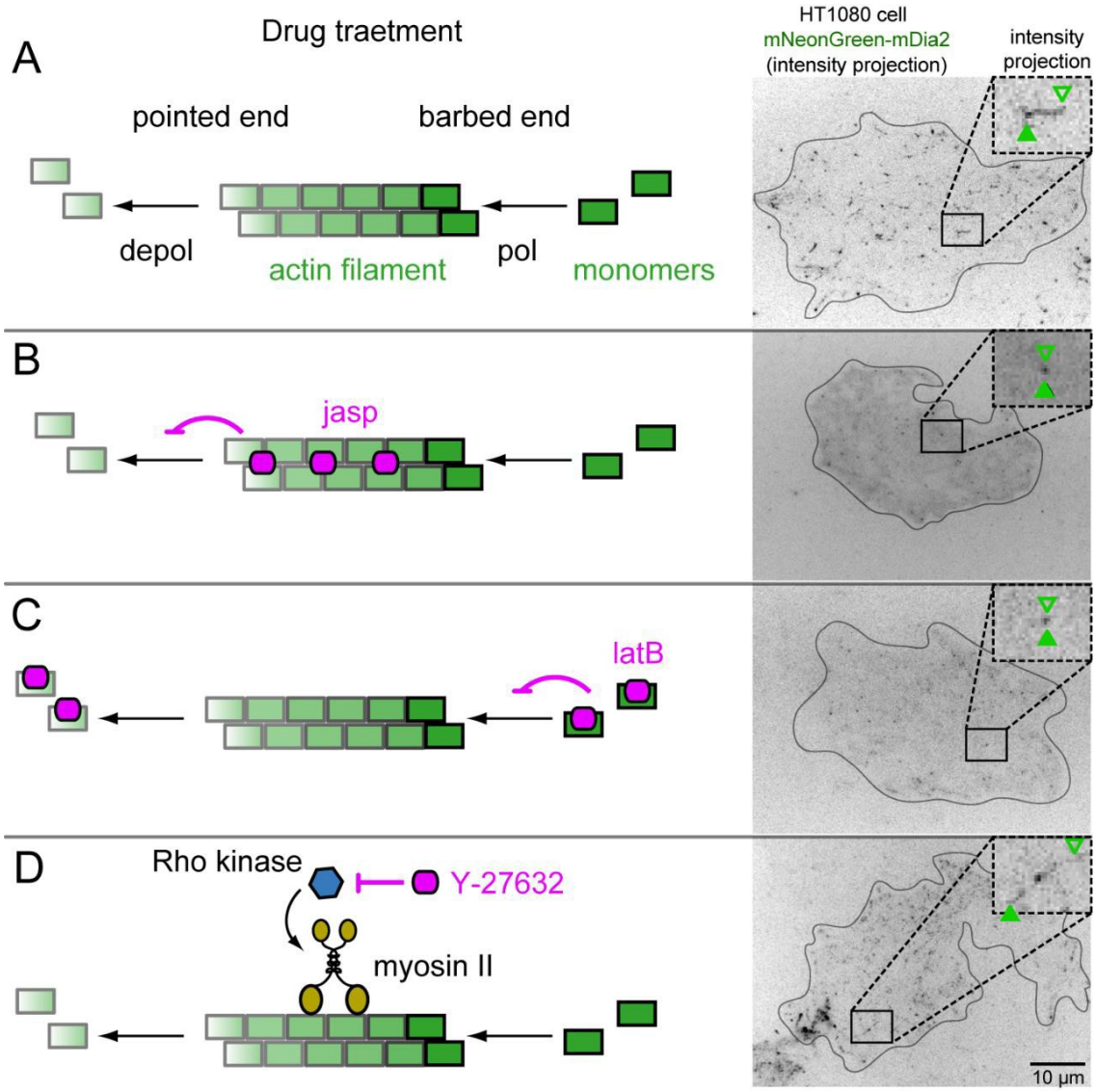

Figure 30: TIRF in vivo single molecule control experiments.Left: Schematic of actin inhibitors: A-D, no treatment, jasplakinolide, latrunculin B, y-27632 (modified from (Peng et al., 2011)). Right: Intensity projections of single mNeonGreen-mDia2 molecules in HT1080 cells, inset: intensity projection of one representative molecule. A. No Drug treatment. Actin filaments polymerize from free monomers on their barbed end and depolymerize on their pointed end. B. Treatment with 8 µM jasplakinolide (jasp) for 10 min. Jasp binds to the actin filament side and inhibits the depolymerization of filaments. After jasp treatment, no actin dynamics are visible anymore since all monomers have been polymerized into filaments. C. Treatment with 0.5 µM latrunculin B (latB) for 10 min. Latrunculin B binds to actin monomers and prevents nucleation and incorporation into actin filaments. After latB treatment, no actin dynamics are visible anymore since all monomers are blocked for polymerization. D. Treatment with 10 µM y-27632 for 10 min. Y-27632 is a ROCK inhibitor that inhibits Rho kinase activity which prevents the activation of myosin-II. After y-27632 treatment, actin dynamics are visible since all formin-mediated filament polymerization dynamics are independent of myosin-II activity.

The single molecules expressed in vivo were moving with formin characteristic speeds where mDia1 speed was much faster (~ 2x-fold) compared to the speed of mDia2

(Figure 31D). Interestingly, the observed speed of either mDia1 or mDia2 formin molecules were very similar between the two specifically selected cell types. While mDia1 driven barbed end polymerization was moving with mean rates of 1286 monomers/s in HT1080 and 1463 monomers/s in EL4 cells, mDia2 mediated filament polymerization showed lower average rates of 712 or 868 monomers/s in HT1080 or EL4 cells, respectively. Moreover, both mDia1 and mDia2 velocities were comparable to the formin mDia1/mDia2 mediated maximum filament polymerization speed observed in our in vitro single filament polymerization assays (1453 and 843 monomers/s for mDia1 and mDia2, respectively) described in the previous section (see section 6.8).

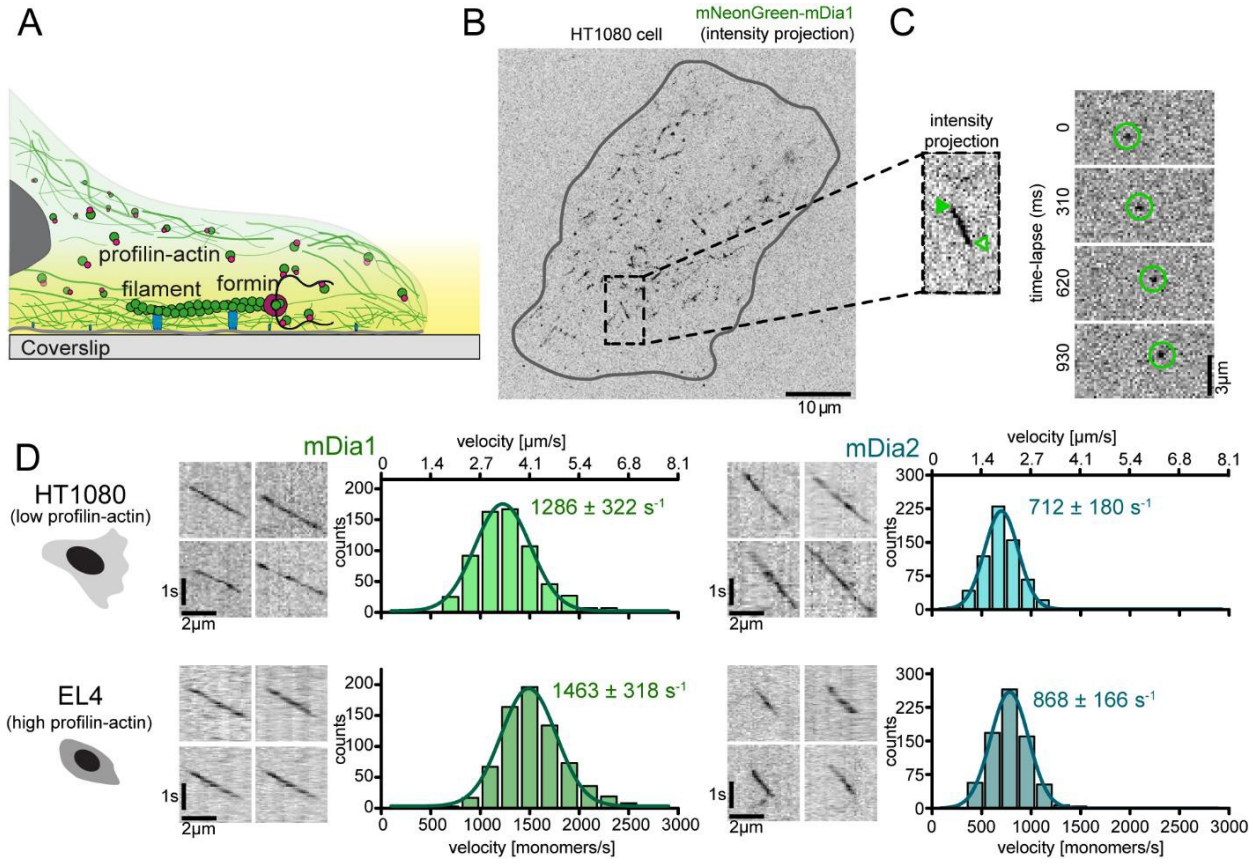

Figure 31: Formin single molecules in vivo. A. Experimental scheme of single constitutively active formin molecules mediating actin filament polymerization in a cell. B. Maximum intensity projection of a TIRF-M time-lapse from single mNeonGreen-mDia1 molecule movement trajectories in a HT1080 cell. C. Left: Inset of B. Close-up of an individual mNeonGreen-mDia1 intensity projection. Right: TIRF-M time-lapse images (in ms) of an individual mNeonGreen-mDia1 molecule. D. Measurements of mDia1 and mDia2 elongation velocities in HT1080 (upper) and EL4 (lower) cells. Left to right: scheme of cell type, kymographs of individual mNeonGreen-mDia1 (left) and mDia2 (right) molecules and their corresponding velocity distribution. Lines are Gaussian fits. Calculated mean velocities and SD errors are indicated in the graphs [per condition: $N_{cells} \geq 10$, $n_{molecules/cell} \geq 30$, $n_{total} \geq 650$].

Together, our formin single molecule in vivo data suggests that actin filament polymerization mediated by formins (here mDia1 and 2) is very robust against variations in the amount of available profilin-actin substrate when comparing different mammalian cell types.

6.12 Perturbation of profilin and actin concentrations in vivo

Our results from the previous sections suggest that actin filament elongation mediated by formins is robust against changes in the profilin-actin concentration in vitro and in vivo. To test whether the invariance in formin-mediated actin elongation speed in vivo is cell-type specific, we perturbed the levels of profilin-actin in HT1080 cells. We choose this cell type because of its low amounts of profilin-actin (see section 6.1) which can be easily increased by profilin-actin overexpression (Figure 32A&B). Both, profilin and actin, were co-overexpressed in a nearly stoichiometric manner to prevent any side-effects: i) the overexpression of actin alone would result in uncontrolled spontaneous nucleation of many filaments within the cell, whereas the overexpression of profilin alone would cause a slowdown in filament elongation by blocking filament barbed ends. To overexpress profilin and actin in a 1:1 stoichiometry, we used a poly-cistronic construct containing the following sequence elements starting from the N-terminus: human β-actin, P2A (1st ribosomal skip site), mScarlet-I (as a fluorescent expression-marker), T2A (2nd ribosomal skip site), human profilin1 (Figure 32C). After the generation of cells which stably express profilin and actin, we sorted the heterogeneous expressing cell pool. Depending on their mScarlet-I fluorescent signal, we sorted the cells into four distinct sub-populations (Figure 32D). We then quantified the actin and profilin protein concentrations as described previously (see section 6.1). This quantification revealed a ~2x –fold overexpression of both, profilin and actin in the sub-population which showed the highest signal for mScarlet-I (Figure 32D). Importantly, profilin and actin were expressed in nearly balanced amounts, and no other high molecular-weight actin contaminants as for instance arising from ribosomal read-through could be detected (Figure 32E). After applying a pharmacological arrest cocktail (Peng et al., 2011) we confirmed that the profilin fraction was completely soluble.

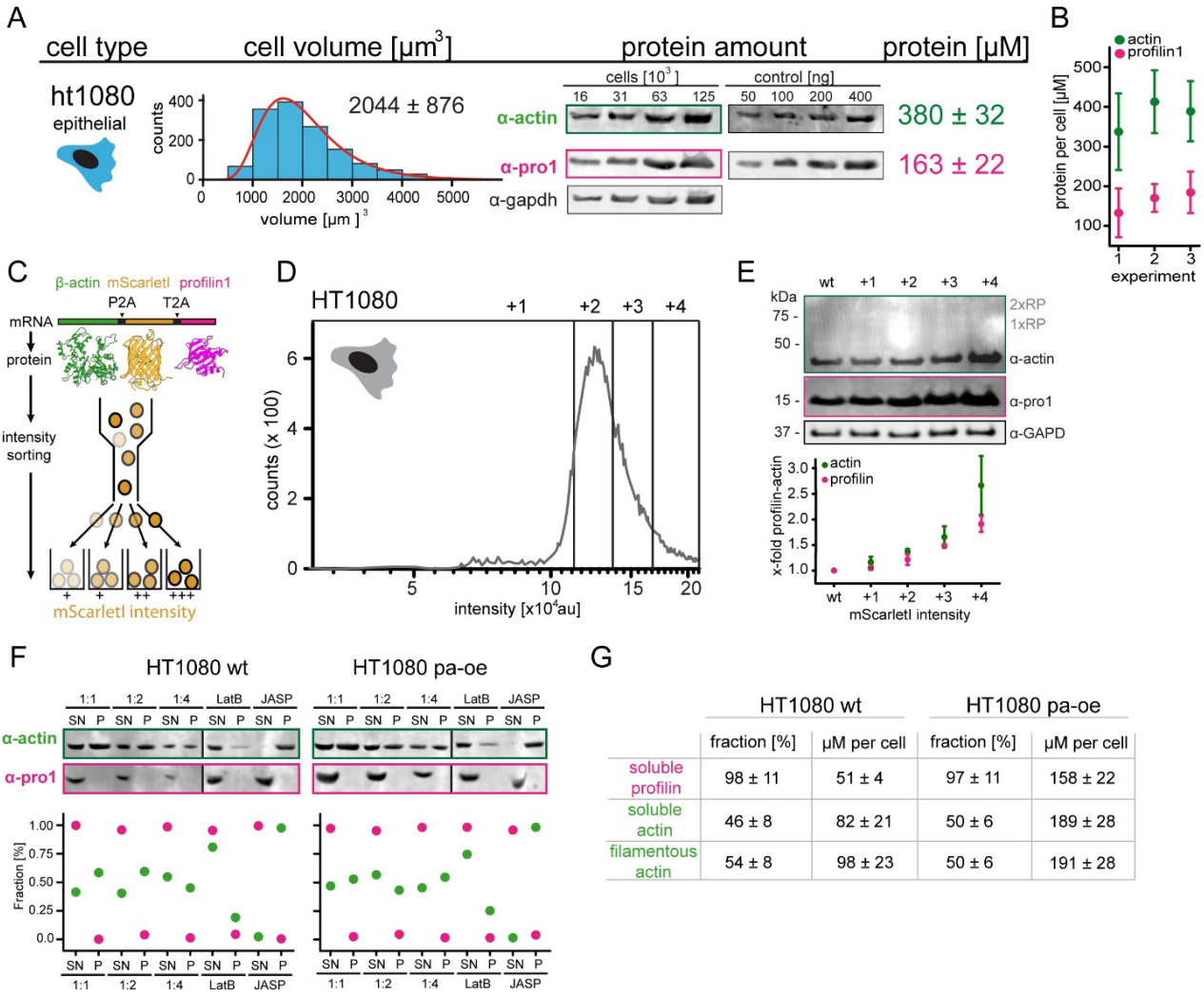

G

	HT1080 wt		HT1080 pa-oe	
	fraction [%]	µM per cell	fraction [%]	µM per cell
soluble profilin	98 ± 11	51 ± 4	97 ± 11	158 ± 22
soluble actin	46 ± 8	82 ± 21	50 ± 6	189 ± 28
filamentous actin	54 ± 8	98 ± 23	50 ± 6	191 ± 28

Figure 32: Overexpression of profilin and actin in vivo. A. Measurements of profilin1 and actin concentrations in HT1080 cells overexpressing profilin1 and β-actin. Left to right: scheme of cell type, histogram of the single cell volumes determined by fluorescence eXclusion, determination of profilin1 and actin amounts by quantitative western blot analysis (left: titration of specific cell numbers, right: reference curve of respective recombinant proteins), calculated mean profilin1 and actin protein concentrations per cell [µM] with SD error B. Profilin1 and actin concentrations per HT1080 cell from three individual experiments. C. Experimental workflow to generate profilin1 and β-actin overexpressing HT1080 cell. Top to bottom: design of polycistronic constructs (β-actin-P2A-mScarletI-T2A-profilin1) that were integrated into the genome via PiggyBac strategies, cell sorting via mScarletI intensity (see D) into subpopulations D. FACS analysis histogram representing the mScarletI intensity distribution of a polyclonal HT1080 population. The population was distributed into four subpopulations from low to high (+1 to +4) mScarletI intensity. E. Control experiments for relative profilin1 and actin overexpression in HT1080 cells. Top: western blot for wt and profilin-actin overexpressing cell populations (+1 tot +4). Only full-length proteins and no translational read-through protein products (1xRP: actin-mScarletI, 2xRP: actin-mScarletI-profilin1 at expected molecular weight) are visible. Bottom: relative profilin1 and actin amounts in x-fold over wt for all tested populations respectively. F. Control experiments for the determination of soluble and non-soluble fractions of actin and profilin in HT1080 wt and profilin-actin overexpressing cells. After actin arrest (see methods), profilin1 and actin amounts were determined in soluble and non-soluble fractions by quantitative western blot analysis. G. Summarizing table for wt and profilin-actin overexpressing HT1080 cells (see F) showing the calculated fractions [%] as well as protein concentrations per cell [µM] of soluble profilin/actin and filamentous actin.

Actin, however, separated into soluble (monomers) and non-soluble fractions (filaments) (Figure 32F&G). The concentration of soluble actin was increasing by similar amounts as the soluble profilin concentration in all overexpressing cell-populations. Additionally, the amount of soluble actin was always higher than the amount of profilin1 (for both HT1080 wt and profilin-actin overexpression, Figure 32G). This suggests that the majority of the profilin molecules in vivo are bound to actin monomers since profilin has a very high monomer binding-affinity (K_D~18 nM, Figure 13A).

We then carried out formin single molecule tracking experiments to visualize formin-driven actin filament elongation in cells overexpressing profilin-actin. In line with previous results, formin velocities in the profilin-actin overexpressing cells (HT1080 PA-OE) were very similar to rates in HT1080 wt cells (Figure 33A). Both mDia1 and mDia2 speeds were only mildly increased by 20 and 12%, respectively. We then plotted these in vivo formin velocities against the relative profilin-actin amounts measured previously (Figure 33B). Strikingly, this reveals that the formin-mediated filament elongation speed does not correlate in a linear fashion with the amount of available profilin-actin (Figure 33B&C). In addition, we could show that the observed non-linearity also holds true for other cell types (HT1080 wt/PA-OE and EL4) containing various absolute amounts of profilin-actin. Instead, the formin velocities measured in different cell types containing different profilin-actin amounts (either wt or profilin-actin overexpression), could be well fit to a hyperbola similar to the in vitro data (Figure 33B). Interestingly, the maximum mDia1 and mDia2 formin speeds obtained from the hyperbola fits were very similar to the respective formin kinetics found in vitro.

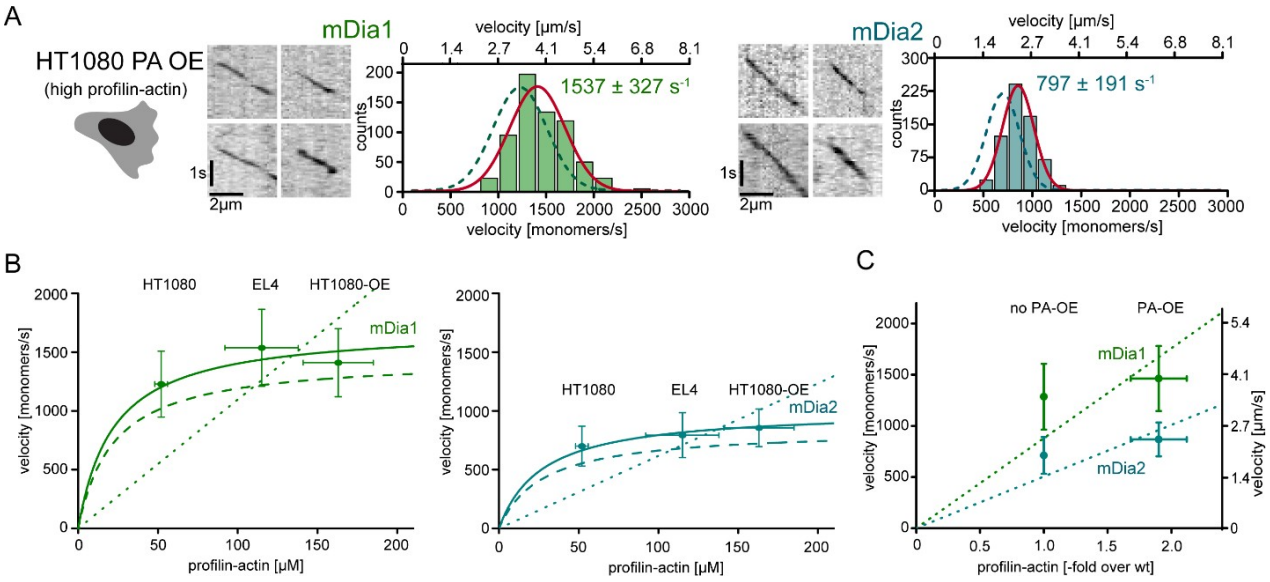

Figure 33: Formin single molecules in profilin-actin overexpressing cells. A. Measurements of mDia1 and mDia2 elongation velocities in profilin-actin overexpressing HT1080 cells. Left to right: scheme of cell type, kymographs of individual mNeonGreen-mDia1 (left) and mDia2 (right) molecules and their corresponding velocity distribution. Lines are Gaussian fits with a red = PA-OE and dashed = wt. Calculated mean velocities and SD errors are indicated in the graphs [per condition: $N_{cells} \geq 10$, $n_{molecules/cell} \geq 30$, $n_{total} \geq 650$]. B. mDia1 (left) and 2 (right) mean velocities for HT1080 wt, PA-OE and EL4 cells plotted against the quantified profilin-actin concentration. Solid line = hyperbola fit of in vivo formin velocity data (with a $K_{0.5}$ (profilin-actin concentration at half-maximal elongation speed) fixed to the value of the vitro data), dashed line = formin speeds from in vitro data, dotted line = linear fits through the origin (see also C). C. mDia1 and 2 mean velocities for HT1080 wt and PA-OE cells plotted against the relative profilin-actin concentration, error = SD, dashed lines = linear fits through the origin (see also B).

Collectively, our findings suggest that actin filament polymerization mediated by formins is robust against changes in profilin-actin concentrations in vitro and in vivo. Moreover, we show, that cells maintain their profilin-actin levels close to saturation. This reveals that profilin and formins together mediate and control for the kinetic limit of actin filament elongation in cells similarly as they do in vitro.

7 Discussion

7.1 Actin filament assembly from profilin-actin complexes is kinetically limited at physiological concentrations

We showed that the polymerizable actin pool in vivo is large, but also highly variable among different mammalian cell types. Earlier estimates of the monomeric actin pool from distinct eukaryotic cells diverge even more (Koestler et al., 2009; Raz-Ben Aroush et al., 2017). If actin polymerization would linearly scale with the monomer concentration as previously predicted (Amann and Pollard, 2001; Kuhn and Pollard, 2005; Wegner and Engel, 1975), what would be the consequences? We determined the association rate constant of ATP-bound actin for the filament barbed end to be ~10^7 M^{-1} s^{-1} which is in line with rates previously reported (Drenckhahn and Pollard, 1986; Pollard and Mooseker, 1981). Under physiological substrate concentrations, as we found them in cells, this would translate to a wide range of barbed end elongation rates between 520 s^{-1} to 1440 s^{-1}. From these calculations we predict that actin assembly would result in dramatically different and very fast filament growth speeds among different cell types and within different location of cells. Such expeditious rates would likely result in rapid depletion of polymerizable actin in vivo. As a consequence, intracellular actin architectures, which highly depend on the filament elongation speed, might become disorganized. Another issue to consider is the balance between actin assembly and disassembly inside living cells. Actin filaments within cellular networks are believed to depolymerize from their pointed end. Regulatory actin proteins such as cofilin/ADF and CAP are known to promote pointed-end disassembly up to rates of 50 s^{-1} (Jansen et al., 2015; Johnston et al., 2015; Kotila et al., 2019). How pointed end depolymerization would keep up with orders-of-magnitude faster rates of barbed end polymerization is currently not understood. Clearly, severing proteins such as cofilin, which fragment filaments and thus increase the number of ends from which filaments can depolymerize (Bamburg et al., 1980; Nishida et al., 1984) might offer part of the answer. However, it is not known whether these proteins could help to replenish the monomer pool fast enough to compensate for such high monomer consumptions we would expect at in vivo monomer levels.

The use of improved TIRF-M assays and the use of mammalian cytoplasmic actin enabled us to monitor filament elongation for the first time at physiologically relevant conditions. We thereby uncovered a biochemical mechanism, which limits the actin assembly speed at physiological monomer levels. Therefore, that the large differences in physiological profilin-actin concentrations cannot be anticipated to result in large changes in the filament growth rate. The underlying mechanism is a kinetic limiting reaction in actin filament elongation, which provides robust filament dynamics. Our findings deviate from the textbook view of actin assembly (Amann and Pollard, 2001; Kuhn and Pollard, 2005; Wegner and Engel, 1975), which posits that the actin filament elongation rate scales with the concentration of available substrate and is limited by diffusional collisions of actin subunits and the filament barbed ends (Drenckhahn and Pollard, 1986). We reveal that the assembly of actin is buffered against changes in physiologically relevant substrate concentrations. This mechanism is based on two central biochemical elements: i) the limit in filament growth which is caused by a kinetic bottleneck within the actin elongation cycle and ii) the maintenance of substrate concentrations near saturation. The mechanism we reveal has likely evolved to maintain robust actin dynamics.

7.2 Profilin release from the terminal barbed end protomer limits the actin elongation cycle

In vivo actin monomers are largely bound to monomer binding proteins to prevent spontaneous actin nucleation. Profilin is the most relevant monomer binding protein from the perspective of filament assembly because of its abundance and its ability to elongate filaments. The latter ability stems from its differential affinities for ATP-bound actin monomers (K_D ~ 18 nM) and the terminal protomers at the barbed end (K_D ~ 20 - 200 µM) (Courtemanche and Pollard, 2013; Pernier et al., 2016). Profilin-actin complexes consumed in elongation can quickly be replenished, because profilin should outcompete other abundant actin monomer binding proteins such as thymosin-β_4, which generally bind ATP-bound actin monomers with much lower affinity. Hence, the total amount of profilin should approximate the amount of polymerization competent profilin-

actin complexes as long as the following conditions are fulfilled: 1. The soluble actin pool is larger than the total amount of profilin and 2. The majority of all soluble actin subunits are bound in the ATP-state (Paavilainen et al., 2004; Rosenblatt et al., 1995). We found that despite profilin release from the filament barbed end being very rapid, it nonetheless constitutes the rate-limiting reaction in actin elongation. Thus we reveal two central elements in filament elongation which both originate from the versatile biochemical properties of profilin: i) through its high actin monomer binding affinity, profilin maintains the concentration of polymerizable profilin-actin close to saturation and ii) profilin limits filament elongation rate through its dissociation from the filament barbed end. Both of these features are essential to maintain rapid and robust filament assembly in vivo. We believe that other reactions within the actin elongation cycle such as the structural actin monomer-to-filament transition that causes the drop in profilin affinity for actin are likely faster than profilin dissociation itself. This is in line with a recent structural study (Merino et al., 2018) on the conformation of actin filaments in presence of different nucleotides, which revealed that actin subunits in the filaments bound to hydrolyzed ADP + P_i, ADP or to non-hydrolyzed AMPPNP (ATP-analogue) have similar conformations that are very different from the monomer state. Hence, major structural changes in the actin accompanying polymerization are independent of changes in the nucleotide state. Importantly, our results suggest that the majority of the growing actin filaments in vivo is decorated with profilin which transiently caps the filament end and thus limits actin monomer binding. However, we believe that it is unlikely that profilin targets filament barbed ends based on equilibrium binding because of two reasons: i) the profilin binding affinity for filament ends is orders of magnitude lower than for monomers and ii) the amount of soluble actin monomers is found to exceed the profilin concentration. Hence, in vivo it is very unlikely that free profilin would accumulate to the high concentrations required for direct barbed end binding from solution. Instead, we reveal that profilin limits filament elongation through a polymerization-coupled mechanism where profilin dissociation from the filament barbed end limits the association of new profilin-actin complexes.

7.3 Formins accelerate profilin release from the filament end and tune barbed end assembly through their FH2 domains

Our results demonstrate that formins are capable of promoting the rate-limiting reaction in actin elongation at physiologically relevant profilin-actin levels. Like previously shown under conditions of limiting profilin-actin concentration (Hansen and Mullins, 2010; Jegou et al., 2013; Kovar et al., 2006; Romero et al., 2004), formins accelerate the elongation of filaments also at saturating substrate concentrations, although through another mechanism. We propose that they accelerate profilin dissociation from the filament barbed end through the action of their conserved FH2 domains. This is in agreement with earlier findings (Pernier et al., 2016) which show that profilin and formin bound to the filament barbed end mutually destabilize each other. In line, our structural model (Figure 34) of an actin filament barbed end bound to profilin and a FH2 dimer shows structural clashes of the two proteins at the barbed end. When superimposing the profilin structure onto the formin-bound ultimate actin subunit, steric clashes between profilin and the knob region of the leading FH2 are visible. It is therefore conceivable that the formins FH2 domain increases the dissociation of profilin from the barbed end when stepping onto the terminal protomer.

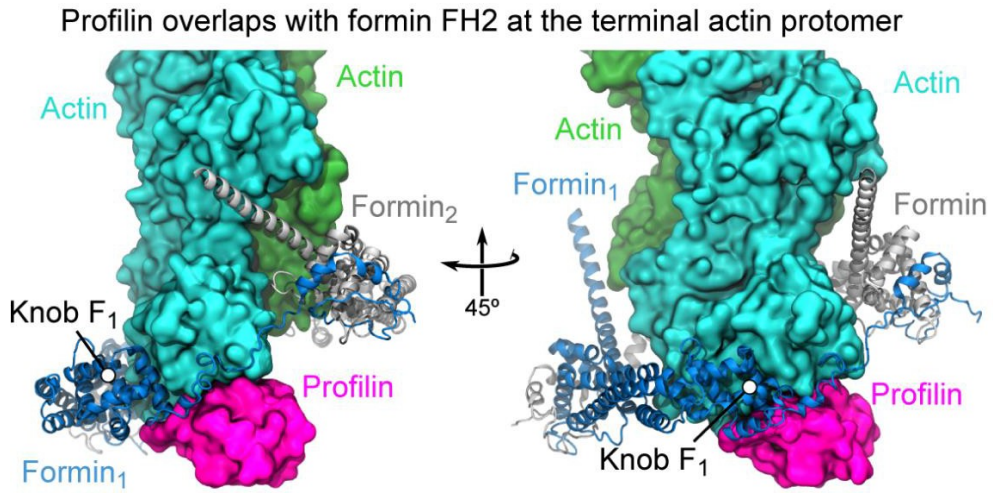

Figure 34: Structural model of the actin filament barbed end decorated with profilin1 and mDia1 FH2 domains. Surface model of profilin1 (magenta) bound to the terminal protomer of an actin filament (green). The FH2 domain of mDia1 (blue) is clashing with the profilin structure with its FH2 knob region.

Alternatively, formins could change the configuration of the actin filament barbed end (Aydin et al., 2018) and thereby promoting the dissociation of the profilin from the terminal protomer in an allosteric manner. To refute or directly confirm either mechanism in molecular detail, further structural analysis of formin and profilin decorated barbed ends will be required. Regardless of the mechanism, our results imply that under saturating substrate concentrations formins do not only promote filament elongation rates by increasing the monomer association onto filament ends like previously suggested (Goode and Eck, 2007; Schonichen and Geyer, 2010). At saturation, and in contrast to reactions at low substrate concentration, the number of profilin-actin complexes recruited by the FH1 domains should not affect the speed of formin-mediated actin growth. Interestingly, formins contain different numbers of poly-proline repeats within their FH1 domains (Petrella et al., 1996) which have a positive effect on the profilin-actin association rate to filament barbed ends under substrate limiting conditions. We show that the identity of the formin FH1 domain does not greatly affect the elongation rate at saturating profilin-actin levels.

Our experiments uncover an important second formin function depending on the amount of available substrate: i). Formins FH1 domains enhance the association rate of profilin-actin onto the filament barbed end under substrate limiting conditions through dimensionality reduction and ii). FH2 domains enhance profilin dissociation from filament ends under non-limiting substrate conditions as an additional new formin function. Both of these activities are matched to fix the formin-mediated actin growth speed to a limited range that does not allow for large variances in elongation speed.

7.4 FH2 translocation at the filament barbed end as a direct regulator of profilin dissociation

Interestingly, even formin types that are evolutionary closely related are significantly different in their capacity to accelerate profilin dissociation from the filament barbed end at saturating profilin-actin levels. The processive association of formins with the elongating filament barbed end requires the FH2 domain to translocate at the barbed end upon the addition of new actin subunits (Harris et al., 2004; Kovar et al., 2003; Moseley et al., 2004; Zigmond et al., 2003). Previous studies (Otomo et al., 2005b; Xu et

al., 2004) on Bni1p FH2 domains suggest specific actin interaction sites (knob and post region) for FH2 binding and translocation on filament ends. Up to this point, several mechanisms on formin translocation have been discussed. In general, the FH2 dimer has to step and therefore undergoes conformational changes between open and closed states which either allow or prevent monomer addition respectively (Otomo et al., 2005b). Currently, there are two main hypotheses how formins step on the filament end: i) the stair-stepping model (Otomo et al., 2005b; Xu et al., 2004). In this scenario, the trailing FH2 first dissociates from the barbed end (open state) followed by the addition of a new actin subunit and FH2 binding (closed state). ii) the stepping second model (Paul and Pollard, 2009) in which a new actin subunits is added onto the barbed end (open state), followed by the translocation of the trailing FH2 (closed state). Our experiments do not allow us to discriminate between these two mechanisms. Structures of formin- decorated end would be needed to answer whether and which of the two stepping hypothesis holds true for formin-mediated actin elongation.

However, we find that the actin growth speeds we observe for different formin types might be explained by their distinct gating factor. The gating factor is defined as the fraction of time the barbed end spends in the open state. In agreement with our measurement, mDia1 is known to exhibit a high gating factor (Aydin et al., 2018) compared to other formins and therefore accelerates actin assembly more potently. Collectively, our results reveal that the limiting reaction of filament elongation caused by profilin dissociation kinetics can be actively modulated by the formin FH2 domain (Figure 35). We reveal that formins acting as pacemakers to generate formin-specific speeds which is in agreement with the specific location they are found inside cells: Diaphanous formins which are found in filopodia (Yang et al., 2007), mediate actin assembly on sites that require very rapid polymerization of unbranched filaments.

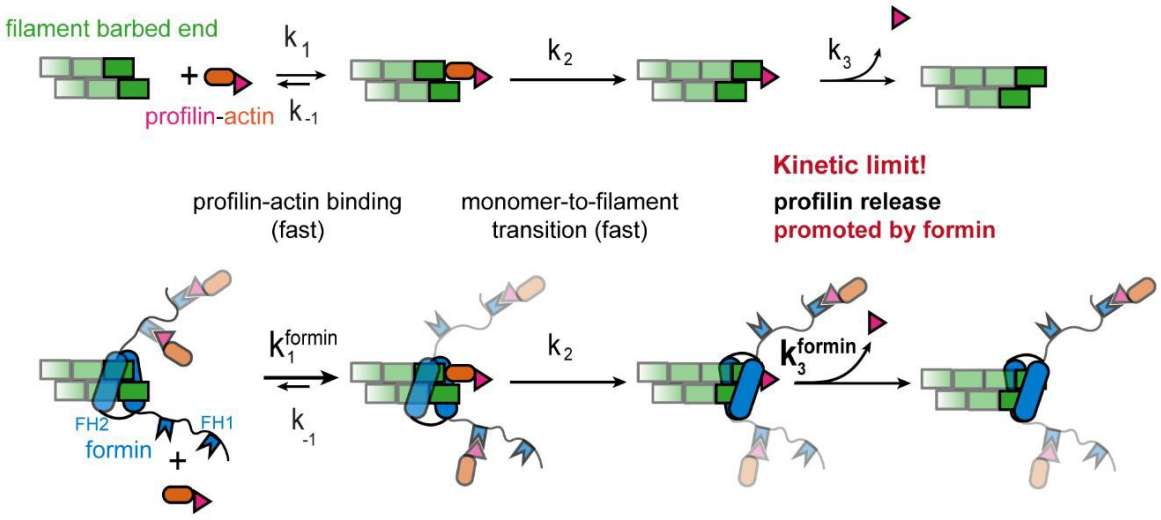

Figure 35: Scheme of filament barbed end elongation in absence and presence of formins. Upper: Barbed end elongation only from profilin-actin complexes in absence of formins Lower: Barbed end elongation from profilin-actin complexes in presence of formins. The release of profilin from the terminal subunit as a kinetic limiting reaction (k_3) is promoted by the formin FH2 stepping on the filament barbed end.

Do formin-interacting proteins regulate their ability to tune the rate-limiting step in actin assembly? The formin-mediated actin growth speeds we observe in mammalian cells agree very well with our estimates of their profilin-actin concentrations and with the formin-rates measured in vitro under substrate saturating conditions. This is intriguing, because the formin-mediated actin assembly in vitro are examined in absence of potential formin regulators. Previous in vitro studies (Henty-Ridilla et al., 2016) suggest that the microtubule plus end associated protein CLIP-170 tightly binds to formins and can accelerate formin-mediated filament assembly at least for diaphanous-type formins at low substrate concentrations. Whether formin accessory proteins such as CLIP-170 can tune formins ability to promote profilin release from the filament barbed end remains to be investigated. More importantly, whether and how other actin elongating proteins such as Ena/VASP (Hansen and Mullins, 2010; Winkelman et al., 2014) which are evolutionary unrelated to formins promote profilin release from the filament end at physiologically relevant profilin-actin concentrations will be essential to study in the future.

7.5 Profilin dissociation from the filament barbed end is independent of actins ATP hydrolysis in absence or presence of formins

Aside from structural changes in the terminal protomer, changes in the nucleotide state have been suggested to drive profilin release from the barbed end (Carlier and Pantaloni, 1986, 1988; Pernier et al., 2016; Romero et al., 2004). This could either be the release of inorganic phosphate or the preceding cleavage of the β – γ bond in the terminal actin subunit (Yarmola et al., 2008). However, we found that profilin dissociation is independent of ATP hydrolysis and phosphate cleavage in presence and absence of formins. This observation is in agreement with the timescales at which ATP hydrolysis and actin assembly are thought to occur. Both reactions should be too slow to account for the rapid polymerization speeds we observe at saturating profilin-actin concentrations. Under these conditions, actin assembly proceeds much faster than previously determined ATP hydrolysis rates (Blanchoin and Pollard, 2002; Pollard, 1986b). Both nucleotide hydrolysis and inorganic phosphate release can be uncoupled from profilin release at the filament barbed end and are not required for actin assembly as such. Why is ATPase activity essential for actin function then? Progressive nucleotide-state changes and the resulting gradient of ATP, ADP + P_i and ADP along the filament is likely key to gate the activity of distinct regulatory proteins to regions of different filament “age”. The actin subunits within the filament experience at least three different conformational changes according to their nucleotide state (Combeau and Carlier, 1988; Merino et al., 2018). These changes along the filament act as a “molecular timer”. Multiple actin filament binding proteins recognize the nucleotide state of the actin filament (Cai et al., 2007). This mechanism is essential to an active remodeling of the actin cytoskeleton within cells and especially requires actin binding proteins linked to disassembly such as cofilin (Blanchoin and Pollard, 1999; Suarez et al., 2011) and coronin 1B (Cai et al., 2007). The severing protein cofilin for example binds filamentous ADP actin with higher affinity than ATP or ADP + P_i actin subunits and thus detects its specific position to cleave the filament (Cao et al., 2006) resulting in the selective depolymerization of “aged” filaments. Importantly, however, the actin nucleotide state does not only affect filament severing and depolymerization but also regulates actin network architectures. In particular branched networks are affected since the Arp2/3

complex, which forms an actin nucleus at the filament branching point, has been proposed to be sensitive to actin nucleotide states as well. The affinity of the Arp2/3 complex for the actin filament decreases upon phosphate release which leads to debranching of aged actin networks (Blanchoin et al., 2000). This suggests that nucleotide state changes upon ATP hydrolysis indeed are very important to control for multiple molecular interactions involved in the global turnover in the actin system that maintains itself far from thermodynamic equilibrium.

7.6 Implications for polymerization-mediated force generation

How different formins impact actin filament elongation in vivo has never been studied in kinetic detail. Here we unravel that formins together with profilin promote a system for robust actin filament assembly both under physiological conditions in vitro and in live mammalian cells. This biochemical system actively buffers against large changes of cell-type specific profilin-actin levels. If the mechanism we propose holds true in vivo, we can ask whether all filaments within a cell elongate with their maximal speed, which should be dictated by the rate of profilin dissociation. This is unlikely true since the formin mediated actin elongation rates we observe in mammalian cells are very fast (up to ~4 µm/s). Indeed, these actin growth speeds are significantly faster than the movement of most actin networks, even in very rapidly moving cells, which are involved in cell-protrusion with rates of 5-30 µm/min (Renkawitz et al., 2009).

But why does the speed of formin mediated actin growth not match the dynamics of cellular structures that are generated by the actin cytoskeleton? This paradox might be explained by multiple reasons such as variations in filament orientation. Most filaments might not be aligned at an orthogonal angle towards the membrane they push against. More importantly, the mismatch of filament and network speed could originate from compressive forces filaments experience when pushing against the plasma membrane resulting in a decrease in actin growth speed (Bieling et al., 2016; Mueller et al., 2017). We anticipate that these compressive forces will dominantly slow down the binding of profilin-actin rather than affecting other reactions in the actin elongation cycle. During barbed end elongation, the plasma membrane will obstruct the Brownian motions of the elongating filaments due to pushing forces on these filaments. The pressure being

exerted onto the filament end should strongly inhibit the binding of profilin-actin resulting in a slowdown of actin assembly. To continue the elongation cycle by the addition of actin monomers onto the filament barbed end, thermal fluctuations are required to generate sufficiently sized gaps (2.7 nm) for monomer-filament interactions (Mogilner and Oster, 1996). This mechanism has been described as Brownian ratchet model, which predicts that the frequency of created gaps between plasma membrane and filament ends is limiting the elongation reaction at protrusive sites. As a consequence, the binding of profilin-actin onto filament ends under compressive forces should be significantly decreased. Filaments which experience compressive force are not only formin-bound but also freely growing such as branched networks generated through the Arp2/3 complex that push against the plasma membrane. An increase in the profilin-actin concentration might thus still accelerate the growth of filaments experiencing compression and at the same time determine the pushing force these filaments can generate. This is in agreement with the significantly increased profilin-actin concentrations we found in rapidly moving cells such as the ones of the immune system.

7.7 Competition for polymerization competent actin monomers and the regulation of actin network dynamics

How do cells regulate and control for actin growth in different actin networks? To maintain intracellular organization cells need to control for the size and homoeostatic balance of different co-existing sub-cellular structures such as formin mediated parallel actin bundles in filopodia or branched networks in lamellipodia generated by the Arp2/3 complex. Importantly, however, these distinct structures have to grow for a shared pool of actin monomers (Suarez and Kovar, 2016). Competition for a limited pool of monomers has been proposed to explain mutual inhibition that can be observed between these specific actin networks in some cell-types (Rotty et al., 2015; Suarez et al., 2015). How can this be reconciled with the robust actin assembly rates from vast profilin-actin levels we observe? We speculate that direct competition for a limiting actin monomer source might not be the cause of mutual inhibition. Actin monomers that are incorporated into filaments can be released by filament disassembly. Filament disassembly of entire actin networks can be triggered by for example either genetic or

pharmacological inhibition of actin filament nucleators. Upon the inhibition of these nucleators such as formins or the Arp2/3 complex, actin filaments will transiently disassemble into monomers. The transient increase in the monomer concentration might exceed the concentration of free profilin. Exceeding the profilin binding capacity should result in the accumulation of free actin monomers. Since actin nucleation from free unbound monomers is not only catalyzed through nucleators but is also initiated spontaneously, filament homeostasis might be triggered through alternative nucleation mechanisms. Such a compensatory nucleation mechanism has been suggested for formin-mediated filament nucleation (Higashida et al., 2013). In particular, formins were shown to trigger rapid actin nucleation in response to actin cortex disassembly. However, to understand the effect of different free or profilin bound monomers on local actin network dynamics in vivo, new methods are needed to discriminate between distinct actin monomer states (Skruber et al., 2018).

8 Conclusion and future perspectives

In this work I have uncovered a fundamental mechanism that controls and limits the assembly of actin filaments at high profilin-actin concentrations which are characteristic for mammalian cells. This mechanism buffers the speed of filament assembly against changes in the concentration of the polymerizable actin pool and therefore provides robustness to actin dynamics in different cellular contexts and across cell-types. Importantly, actin assembly is nonetheless tunable through accessory proteins such as actin polymerases, which can directly modulate the rate-limiting reaction in actin filament elongation. This allows us to understand the mechanisms that regulate the dynamics of actin assembly and their most immediate consequences. Interestingly, many actin polymerases perform activities beyond actin assembly such as bundling of actin filaments, filament depolymerization and severing or microtubule binding (Harris et al., 2010; Harris et al., 2004; Henty-Ridilla et al., 2016; Moseley and Goode, 2005). These additional actin polymerase functions are still not very well understood and deserve further attention in the future. Therefore, the generation of actin polymerase mutants which separately perturb individual polymerase functions will be an important tool to better understand the regulation of polymerase-mediated actin dynamics in vivo.

In our work we revealed the functional relevance of two major actin binding proteins (ABPs), profilin and formin actin polymerases, on actin filament dynamics. ABPs not only control for actin assembly dynamics by interacting with filament barbed ends but also they interact with each other and are involved in a plethora of different actin regulatory processes. Therefore, further investigation of actin dynamics, not only in linear filaments but also in branched actin networks, in presence of different ABPs will become very important in the near future to holistically understand the actin economy through systems reconstitution. Here the combination of new biochemical experiments together with structural analysis can provide tremendous advances for our understanding the molecular mechanisms controlling actin network dynamics. Especially structural analysis of both actin filament ends together with ABPs will solve many open questions about the detailed biochemical mechanisms governing filament end dynamics. One important question, which needs to be clarified by structural end analysis, is the mechanistic basis

of formin processivity. Formin FH2 domain structures bound to the filament barbed end in different gating states (open and closed) should unravel the formin stepping mechanism. Furthermore, a lot has to be learned regarding the biochemical differences between soluble actin monomers and those ones that are bound at filament ends. Structures of filament ends could potentially explain the reason for the large kinetic difference of the two actin ends. Part of my future work will be dedicated to the development of new methods to solve filament end structures at high resolution.

Moreover, it will be important to understand how ABPs sense different actin nucleotide states and if this is specific to individual ABPs or whether it is regulated through a common mechanism. To investigate these questions structural analysis combined with new biochemical tools, such as ABP mutants with altered or modified actin binding sites, will be required. Since the direct visualization of filament polymerization in vivo is not possible up to this point due to high actin densities, remarkably little is known about actin filament lifetimes. Thus the generation of actin monomer and filament binding probes, which only sense specific filament conformational states, would be of interest to understand filament lifetime and turnover at different locations in cells. We showed that actin elongation is robust in vivo and it will be an important further challenge to learn more about the regulation and adaptation of actin filament polymerization dynamics inside cells. As the next step in this direction, it will be necessary to perturb the actin system by manipulating for instance the binding affinity of profilin-actin. This could be achieved through genetic replacement of profilin with the mutants we have studied here through CRISPR/Cas mediated gene editing. Specifically, much remains to be learned about the spatio-temporal distribution of distinct monomer species such as profilin- and/or thymosin-β_4 –bound actin (Rotty et al., 2015; Suarez et al., 2015; Suarez and Kovar, 2016). Importantly, the availability and distribution of polymerizable actin monomers has not yet been directly visualized inside living cells. Development of novel probes able to sense different soluble monomer states will be necessary to better understand the molecular details of local monomer consumption in different actin networks in vivo.

9 References

Aitken, C.E., Marshall, R.A., and Puglisi, J.D. (2008). An oxygen scavenging system for improvement of dye stability in single-molecule fluorescence experiments. Biophys J *94*, 1826-1835.
Alberts, A.S. (2001). Identification of a carboxyl-terminal diaphanous-related formin homology protein autoregulatory domain. J Biol Chem *276*, 2824-2830.
Amann, K.J., and Pollard, T.D. (2001). The Arp2/3 complex nucleates actin filament branches from the sides of pre-existing filaments. Nat Cell Biol *3*, 306-310.
Aydin, F., Courtemanche, N., Pollard, T.D., and Voth, G.A. (2018). Gating mechanisms during actin filament elongation by formins. Elife *7*.
Baker, J.L., Courtemanche, N., Parton, D.L., McCullagh, M., Pollard, T.D., and Voth, G.A. (2015). Electrostatic interactions between the Bni1p Formin FH2 domain and actin influence actin filament nucleation. Structure *23*, 68-79.
Bamburg, J.R., Harris, H.E., and Weeds, A.G. (1980). Partial-Purification and Characterization of an Actin Depolymerizing Factor from Brain. Febs Letters *121*, 178-182.
Barkalow, K., and Hartwig, J.H. (1995). The role of actin filament barbed-end exposure in cytoskeletal dynamics and cell motility. Biochem Soc Trans *23*, 451-456.
Berger, S., Procko, E., Margineantu, D., Lee, E.F., Shen, B.W., Zelter, A., Silva, D.A., Chawla, K., Herold, M.J., Garnier, J.M*., et al.* (2016). Computationally designed high specificity inhibitors delineate the roles of BCL2 family proteins in cancer. Elife *5*.
Bieling, P., Hansen, S.D., Akin, O., Li, T.D., Hayden, C.C., Fletcher, D.A., and Mullins, R.D. (2018). WH2 and proline-rich domains of WASP-family proteins collaborate to accelerate actin filament elongation. EMBO J *37*, 102-121.
Bieling, P., Li, T.D., Weichsel, J., McGorty, R., Jreij, P., Huang, B., Fletcher, D.A., and Mullins, R.D. (2016). Force Feedback Controls Motor Activity and Mechanical Properties of Self-Assembling Branched Actin Networks. Cell *164*, 115-127.
Bieling, P., Telley, I.A., Hentrich, C., Piehler, J., and Surrey, T. (2010). Fluorescence microscopy assays on chemically functionalized surfaces for quantitative imaging of microtubule, motor, and +TIP dynamics. Methods Cell Biol *95*, 555-580.
Blanchoin, L., and Pollard, T.D. (1999). Mechanism of interaction of Acanthamoeba actophorin (ADF/Cofilin) with actin filaments. J Biol Chem *274*, 15538-15546.
Blanchoin, L., and Pollard, T.D. (2002). Hydrolysis of ATP by polymerized actin depends on the bound divalent cation but not profilin. Biochemistry *41*, 597-602.
Blanchoin, L., Pollard, T.D., and Mullins, R.D. (2000). Interactions of ADF/cofilin, Arp2/3 complex, capping protein and profilin in remodeling of branched actin filament networks. Curr Biol *10*, 1273-1282.
Boopathy, S., Silvas, T.V., Tischbein, M., Jansen, S., Shandilya, S.M., Zitzewitz, J.A., Landers, J.E., Goode, B.L., Schiffer, C.A., and Bosco, D.A. (2015). Structural basis for mutation-induced destabilization of profilin 1 in ALS. Proc Natl Acad Sci U S A *112*, 7984-7989.
Bottier, C., Gabella, C., Vianay, B., Buscemi, L., Sbalzarini, I.F., Meister, J.J., and Verkhovsky, A.B. (2011). Dynamic measurement of the height and volume of migrating cells by a novel fluorescence microscopy technique. Lab Chip *11*, 3855-3863.
Breitsprecher, D., Jaiswal, R., Bombardier, J.P., Gould, C.J., Gelles, J., and Goode, B.L. (2012). Rocket launcher mechanism of collaborative actin assembly defined by single-molecule imaging. Science *336*, 1164-1168.
Breitsprecher, D., Kiesewetter, A.K., Linkner, J., and Faix, J. (2009). Analysis of actin assembly by in vitro TIRF microscopy. Methods Mol Biol *571*, 401-415.

Burkel, B.M., von Dassow, G., and Bement, W.M. (2007). Versatile fluorescent probes for actin filaments based on the actin-binding domain of utrophin. Cell Motil Cytoskeleton *64*, 822-832.
Cadart, C., Zlotek-Zlotkiewicz, E., Venkova, L., Thouvenin, O., Racine, V., Le Berre, M., Monnier, S., and Piel, M. (2017). Fluorescence eXclusion Measurement of volume in live cells. Methods Cell Biol *139*, 103-120.
Cai, L., Makhov, A.M., and Bear, J.E. (2007). F-actin binding is essential for coronin 1B function in vivo. J Cell Sci *120*, 1779-1790.
Cao, W., Goodarzi, J.P., and De La Cruz, E.M. (2006). Energetics and kinetics of cooperative cofilin-actin filament interactions. J Mol Biol *361*, 257-267.
Carlier, M.F., Husson, C., Renault, L., and Didry, D. (2011). Control of actin assembly by the WH2 domains and their multifunctional tandem repeats in Spire and Cordon-Bleu. Int Rev Cell Mol Biol *290*, 55-85.
Carlier, M.F., Jean, C., Rieger, K.J., Lenfant, M., and Pantaloni, D. (1993). Modulation of the interaction between G-actin and thymosin beta 4 by the ATP/ADP ratio: possible implication in the regulation of actin dynamics. Proc Natl Acad Sci U S A *90*, 5034-5038.
Carlier, M.F., and Pantaloni, D. (1986). Direct evidence for ADP-Pi-F-actin as the major intermediate in ATP-actin polymerization. Rate of dissociation of Pi from actin filaments. Biochemistry *25*, 7789-7792.
Carlier, M.F., and Pantaloni, D. (1988). Binding of phosphate to F-ADP-actin and role of F-ADP-Pi-actin in ATP-actin polymerization. J Biol Chem *263*, 817-825.
Carlier, M.F., Pernier, J., Montaville, P., Shekhar, S., Kuhn, S., Cytoskeleton, D., and Motility, g. (2015). Control of polarized assembly of actin filaments in cell motility. Cell Mol Life Sci *72*, 3051-3067.
Carlier, M.F., and Shekhar, S. (2017). Global treadmilling coordinates actin turnover and controls the size of actin networks. Nat Rev Mol Cell Biol *18*, 389-401.
Carlsson, A.E. (2010). Actin dynamics: from nanoscale to microscale. Annu Rev Biophys *39*, 91-110.
Castrillon, D.H., and Wasserman, S.A. (1994). Diaphanous is required for cytokinesis in Drosophila and shares domains of similarity with the products of the limb deformity gene. Development *120*, 3367-3377.
Chang, F., Drubin, D., and Nurse, P. (1997). cdc12p, a protein required for cytokinesis in fission yeast, is a component of the cell division ring and interacts with profilin. J Cell Biol *137*, 169-182.
Chesarone, M.A., DuPage, A.G., and Goode, B.L. (2010). Unleashing formins to remodel the actin and microtubule cytoskeletons. Nat Rev Mol Cell Biol *11*, 62-74.
Chesarone, M.A., and Goode, B.L. (2009). Actin nucleation and elongation factors: mechanisms and interplay. Curr Opin Cell Biol *21*, 28-37.
Combeau, C., and Carlier, M.F. (1988). Probing the mechanism of ATP hydrolysis on F-actin using vanadate and the structural analogs of phosphate BeF-3 and A1F-4. J Biol Chem *263*, 17429-17436.
Courtemanche, N. (2018). Mechanisms of formin-mediated actin assembly and dynamics. Biophys Rev *10*, 1553-1569.
Courtemanche, N., and Pollard, T.D. (2013). Interaction of profilin with the barbed end of actin filaments. Biochemistry *52*, 6456-6466.
Didry, D., Cantrelle, F.X., Husson, C., Roblin, P., Moorthy, A.M., Perez, J., Le Clainche, C., Hertzog, M., Guittet, E., Carlier, M.F*., et al.* (2012). How a single residue in individual beta-thymosin/WH2 domains controls their functions in actin assembly. EMBO J *31*, 1000-1013.
Dimchev, G., Steffen, A., Kage, F., Dimchev, V., Pernier, J., Carlier, M.F., and Rottner, K. (2017). Efficiency of lamellipodia protrusion is determined by the extent of cytosolic actin assembly. Mol Biol Cell *28*, 1311-1325.
Dominguez, R. (2004). Actin-binding proteins--a unifying hypothesis. Trends Biochem Sci *29*, 572-578.
Dominguez, R. (2010). Structural insights into de novo actin polymerization. Curr Opin Struct Biol *20*, 217-225.
Dominguez, R. (2016). The WH2 Domain and Actin Nucleation: Necessary but Insufficient. Trends Biochem Sci *41*, 478-490.

dos Remedios, C.G., Chhabra, D., Kekic, M., Dedova, I.V., Tsubakihara, M., Berry, D.A., and Nosworthy, N.J. (2003). Actin binding proteins: regulation of cytoskeletal microfilaments. Physiol Rev *83*, 433-473.

Drenckhahn, D., and Pollard, T.D. (1986). Elongation of actin filaments is a diffusion-limited reaction at the barbed end and is accelerated by inert macromolecules. J Biol Chem *261*, 12754-12758.

Duellberg, C., Cade, N.I., Holmes, D., and Surrey, T. (2016). The size of the EB cap determines instantaneous microtubule stability. Elife *5*.

Edelstein, A.D., Tsuchida, M.A., Amodaj, N., Pinkard, H., Vale, R.D., and Stuurman, N. (2014). Advanced methods of microscope control using muManager software. J Biol Methods *1*.

Evangelista, M., Blundell, K., Longtine, M.S., Chow, C.J., Adames, N., Pringle, J.R., Peter, M., and Boone, C. (1997). Bni1p, a yeast formin linking cdc42p and the actin cytoskeleton during polarized morphogenesis. Science *276*, 118-122.

Faix, J., and Grosse, R. (2006). Staying in shape with formins. Dev Cell *10*, 693-706.

Ferron, F., Rebowski, G., Lee, S.H., and Dominguez, R. (2007). Structural basis for the recruitment of profilin-actin complexes during filament elongation by Ena/VASP. EMBO J *26*, 4597-4606.

Fleishman, S.J., Leaver-Fay, A., Corn, J.E., Strauch, E.M., Khare, S.D., Koga, N., Ashworth, J., Murphy, P., Richter, F., Lemmon, G.*, et al.* (2011). RosettaScripts: a scripting language interface to the Rosetta macromolecular modeling suite. PLoS One *6*, e20161.

Fujii, T., Iwane, A.H., Yanagida, T., and Namba, K. (2010). Direct visualization of secondary structures of F-actin by electron cryomicroscopy. Nature *467*, 724-728.

Fujiwara, I., Vavylonis, D., and Pollard, T.D. (2007). Polymerization kinetics of ADP- and ADP-Pi-actin determined by fluorescence microscopy. Proc Natl Acad Sci U S A *104*, 8827-8832.

Galkin, V.E., Orlova, A., Schroder, G.F., and Egelman, E.H. (2010). Structural polymorphism in F-actin. Nat Struct Mol Biol *17*, 1318-1323.

Gibson, D.G. (2011). Enzymatic assembly of overlapping DNA fragments. Methods Enzymol *498*, 349-361.

Gibson, D.G., Young, L., Chuang, R.Y., Venter, J.C., Hutchison, C.A., 3rd, and Smith, H.O. (2009). Enzymatic assembly of DNA molecules up to several hundred kilobases. Nat Methods *6*, 343-345.

Goode, B.L., and Eck, M.J. (2007). Mechanism and function of formins in the control of actin assembly. Annu Rev Biochem *76*, 593-627.

Gutsche-Perelroizen, I., Lepault, J., Ott, A., and Carlier, M.F. (1999). Filament assembly from profilin-actin. J Biol Chem *274*, 6234-6243.

Hansen, S.D., and Mullins, R.D. (2010). VASP is a processive actin polymerase that requires monomeric actin for barbed end association. J Cell Biol *191*, 571-584.

Harris, E.S., Gauvin, T.J., Heimsath, E.G., and Higgs, H.N. (2010). Assembly of filopodia by the formin FRL2 (FMNL3). Cytoskeleton (Hoboken) *67*, 755-772.

Harris, E.S., Li, F., and Higgs, H.N. (2004). The mouse formin, FRLalpha, slows actin filament barbed end elongation, competes with capping protein, accelerates polymerization from monomers, and severs filaments. J Biol Chem *279*, 20076-20087.

Hartwig, J.H. (1992). Mechanisms of actin rearrangements mediating platelet activation. J Cell Biol *118*, 1421-1442.

Hatano, T., Alioto, S., Roscioli, E., Palani, S., Clarke, S.T., Kamnev, A., Hernandez-Fernaud, J.R., Sivashanmugam, L., Chapa, Y.L.B., Jones, A.M.E.*, et al.* (2018). Rapid production of pure recombinant actin isoforms in Pichia pastoris. J Cell Sci *131*.

Henty-Ridilla, J.L., Rankova, A., Eskin, J.A., Kenny, K., and Goode, B.L. (2016). Accelerated actin filament polymerization from microtubule plus ends. Science *352*, 1004-1009.

Herman, I.M. (1993). Actin isoforms. Curr Opin Cell Biol *5*, 48-55.

Higashida, C., Kiuchi, T., Akiba, Y., Mizuno, H., Maruoka, M., Narumiya, S., Mizuno, K., and Watanabe, N. (2013). F- and G-actin homeostasis regulates mechanosensitive actin nucleation by formins. Nat Cell Biol *15*, 395-405.

Higashida, C., Miyoshi, T., Fujita, A., Oceguera-Yanez, F., Monypenny, J., Andou, Y., Narumiya, S., and Watanabe, N. (2004). Actin polymerization-driven molecular movement of mDia1 in living cells. Science *303*, 2007-2010.

Higgs, H.N., and Peterson, K.J. (2005). Phylogenetic analysis of the formin homology 2 domain. Mol Biol Cell *16*, 1-13.

Holmes, K.C., Popp, D., Gebhard, W., and Kabsch, W. (1990). Atomic model of the actin filament. Nature *347*, 44-49.

Hudson, E.N., and Weber, G. (1973). Synthesis and characterization of two fluorescent sulfhydryl reagents. Biochemistry *12*, 4154-4161.

Imamura, H., Tanaka, K., Hihara, T., Umikawa, M., Kamei, T., Takahashi, K., Sasaki, T., and Takai, Y. (1997). Bni1p and Bnr1p: downstream targets of the Rho family small G-proteins which interact with profilin and regulate actin cytoskeleton in Saccharomyces cerevisiae. EMBO J *16*, 2745-2755.

Jansen, S., Collins, A., Chin, S.M., Ydenberg, C.A., Gelles, J., and Goode, B.L. (2015). Single-molecule imaging of a three-component ordered actin disassembly mechanism. Nat Commun *6*, 7202.

Jansen, S., Collins, A., Golden, L., Sokolova, O., and Goode, B.L. (2014). Structure and mechanism of mouse cyclase-associated protein (CAP1) in regulating actin dynamics. J Biol Chem *289*, 30732-30742.

Jegou, A., Carlier, M.F., and Romet-Lemonne, G. (2013). Formin mDia1 senses and generates mechanical forces on actin filaments. Nat Commun *4*, 1883.

Johnston, A.B., Collins, A., and Goode, B.L. (2015). High-speed depolymerization at actin filament ends jointly catalysed by Twinfilin and Srv2/CAP. Nat Cell Biol *17*, 1504-1511.

Kabsch, W., Mannherz, H.G., Suck, D., Pai, E.F., and Holmes, K.C. (1990). Atomic structure of the actin:DNase I complex. Nature *347*, 37-44.

Kaiser, D.A., Vinson, V.K., Murphy, D.B., and Pollard, T.D. (1999). Profilin is predominantly associated with monomeric actin in Acanthamoeba. J Cell Sci *112 (Pt 21)*, 3779-3790.

Kerkhoff, E. (2006). Cellular functions of the Spir actin-nucleation factors. Trends Cell Biol *16*, 477-483.

Kibbe, W.A. (2007). OligoCalc: an online oligonucleotide properties calculator. Nucleic Acids Res *35*, W43-46.

Kinosian, H.J., Selden, L.A., Estes, J.E., and Gershman, L.C. (1993). Nucleotide binding to actin. Cation dependence of nucleotide dissociation and exchange rates. J Biol Chem *268*, 8683-8691.

Kinosian, H.J., Selden, L.A., Gershman, L.C., and Estes, J.E. (2000). Interdependence of profilin, cation, and nucleotide binding to vertebrate non-muscle actin. Biochemistry *39*, 13176-13188.

Kinosian, H.J., Selden, L.A., Gershman, L.C., and Estes, J.E. (2002). Actin filament barbed end elongation with nonmuscle MgATP-actin and MgADP-actin in the presence of profilin. Biochemistry *41*, 6734-6743.

Koestler, S.A., Rottner, K., Lai, F., Block, J., Vinzenz, M., and Small, J.V. (2009). F- and G-actin concentrations in lamellipodia of moving cells. PLoS One *4*, e4810.

Korenbaum, E., Nordberg, P., Bjorkegren-Sjogren, C., Schutt, C.E., Lindberg, U., and Karlsson, R. (1998). The role of profilin in actin polymerization and nucleotide exchange. Biochemistry *37*, 9274-9283.

Kotila, T., Wioland, H., Enkavi, G., Kogan, K., Vattulainen, I., Jegou, A., Romet-Lemonne, G., and Lappalainen, P. (2019). Mechanism of synergistic actin filament pointed end depolymerization by cyclase-associated protein and cofilin. Nat Commun *10*, 5320.

Kovar, D.R., Harris, E.S., Mahaffy, R., Higgs, H.N., and Pollard, T.D. (2006). Control of the assembly of ATP- and ADP-actin by formins and profilin. Cell *124*, 423-435.

Kovar, D.R., Kuhn, J.R., Tichy, A.L., and Pollard, T.D. (2003). The fission yeast cytokinesis formin Cdc12p is a barbed end actin filament capping protein gated by profilin. Journal of Cell Biology *161*, 875-887.

Kovar, D.R., and Pollard, T.D. (2004). Insertional assembly of actin filament barbed ends in association with formins produces piconewton forces. Proc Natl Acad Sci U S A *101*, 14725-14730.

Kuhn, J.R., and Pollard, T.D. (2005). Real-time measurements of actin filament polymerization by total internal reflection fluorescence microscopy. Biophys J *88*, 1387-1402.

Laki, K. (1951). The polymerization of proteins; the action of thrombin on fibrinogen. Arch Biochem Biophys *32*, 317-324.
Leaver-Fay, A., Tyka, M., Lewis, S.M., Lange, O.F., Thompson, J., Jacak, R., Kaufman, K., Renfrew, P.D., Smith, C.A., Sheffler, W.*, et al.* (2011). ROSETTA3: an object-oriented software suite for the simulation and design of macromolecules. Methods Enzymol *487*, 545-574.
Li, F., and Higgs, H.N. (2003). The mouse Formin mDia1 is a potent actin nucleation factor regulated by autoinhibition. Curr Biol *13*, 1335-1340.
Lu, J., Meng, W., Poy, F., Maiti, S., Goode, B.L., and Eck, M.J. (2007). Structure of the FH2 domain of Daam1: implications for formin regulation of actin assembly. J Mol Biol *369*, 1258-1269.
Melki, R., Fievez, S., and Carlier, M.F. (1996). Continuous monitoring of Pi release following nucleotide hydrolysis in actin or tubulin assembly using 2-amino-6-mercapto-7-methylpurine ribonucleoside and purine-nucleoside phosphorylase as an enzyme-linked assay. Biochemistry *35*, 12038-12045.
Merino, F., Pospich, S., Funk, J., Wagner, T., Kullmer, F., Arndt, H.D., Bieling, P., and Raunser, S. (2018). Structural transitions of F-actin upon ATP hydrolysis at near-atomic resolution revealed by cryo-EM. Nat Struct Mol Biol *25*, 528-537.
Merino, F., Pospich, S., and Raunser, S. (2019). Towards a structural understanding of the remodeling of the actin cytoskeleton. Semin Cell Dev Biol.
Miki, M., Barden, J.A., dos Remedios, C.G., Phillips, L., and Hambly, B.D. (1987). Interaction of phalloidin with chemically modified actin. Eur J Biochem *165*, 125-130.
Mogilner, A., and Oster, G. (1996). Cell motility driven by actin polymerization. Biophys J *71*, 3030-3045.
Moseley, J.B., and Goode, B.L. (2005). Differential activities and regulation of Saccharomyces cerevisiae formin proteins Bni1 and Bnr1 by Bud6. J Biol Chem *280*, 28023-28033.
Moseley, J.B., Sagot, I., Manning, A.L., Xu, Y., Eck, M.J., Pellman, D., and Goode, B.L. (2004). A conserved mechanism for Bni1- and mDia1-induced actin assembly and dual regulation of Bni1 by Bud6 and profilin. Mol Biol Cell *15*, 896-907.
Mouneimne, G., Hansen, S.D., Selfors, L.M., Petrak, L., Hickey, M.M., Gallegos, L.L., Simpson, K.J., Lim, J., Gertler, F.B., Hartwig, J.H.*, et al.* (2012). Differential remodeling of actin cytoskeleton architecture by profilin isoforms leads to distinct effects on cell migration and invasion. Cancer Cell *22*, 615-630.
Mueller, J., Szep, G., Nemethova, M., de Vries, I., Lieber, A.D., Winkler, C., Kruse, K., Small, J.V., Schmeiser, C., Keren, K.*, et al.* (2017). Load Adaptation of Lamellipodial Actin Networks. Cell *171*, 188-200 e116.
Nakano, K., Imai, J., Arai, R., Toh, E.A., Matsui, Y., and Mabuchi, I. (2002). The small GTPase Rho3 and the diaphanous/formin For3 function in polarized cell growth in fission yeast. J Cell Sci *115*, 4629-4639.
Narita, A., Oda, T., and Maeda, Y. (2011). Structural basis for the slow dynamics of the actin filament pointed end. Embo Journal *30*, 1230-1237.
Neidt, E.M., Skau, C.T., and Kovar, D.R. (2008). The cytokinesis formins from the nematode worm and fission yeast differentially mediate actin filament assembly. J Biol Chem *283*, 23872-23883.
Nezami, A., Poy, F., Toms, A., Zheng, W., and Eck, M.J. (2010). Crystal structure of a complex between amino and carboxy terminal fragments of mDia1: insights into autoinhibition of diaphanous-related formins. PLoS One *5*.
Nishida, E., Maekawa, S., and Sakai, H. (1984). Cofilin, a Protein in Porcine Brain That Binds to Actin-Filaments and Inhibits Their Interactions with Myosin and Tropomyosin. Zool Sci *1*, 903-903.
Noguchi, T.Q., Kanzaki, N., Ueno, H., Hirose, K., and Uyeda, T.Q. (2007). A novel system for expressing toxic actin mutants in Dictyostelium and purification and characterization of a dominant lethal yeast actin mutant. J Biol Chem *282*, 27721-27727.
Oda, T., Iwasa, M., Aihara, T., Maeda, Y., and Narita, A. (2009). The nature of the globular- to fibrous-actin transition. Nature *457*, 441-445.

Ohki, T., Ohno, C., Oyama, K., Mikhailenko, S.V., and Ishiwata, S. (2009). Purification of cytoplasmic actin by affinity chromatography using the C-terminal half of gelsolin. Biochem Biophys Res Commun *383*, 146-150.

Oosawa, F., and Asakura, S. (1975). Thermodynamics of the polymerization of protein (London ; New York: Academic Press).

Otomo, T., Otomo, C., Tomchick, D.R., Machius, M., and Rosen, M.K. (2005a). Structural basis of Rho GTPase-mediated activation of the formin mDia1. Mol Cell *18*, 273-281.

Otomo, T., Tomchick, D.R., Otomo, C., Panchal, S.C., Machius, M., and Rosen, M.K. (2005b). Structural basis of actin filament nucleation and processive capping by a formin homology 2 domain. Nature *433*, 488-494.

Paavilainen, V.O., Bertling, E., Falck, S., and Lappalainen, P. (2004). Regulation of cytoskeletal dynamics by actin-monomer-binding proteins. Trends Cell Biol *14*, 386-394.

Pantaloni, D., and Carlier, M.F. (1993). How profilin promotes actin filament assembly in the presence of thymosin beta 4. Cell *75*, 1007-1014.

Paul, A.S., and Pollard, T.D. (2008). The role of the FH1 domain and profilin in formin-mediated actin-filament elongation and nucleation. Curr Biol *18*, 9-19.

Paul, A.S., and Pollard, T.D. (2009). Review of the mechanism of processive actin filament elongation by formins. Cell Motil Cytoskeleton *66*, 606-617.

Peng, G.E., Wilson, S.R., and Weiner, O.D. (2011). A pharmacological cocktail for arresting actin dynamics in living cells. Mol Biol Cell *22*, 3986-3994.

Perelroizen, I., Didry, D., Christensen, H., Chua, N.H., and Carlier, M.F. (1996). Role of nucleotide exchange and hydrolysis in the function of profilin in action assembly. J Biol Chem *271*, 12302-12309.

Pernier, J., Shekhar, S., Jegou, A., Guichard, B., and Carlier, M.F. (2016). Profilin Interaction with Actin Filament Barbed End Controls Dynamic Instability, Capping, Branching, and Motility. Dev Cell *36*, 201-214.

Petrella, E.C., Machesky, L.M., Kaiser, D.A., and Pollard, T.D. (1996). Structural requirements and thermodynamics of the interaction of proline peptides with profilin. Biochemistry *35*, 16535-16543.

Pollard, T.D. (1982). Myosin purification and characterization. Methods Cell Biol *24*, 333-371.

Pollard, T.D. (1986a). Assembly and dynamics of the actin filament system in nonmuscle cells. J Cell Biochem *31*, 87-95.

Pollard, T.D. (1986b). Rate constants for the reactions of ATP- and ADP-actin with the ends of actin filaments. J Cell Biol *103*, 2747-2754.

Pollard, T.D. (2007). Regulation of actin filament assembly by Arp2/3 complex and formins. Annu Rev Biophys Biomol Struct *36*, 451-477.

Pollard, T.D., Blanchoin, L., and Mullins, R.D. (2000). Molecular mechanisms controlling actin filament dynamics in nonmuscle cells. Annu Rev Biophys Biomol Struct *29*, 545-576.

Pollard, T.D., and Borisy, G.G. (2003). Cellular motility driven by assembly and disassembly of actin filaments. Cell *112*, 453-465.

Pollard, T.D., and Cooper, J.A. (1984). Quantitative analysis of the effect of Acanthamoeba profilin on actin filament nucleation and elongation. Biochemistry *23*, 6631-6641.

Pollard, T.D., and Cooper, J.A. (1986). Actin and actin-binding proteins. A critical evaluation of mechanisms and functions. Annu Rev Biochem *55*, 987-1035.

Pollard, T.D., and Cooper, J.A. (2009). Actin, a central player in cell shape and movement. Science *326*, 1208-1212.

Pollard, T.D., and Mooseker, M.S. (1981). Direct measurement of actin polymerization rate constants by electron microscopy of actin filaments nucleated by isolated microvillus cores. J Cell Biol *88*, 654-659.

Pospich, S., Kumpula, E.P., von der Ecken, J., Vahokoski, J., Kursula, I., and Raunser, S. (2017). Near-atomic structure of jasplakinolide-stabilized malaria parasite F-actin reveals the structural basis of filament instability. Proc Natl Acad Sci U S A *114*, 10636-10641.

Pring, M., Evangelista, M., Boone, C., Yang, C., and Zigmond, S.H. (2003). Mechanism of formin-induced nucleation of actin filaments. Biochemistry *42*, 486-496.
Pring, M., Weber, A., and Bubb, M.R. (1992). Profilin-actin complexes directly elongate actin filaments at the barbed end. Biochemistry *31*, 1827-1836.
Pruyne, D., Evangelista, M., Yang, C., Bi, E., Zigmond, S., Bretscher, A., and Boone, C. (2002). Role of formins in actin assembly: nucleation and barbed-end association. Science *297*, 612-615.
Ramalingam, N., Zhao, H., Breitsprecher, D., Lappalainen, P., Faix, J., and Schleicher, M. (2010). Phospholipids regulate localization and activity of mDia1 formin. Eur J Cell Biol *89*, 723-732.
Rasnik, I., McKinney, S.A., and Ha, T. (2006). Nonblinking and long-lasting single-molecule fluorescence imaging. Nat Methods *3*, 891-893.
Raz-Ben Aroush, D., Ofer, N., Abu-Shah, E., Allard, J., Krichevsky, O., Mogilner, A., and Keren, K. (2017). Actin Turnover in Lamellipodial Fragments. Curr Biol *27*, 2963-2973 e2914.
Renault, L., Bugyi, B., and Carlier, M.F. (2008). Spire and Cordon-bleu: multifunctional regulators of actin dynamics. Trends Cell Biol *18*, 494-504.
Renkawitz, J., Schumann, K., Weber, M., Lammermann, T., Pflicke, H., Piel, M., Polleux, J., Spatz, J.P., and Sixt, M. (2009). Adaptive force transmission in amoeboid cell migration. Nat Cell Biol *11*, 1438-1443.
Riedl, J., Crevenna, A.H., Kessenbrock, K., Yu, J.H., Neukirchen, D., Bista, M., Bradke, F., Jenne, D., Holak, T.A., Werb, Z*., et al.* (2008). Lifeact: a versatile marker to visualize F-actin. Nat Methods *5*, 605-607.
Romero, S., Didry, D., Larquet, E., Boisset, N., Pantaloni, D., and Carlier, M.F. (2007). How ATP hydrolysis controls filament assembly from profilin-actin: implication for formin processivity. J Biol Chem *282*, 8435-8445.
Romero, S., Le Clainche, C., Didry, D., Egile, C., Pantaloni, D., and Carlier, M.F. (2004). Formin is a processive motor that requires profilin to accelerate actin assembly and associated ATP hydrolysis. Cell *119*, 419-429.
Rose, R., Weyand, M., Lammers, M., Ishizaki, T., Ahmadian, M.R., and Wittinghofer, A. (2005). Structural and mechanistic insights into the interaction between Rho and mammalian Dia. Nature *435*, 513-518.
Rosenblatt, J., Peluso, P., and Mitchison, T.J. (1995). The bulk of unpolymerized actin in Xenopus egg extracts is ATP-bound. Mol Biol Cell *6*, 227-236.
Rotty, J.D., Wu, C., Haynes, E.M., Suarez, C., Winkelman, J.D., Johnson, H.E., Haugh, J.M., Kovar, D.R., and Bear, J.E. (2015). Profilin-1 serves as a gatekeeper for actin assembly by Arp2/3-dependent and -independent pathways. Dev Cell *32*, 54-67.
Rould, M.A., Wan, Q., Joel, P.B., Lowey, S., and Trybus, K.M. (2006). Crystal structures of expressed non-polymerizable monomeric actin in the ADP and ATP states. J Biol Chem *281*, 31909-31919.
Safer, D., and Nachmias, V.T. (1994). Beta thymosins as actin binding peptides. Bioessays *16*, 590.
Safer, D., Sosnick, T.R., and Elzinga, M. (1997). Thymosin beta 4 binds actin in an extended conformation and contacts both the barbed and pointed ends. Biochemistry *36*, 5806-5816.
Schonichen, A., and Geyer, M. (2010). Fifteen formins for an actin filament: a molecular view on the regulation of human formins. Biochim Biophys Acta *1803*, 152-163.
Schutt, C.E., Myslik, J.C., Rozycki, M.D., Goonesekere, N.C., and Lindberg, U. (1993). The structure of crystalline profilin-beta-actin. Nature *365*, 810-816.
Sept, D., Elcock, A.H., and McCammon, J.A. (1999). Computer simulations of actin polymerization can explain the barbed-pointed end asymmetry. J Mol Biol *294*, 1181-1189.
Sept, D., and McCammon, J.A. (2001). Thermodynamics and kinetics of actin filament nucleation. Biophys J *81*, 667-674.
Shimada, A., Nyitrai, M., Vetter, I.R., Kuhlmann, D., Bugyi, B., Narumiya, S., Geeves, M.A., and Wittinghofer, A. (2004). The core FH2 domain of diaphanous-related formins is an elongated actin binding protein that inhibits polymerization. Mol Cell *13*, 511-522.
Skau, C.T., and Waterman, C.M. (2015). Specification of Architecture and Function of Actin Structures by Actin Nucleation Factors. Annu Rev Biophys *44*, 285-310.

Skruber, K., Read, T.A., and Vitriol, E.A. (2018). Reconsidering an active role for G-actin in cytoskeletal regulation. J Cell Sci *131*.

Straub, F.B., and Feuer, G. (1950). [Adenosine triphosphate, the functional group of actin]. Kiserl Orvostud *2*, 141-151.

Suarez, C., Carroll, R.T., Burke, T.A., Christensen, J.R., Bestul, A.J., Sees, J.A., James, M.L., Sirotkin, V., and Kovar, D.R. (2015). Profilin regulates F-actin network homeostasis by favoring formin over Arp2/3 complex. Dev Cell *32*, 43-53.

Suarez, C., and Kovar, D.R. (2016). Internetwork competition for monomers governs actin cytoskeleton organization. Nat Rev Mol Cell Biol *17*, 799-810.

Suarez, C., Roland, J., Boujemaa-Paterski, R., Kang, H., McCullough, B.R., Reymann, A.C., Guerin, C., Martiel, J.L., De la Cruz, E.M., and Blanchoin, L. (2011). Cofilin tunes the nucleotide state of actin filaments and severs at bare and decorated segment boundaries. Curr Biol *21*, 862-868.

Tinevez, J.Y., Perry, N., Schindelin, J., Hoopes, G.M., Reynolds, G.D., Laplantine, E., Bednarek, S.Y., Shorte, S.L., and Eliceiri, K.W. (2017). TrackMate: An open and extensible platform for single-particle tracking. Methods *115*, 80-90.

Vaillant, D.C., Copeland, S.J., Davis, C., Thurston, S.F., Abdennur, N., and Copeland, J.W. (2008). Interaction of the N- and C-terminal autoregulatory domains of FRL2 does not inhibit FRL2 activity. J Biol Chem *283*, 33750-33762.

van Gisbergen, P.A., Li, M., Wu, S.Z., and Bezanilla, M. (2012). Class II formin targeting to the cell cortex by binding PI(3,5)P(2) is essential for polarized growth. J Cell Biol *198*, 235-250.

Vargas, P., Maiuri, P., Bretou, M., Saez, P.J., Pierobon, P., Maurin, M., Chabaud, M., Lankar, D., Obino, D., Terriac, E.*, et al.* (2016a). Corrigendum: Innate control of actin nucleation determines two distinct migration behaviours in dendritic cells. Nat Cell Biol *18*, 234.

Vargas, P., Maiuri, P., Bretou, M., Saez, P.J., Pierobon, P., Maurin, M., Chabaud, M., Lankar, D., Obino, D., Terriac, E.*, et al.* (2016b). Innate control of actin nucleation determines two distinct migration behaviours in dendritic cells. Nat Cell Biol *18*, 43-53.

Vavylonis, D., Kovar, D.R., O'Shaughnessy, B., and Pollard, T.D. (2006). Model of formin-associated actin filament elongation. Mol Cell *21*, 455-466.

Vinson, V.K., De La Cruz, E.M., Higgs, H.N., and Pollard, T.D. (1998). Interactions of Acanthamoeba profilin with actin and nucleotides bound to actin. Biochemistry *37*, 10871-10880.

Wang, Z.X. (1995). An exact mathematical expression for describing competitive binding of two different ligands to a protein molecule. FEBS Lett *360*, 111-114.

Watanabe, N., Madaule, P., Reid, T., Ishizaki, T., Watanabe, G., Kakizuka, A., Saito, Y., Nakao, K., Jockusch, B.M., and Narumiya, S. (1997). p140mDia, a mammalian homolog of Drosophila diaphanous, is a target protein for Rho small GTPase and is a ligand for profilin. EMBO J *16*, 3044-3056.

Webb, B., and Sali, A. (2016). Comparative Protein Structure Modeling Using MODELLER. Curr Protoc Protein Sci *86*, 2 9 1-2 9 37.

Wegner, A. (1976). Head to tail polymerization of actin. J Mol Biol *108*, 139-150.

Wegner, A., and Engel, J. (1975). Kinetics of the cooperative association of actin to actin filaments. Biophys Chem *3*, 215-225.

Winkelman, J.D., Bilancia, C.G., Peifer, M., and Kovar, D.R. (2014). Ena/VASP Enabled is a highly processive actin polymerase tailored to self-assemble parallel-bundled F-actin networks with Fascin. Proc Natl Acad Sci U S A *111*, 4121-4126.

Winterhoff, M., Bruhmann, S., Franke, C., Breitsprecher, D., and Faix, J. (2016). Visualization of Actin Assembly and Filament Turnover by In Vitro Multicolor TIRF Microscopy. Methods Mol Biol *1407*, 287-306.

Witke, W., Sutherland, J.D., Sharpe, A., Arai, M., and Kwiatkowski, D.J. (2001). Profilin I is essential for cell survival and cell division in early mouse development. Proc Natl Acad Sci U S A *98*, 3832-3836.

Xu, Y.W., Moseley, J.B., Sagot, I., Poy, F., Pellman, D., Goode, B.L., and Eck, M.J. (2004). Crystal structures of a formin homology-2 domain reveal a tethered dimer architecture. Cell *116*, 711-723.
Xue, B., Leyrat, C., Grimes, J.M., and Robinson, R.C. (2014). Structural basis of thymosin-beta4/profilin exchange leading to actin filament polymerization. Proc Natl Acad Sci U S A *111*, E4596-4605.
Yamashita, M., Higashi, T., Suetsugu, S., Sato, Y., Ikeda, T., Shirakawa, R., Kita, T., Takenawa, T., Horiuchi, H., Fukai, S*., et al.* (2007). Crystal structure of human DAAM1 formin homology 2 domain. Genes Cells *12*, 1255-1265.
Yang, C., Czech, L., Gerboth, S., Kojima, S., Scita, G., and Svitkina, T. (2007). Novel roles of formin mDia2 in lamellipodia and filopodia formation in motile cells. PLoS Biol *5*, e317.
Yarmola, E.G., and Bubb, M.R. (2004). Effects of profilin and thymosin beta4 on the critical concentration of actin demonstrated in vitro and in cell extracts with a novel direct assay. J Biol Chem *279*, 33519-33527.
Yarmola, E.G., and Bubb, M.R. (2006). Profilin: emerging concepts and lingering misconceptions. Trends Biochem Sci *31*, 197-205.
Yarmola, E.G., Dranishnikov, D.A., and Bubb, M.R. (2008). Effect of profilin on actin critical concentration: a theoretical analysis. Biophys J *95*, 5544-5573.
Zalevsky, J., Grigorova, I., and Mullins, R.D. (2001). Activation of the Arp2/3 complex by the Listeria acta protein. Acta binds two actin monomers and three subunits of the Arp2/3 complex. J Biol Chem *276*, 3468-3475.
Zigmond, S.H., Evangelista, M., Boone, C., Yang, C., Dar, A.C., Sicheri, F., Forkey, J., and Pring, M. (2003). Formin leaky cap allows elongation in the presence of tight capping proteins. Curr Biol *13*, 1820-1823.

Publications

Parts of this work were originally published in the following publication submitted on the 8th of August 2019 and accepted on the 24th of October 2019:

Funk J., Merino F., Venkova L., Heydenreich L., Kierfeld J., Vargas P., Raunser S., Piel M. and Bieling P. Profilin and formin constitute a pacemaker system for robust actin filament growth. *eLife (**2019**). DOI: 10.7554/eLife.50963.*

For this thesis, text and figures of the original publication (*Funk et al., 2019*) were rewritten and reformatted, respectively. Particularly, changes in figure numbering according to the text of this thesis were performed. In addition, figure panels were partly split into several sections to improve the quality of the reading sequence. Original supplementary movies were not shown in this thesis but can be requested from the online version of the publication *Funk et al., 2019* on the *elife* webpage. Furthermore, improved and more detailed Material and Methods sections (section 5.1 and 5.2) as well as a more generalized Introduction (section 3) were incorporated in this thesis, respectively.

Eidesstattliche Versicherung (Affidavit)

Funk, Johanna
Name, Vorname
(Surname, first name)

191100
Matrikel-Nr.
(Enrolment number)

Belehrung:
Wer vorsätzlich gegen eine die Täuschung über Prü fungsleistungen betreffende Regelung einer Hochschul prüfungsordnung verstößt, handelt ordnungswidrig. Die Ordnungswidrigkeit kann mit einer Geldbuße von bis zu 50.000,00 € geahndet werden. Zuständige Verwaltungs behörde für die Verfolgung und Ahndung von Ordnungswidrigkeiten ist der Kanzler/die Kanzlerin der Technischen Universität Dortmund. Im Falle eines mehrfachen oder sonstigen schwerwiegenden Täuschungsversu ches kann der Prüfling zudem exmatrikuliert werden, § 63 Abs. 5 Hochschulgesetz NRW.

Die Abgabe einer falschen Versicherung an Eides statt ist strafbar.

Wer vorsätzlich eine falsche Versicherung an Eides statt abgibt, kann mit einer Freiheitsstrafe bis zu drei Jahren oder mit Geldstrafe bestraft werden, § 156 StGB. Die fahrlässige Abgabe einer falschen Versicherung an Eides statt kann mit einer Freiheitsstrafe bis zu einem Jahr oder Geldstrafe bestraft werden, § 161 StGB.

Die oben stehende Belehrung habe ich zur Kenntnis genommen:

Official notification:

Any person who intentionally breaches any regulation of university examination regulations relating to deception in examination performance is acting improperly. This offence can be punished with a fine of up to EUR 50,000.00. The competent administrative authority for the pursuit and prosecution of offences of this type is the chancellor of the TU Dortmund University. In the case of multiple or other serious attempts at deception, the candidate can also be unenrolled, Section 63, paragraph 5 of the Universities Act of North Rhine-Westphalia.

The submission of a false affidavit is punishable.

Any person who intentionally submits a false affidavit can be punished with a prison sentence of up to three years or a fine, Section 156 of the Criminal Code. The negligent submission of a false affidavit can be punished with a prison sentence of up to one year or a fine, Section 161 of the Criminal Code.

I have taken note of the above official notification.

_____ _____

Ort, Datum
(Place, date)

Unterschrift
(Signature)

Titel der Dissertation:
(Title of the thesis):

A biochemical pacemaker system for robust actin growth

Ich versichere hiermit an Eides statt, dass ich die vorliegende Dissertation mit dem Titel selbstständig und ohne unzulässige fremde Hilfe angefertigt habe. Ich habe keine anderen als die angegebenen Quellen und Hilfs mittel benutzt sowie wörtliche und sinngemäße Zitate kenntlich gemacht.
Die Arbeit hat in gegenwärtiger oder in einer anderen Fassung weder der TU Dortmund noch einer anderen Hochschule im Zusammenhang mit einer staatlichen oder akademischen Prüfung vorgelegen.

I hereby swear that I have completed the present dissertation independently and without inadmissible external support. I have not used any sources or tools other than those indicated and have identified literal and analogous quotations.

The thesis in its current version or another version has not been presented to the TU Dortmund University or another university in connection with a state or academic examination.*

*Please be aware that solely the German version of the affidavit ("Eidesstattliche Versicherung") for the PhD thesis is the official and legally binding version.

_____ _____

Ort, Datum
(Place, date)

Unterschrift
(Signature)